# FINAL REPORT

Quantifying Sulfate, Organics, and Lubrication Oil in Particles Emitted from Military Aircraft Engines

## SERDP Project WP-1625

OCTOBER 2012

Richard Miake-Lye
Hsi-Wu Wong
Zhenhong Yu
Jay Peck
Scott C. Herndon
Jon Franklin
Gregory R. Magoon
**Aerodyne Research, Inc.**

David Liscinksy
Meredith Colket
Archer Jennings
Bruce True
**United Technologies Research Center**

Anuj Bhargava
Baris Sen
**Pratt and Whitney**

Mina Jun
Ian A. Waitz
**Massachusetts Institute of Technology**

*This document has been cleared for public release*

**SERDP**
DOD ▪ EPA ▪ DOE

| Report Documentation Page | | Form Approved OMB No. 0704-0188 |
|---|---|---|

| 1. REPORT DATE **OCT 2012** | 2. REPORT TYPE | 3. DATES COVERED **00-00-2012 to 00-00-2012** |
|---|---|---|
| 4. TITLE AND SUBTITLE **Quantifying Sulfate, Organics, and Lubrication Oil in Particles Emitted from Military Aircraft Engines** | | 5a. CONTRACT NUMBER |
| | | 5b. GRANT NUMBER |
| | | 5c. PROGRAM ELEMENT NUMBER |
| 6. AUTHOR(S) | | 5d. PROJECT NUMBER |
| | | 5e. TASK NUMBER |
| | | 5f. WORK UNIT NUMBER |
| 7. PERFORMING ORGANIZATION NAME(S) AND ADDRESS(ES) **Aerodyne Research, Inc.,45 Manning Road ,Billerica,MA,01821-3976** | | 8. PERFORMING ORGANIZATION REPORT NUMBER |
| 9. SPONSORING/MONITORING AGENCY NAME(S) AND ADDRESS(ES) | | 10. SPONSOR/MONITOR'S ACRONYM(S) |
| | | 11. SPONSOR/MONITOR'S REPORT NUMBER(S) |
| 12. DISTRIBUTION/AVAILABILITY STATEMENT **Approved for public release; distribution unlimited** | | |
| 13. SUPPLEMENTARY NOTES | | |

## 14. ABSTRACT

**1.1 Objectives SERDP Project WP1625 was a multi-component effort to understand volatile contributions to particulate matter (PM) emitted from military aircraft engines. Volatile PM formed when condensable gases emitted in the exhaust form new particles or add coatings to emitted soot particles, is getting increasing attention due to potential environmental and health effects, and is coming under increasing regulatory control. Military operations can be constrained if local air quality limits are exceeded. For both these environmental reasons and for the potential impact on aircraft signatures, an improved understanding is sought of volatile PM and the factors that control its formation and evolution. 1.2 Technical Approach WP1625 was structured such that there was an interplay between modeling efforts and several experimental measurement efforts. The project was divided into four components, one focused on modeling and three focused on experimental explorations. Modeling work focused on the development of an advanced particle evolution model considering microphysics involving soot, sulfur, water, and condensable hydrocarbons. Experimental work included a laboratory study on soot interaction with organic species, an oil emissions field study, and a combustor sector rig study of condensation on soot. Experimental and modeling efforts were integrated with experiments providing key parameters needed for model simulations and with model simulations aiding in the interpretation of experimental results. Each of these four components is summarized in further detail below, with a Section of the report dedicated to each. 1.3 Results An existing particle evolution model, which included soot and sulfur/water microphysics has been extended to include hydrocarbon condensable species. This is described in detail in Section 2. The inclusion of a wide range of HC species and their capability to condense on soot surfaces has been successfully finalized and the participation of HCs in forming new, volatile particles in concert with sulfuric acid and water has also been completed. The proposed upgrades to the microphysical code under this SERDP effort are now complete, and the upgraded code has been applied in analyzing measurement data and planning of experiments. The extended microphysical model was used in helping to plan a series of laboratory studies. A key finding of the experiments carried out in the first year was the need to include a thermal denuder to remove hydrocarbons from the soot surface and make soot more representative of military aircraft engine soot. This was achieved and subsequent laboratory studies examined several key condensable HCs in a controlled environment, interacting with the now stripped combustion generated soot particles. The promising results from that study are described in Section 3. The coupling between the experimental data and experiment-model**

## 15. SUBJECT TERMS

| 16. SECURITY CLASSIFICATION OF: | | | 17. LIMITATION OF ABSTRACT | 18. NUMBER OF PAGES | 19a. NAME OF RESPONSIBLE PERSON |
|---|---|---|---|---|---|
| a. REPORT<br>**unclassified** | b. ABSTRACT<br>**unclassified** | c. THIS PAGE<br>**unclassified** | **Same as Report (SAR)** | **120** | |

# Table of Contents

## List of Tables

# List of Figures

# List of Acronyms

| | |
|---|---|
| AMS | Aerosol Mass Spectrometer |
| APEX | Aircraft Particle Emissions eXperiment |
| ARI | Aerodyne Research, Inc. |
| ARP | Aerospace Recommended Practices |
| C-TOFAMS | Compact Time of Flight AMS |
| CAPS | Cavity Attenuated Phase Shift |
| CPC | Condensation Particle Counter |
| CPMA | Couette Centrifugal Particle Mass Analyzer |
| DMA | Differential Mobility Analyzer |
| EC | Elementary Carbon (*cf.* OC) |
| EI | Emission Index |
| EEPS | Engine Exhaust Particle Sizer |
| EPA | Environmental Protection Agency |
| FAA | Federal Aviation Administration |
| GMD | Geometric Mean Diameter of a particle size distribution |
| HFID | Heated Flame Ionization Detector |
| HC | Hydrocarbon |
| HR-TOF | High Resolution Time of Flight |
| JBTS | Jet Burner Test Stand |
| LPM | mass flow in Liters Per Minute |
| MAAP | Multiple Angle Absorption Photometer |
| NDIR | Non-Dispersive InfraRed sensor |
| miniCAST | small Combustion Aerosol STandard generator |
| OC | Organic Carbon (*cf.* EC) |
| P&W | Pratt & Whitney |
| PAH | Polycyclic Aromatic Hydrocarbon |
| PM | Particulate Matter |
| PM2.5 | Particulate Matter less than 2.5 µm in size |
| PTR-MS | Proton Transfer Reaction Mass Spectrometry |
| QUN | Quasi-Unary Nucleation |
| RH | Relative Humidity |
| SAE | Society of Automotive Engineers |
| SMPS | Scanning Mobility Particle Sizer |
| TCP | Tricresyl Phosphate |
| TD | Thermal Denuder |
| TEOM | Tapered Element Oscillating Microbalance |
| UHSAS | Ultra High Sensitivity Aerosol Spectrometer |
| UNIFAC | UNIversal Functional Activity Coefficient |
| UTRC | United Technologies Research Center |
| VMD | Volume Mean Diameter of a particle size distribution |
| VOC | Volatile Organic Compound |

**Keywords**

## Acknowledgements

# 1  Abstract

## 1.1  Objectives

SERDP Project WP1625 was a multi-component effort to understand volatile contributions to particulate matter (PM) emitted from military aircraft engines.  Volatile PM, formed when condensable gases emitted in the exhaust form new particles or add coatings to emitted soot particles, is getting increasing attention due to potential environmental and health effects, and is coming under increasing regulatory control.  Military operations can be constrained if local air quality limits are exceeded. For both these environmental reasons and for the potential impact on aircraft signatures, an improved understanding is sought of volatile PM and the factors that control its formation and evolution.

## 1.2  Technical Approach

WP1625 was structured such that there was an interplay between modeling efforts and several experimental measurement efforts. The project was divided into four components, one focused on modeling and three focused on experimental explorations. Modeling work focused on the development of an advanced particle evolution model considering microphysics involving soot, sulfur, water, and condensable hydrocarbons. Experimental work included a laboratory study on soot interaction with organic species, an oil emissions field study, and a combustor sector rig study of condensation on soot. Experimental and modeling efforts were integrated, with experiments providing key parameters needed for model simulations and with model simulations aiding in the interpretation of experimental results. Each of these four components is summarized in further detail below, with a Section of the report dedicated to each.

## 1.3  Results

An existing particle evolution model, which included soot and sulfur/water microphysics, has been extended to include hydrocarbon condensable species.  This is described in detail in Section 2.  The inclusion of a wide range of HC species and their capability to condense on soot surfaces has been successfully finalized and the participation of HCs in forming new, volatile particles in concert with sulfuric acid and water has also been completed.  The proposed upgrades to the microphysical code under this SERDP effort are now complete, and the upgraded code has been applied in analyzing measurement data and planning of experiments.

The extended microphysical model was used in helping to plan a series of laboratory studies.  A key finding of the experiments carried out in the first year was the need to include a thermal denuder to remove hydrocarbons from the soot surface and make soot more representative of military aircraft engine soot.  This was achieved and subsequent laboratory studies examined several key condensable HCs in a controlled environment, interacting with the now stripped combustion generated soot particles.  The promising results from that study are described in Section 3.  The coupling between the experimental data and experiment-model evaluation has been greatly improved and is also described here.

In parallel with the lab studies, measurements were performed on operating engines to understand the role that lubrication oil has in contributing volatile HCs to the particle phase.  This work is described in Section 4.  The first measurements of their kind were performed in the program's first year on the oil breather vent of several turbofans being operated at the manufacturing facility and at an 'endurance testing facility'.  These results clearly show that

nanometer size particles are being vented from engines, and that their composition is the lube oil used in the turbofan engine lubrication system.  This work has been published in the journal *Environmental Science & Technology*.  In the second year, additional oil emissions measurements were performed on turbofans being operated in endurance testing, in which improved determination of the sample dilution by $O_2$ depletion allowed better quantification of the absolute emissions amounts. In addition, in the third year, a field study focusing on lubrication oil emissions from in-service commercial aircrafts was performed at Chicago Midway Airport (MDW) and O'Hare International Airport (ORD). Lubrication oil was identified in the organic particulate matter (PM) emissions from engine exhaust plumes. The contribution from lubrication oil to total PM organic ranges from 5% to 100%. The research paper about this study has also been accepted for publication in the journal, *Environmental Science & Technology*.

## 1.4   Benefits

The major accomplishments for the project have resulted in significant advances in understanding and in state-of-the-art-modeling tools, which will be documented in archival journal publications (Publications on oil experiments have been accepted and published, modeling work publications are currently in preparation.) A summary of findings is presented in the following table.

# Summary of Findings

| Sub-project | Results |
|---|---|
| Modeling *(Section 2)* | HC in soot coatings is strongly dependent on:<br>▪ initial hydrocarbon concentration<br>▪ mass accommodation coefficients |
| | Unary nucleation of hydrocarbon species is unfavorable<br>▪ homogeneous particle nucleation driven by binary sulfuric acid-water nucleation<br>▪ growth by condensation of hydrocarbon vapors |
| Laboratory Study on Soot Interaction with Organic Species *(Section 3)* | Uptake coefficients of a variety of VOCs by combustion soot were determined.<br>▪ Naphthalene and its derivatives<br>▪ Phenol<br>▪ Water-soluble alcohols |
| | Condensational particle growth was not observed for species with vapor pressure below saturation limit |
| | Coating growth rates were relatively insensitive to temperature (over the tested range) |
| | A correlation between uptake coefficient and aqueous solubility was established |
| | Residence time and VOC concentration controlled coating growth rate |
| | Modeling simulations capture same trends for condensational growth of dicarboxylic acids on soot as observed in lab |
| Oil Emissions Field Study *(Section 4)* | Oil from aircraft deoiling system is an important emission that is independent of combustion process. |
| | Oil contributes to semi-volatile hydrocarbon PM mass<br>▪ thermally and chemically stable<br>▪ made up of pentaerythritol esters |
| | Results published in *Environmental Science and Technology* |
| Condensation on Soot from a Combustor Sector Rig *(Section 5)* | Influence of dilution and sampling conditions on volatile and non-volatile soot composition was investigated using experimental and numerical techniques. Results revealed that:<br>▪ Dilution temperature and ratio have little impact on soot emissions measurements in mass and number, while sampling line diameter does change the measurement slightly<br>▪ Volatile composition of soot, especially sulfate, is very sensitive to dilution temperature. Cold dilution promotes condensation<br>▪ The condensation of organic species increases with higher soot loading while the sulfates are not significantly affected<br>▪ Microphysical modeling provides physical insights for understanding the observed phenomena |

# 2  Gas to Particle Microphysical Evolution Model

## 2.1  Introduction

The hydrophilicity, composition, and size of atmospheric fine particles are critical to understanding their potential environmental, climate, and health impacts. It is believed that particle hydrophilicity is important for cloud formation (Kanakidou et al., 2005) and particle chemical composition affects particle radiative forcing properties (Schwarz et al., 2008). Both particle chemical composition and size were also found to determine their health impact (Seaton et al., 1995; Pope and Dockery, 2006). Aircraft emitted particulate matter (PM) in the atmosphere generally consists of liquid coated soot particles and homogeneous liquid droplets. The volatile (liquid) components of these particles mainly consist of sulfuric acid and condensable organic species. The role of sulfuric acid in the formation and atmospheric evolution of aviation PM has been widely studied (Kärcher, 1998; Wong et al., 2008; Kärcher and Yu, 2009). However, the effects of organic emissions on aviation PM formation and evolution is less understood, even though recent field measurements suggested that they are the most dominant components at low thrust settings due to incomplete combustion (Petzold et al., 2005; Knighton et al., 2007; Yelvington et al., 2007; Onasch et al., 2009; Timko et al., 2010a; Timko et al., 2010b). Clearly, novel experimental and modeling approaches elucidating the role of organic emissions in the atmospheric evolution of hydrophilicity, composition, and size of aircraft emitted aerosols are needed to advance our understanding of the effects of aviation PM emissions on environment and human health.

Since a wide variety of organic species are emitted from aircraft engines, it is very challenging to perform experiments to systematically characterize size-resolved composition of aviation PM emissions. Existing aerosol dynamics modeling tools (Odum et al., 1997; Kulmala et al., 2004) also do not track the detailed interactions between organic vapors and solid soot particles and hydrophilicity of solid soot surfaces. This section presents the development of a detailed kinetic microphysical model that describes the detailed, multi-component interactions between organic vapors and soot particles emitted from aircraft gas turbine engines. A list of surrogate organic species was selected based on their vapor pressure values. Approaches to estimate chemical and physical properties of the particles containing mixtures of sulfuric acid, water, and these surrogate species are presented. Results for parametric sensitivity studies on ambient conditions, engine operating parameters, and engine emissions performance are discussed.

## 2.2  Model Development

The detailed microphysical model developed in this work is based on our previous approach of simulating atmospheric evolution of aircraft-emitted particles. Our previous model includes formation of new liquid droplets via homogeneous nucleation and volatile soot coatings via gaseous condensation (Wong et al., 2008; Wong and Miake-Lye, 2010; Wong et al., 2011). Microphysical processes involving organic emissions, however, were not considered. The subsequent model discussion is divided into two main sections: The first section describes our work to extend our existing knowledge of particle microphysics to incorporate condensation of organic emissions on aircraft emitted soot particles. This is followed by a discussion of updates

to modeling microphysical processes of new droplet formation via homogeneous nucleation involving organic vapors.

## 2.3  Soot Microphysics

### 2.3.1  Updates to Soot Microphysics Modeling

#### 2.3.1.1 Activation of Soot Surfaces

It is generally believed that freshly emitted soot particles from gas turbine engines are completely bare and initially hydrophobic. Activation of soot surfaces is prerequisite for subsequent vapor condensation on soot. In our model, soot surfaces are assumed to be activated by sulfuric acid or water-soluble organic species to become aqueous or by water-insoluble organic species to become non-aqueous. Water is not considered in this activation process because direct adsorption of water on hydrophobic soot surfaces is believed to be very unfavorable. In addition to gaseous adsorption on soot, activation by collisions of nucleated liquid droplets on soot surfaces is also considered. This process, termed "scavenging", is modeled with Brownian coagulation between scavenged liquid droplets and soot particles. In summary, the activation of soot particles in the $i^{th}$ size bin is described in the model by:

$$\frac{d\Theta_{aq,i}}{dt}\bigg|_{activation} = \frac{d\Theta_{aq,i}}{dt}\bigg|_{adsorption} + \frac{d\Theta_{aq,i}}{dt}\bigg|_{scavenging}$$

$$\frac{d\Theta_{non\text{-}aq,i}}{dt}\bigg|_{activation} = \frac{d\Theta_{non\text{-}aq,i}}{dt}\bigg|_{adsorption} + \frac{d\Theta_{non\text{-}aq,i}}{dt}\bigg|_{scavenging}$$

$$\frac{d\Theta_{aq,i}}{dt}\bigg|_{adsorption} = \frac{1}{4}\left[\alpha_{d,S}\bar{c}_S\left(C_S + C_{SO_3}\right) + \sum_{j=ws}\alpha_{d,O_j}\bar{c}_{O_j}C_{O_j}\right]\frac{\left(1-\Theta_{aq,i}-\Theta_{non\text{-}aq,i}\right)N_A}{\sigma_0}$$

$$\frac{d\Theta_{non\text{-}aq,i}}{dt}\bigg|_{adsorption} = \frac{1}{4}\sum_{j=ins}\alpha_{d,O_j}\bar{c}_{O_j}C_{O_j}\frac{\left(1-\Theta_{aq,i}-\Theta_{non\text{-}aq,i}\right)N_A}{\sigma_0} \qquad [2.1]$$

$$\frac{d\Theta_{aq,i}}{dt}\bigg|_{scavenging} = \frac{1}{4}\sum_k\sum_{j=a,ws}B_{ijk}n_{k,j}\left(\frac{d_{k,j}}{d_{s,i}}\right)^2\left(1-\Theta_{aq,i}-\Theta_{non\text{-}aq,i}\right)$$

$$\frac{d\Theta_{non\text{-}aq,i}}{dt}\bigg|_{scavenging} = \frac{1}{4}\sum_k\sum_{j=ins}B_{ijk}n_{k,j}\left(\frac{d_{k,j}}{d_{s,i}}\right)^2\left(1-\Theta_{aq,i}-\Theta_{non\text{-}aq,i}\right)$$

where $\Theta_{aq,i}$ and $\Theta_{non\text{-}aq,i}$ are the activated aqueous and non-aqueous fractions of a soot surface, $\alpha_{d,S}$ and $\alpha_{d,O_j}$ are the mass accommodation coefficients for the adsorption of gaseous sulfuric acid and organic species $j$ on soot (referred to as dry accommodation coefficients), which describe the sticking probabilities of vapor molecules on a bare soot surface, $\bar{c}_S$ and $\bar{c}_{O_j}$ are the mean thermal speed for the vapor phase sulfuric acid and organic species $j$, $C_S$, $C_{SO_3}$, and $C_{O_j}$ are the concentrations of the vapor phase sulfuric acid, SO$_3$, and organic species $j$, $N_A$ is the Avogadro's number, $\sigma_0$ is the number of available adsorption sites per unit surface area on soot (which was set at $5\times10^{18}$ m$^{-2}$), $B_{ijk}$ is the Brownian coagulation kernel between liquid droplets of species $j$ in the $k^{th}$ size bin (with a diameter of $d_{k,j}$) and soot particles in the $i^{th}$ size bin (with a

diameter of $d_{s,i}$), and $n_{k,j}$ is the number density of liquid droplets of species $j$ in the $k^{th}$ size bin. Note that in this equation, $j$ is the species index and '$a$', '$ws$', and '$ins$' in the summation terms stand for sulfuric acid, water-soluble, and water-insoluble organic species.

Derived from Equation 2.1, the mass of sulfuric acid ($m_{S,i}$) and organic species $j$ ($m_{Oj,i}$) on soot particles in the $i^{th}$ size bin due to activation and scavenging is calculated by:

$$\frac{dm_{S,i}}{dt} = \frac{\pi}{4}\left[ \alpha_{d,S}\bar{c}_S \left(C_S M_S + C_{SO_3} M_{SO_3}\right)\left(1-\Theta_{aq,i}-\Theta_{non-aq,i}\right)N_A d_{s,i}^2 + \right.$$

$$\left. \sum_k \sum_{j=a} B_{ijk} n_{k,j}\left(\frac{d_{k,j}}{d_{s,i}}\right)^2 \left(1-\Theta_{aq,i}-\Theta_{non-aq,i}\right)M_{S,k} \right]$$

$$\left.\frac{dm_{Oj,i}}{dt}\right|_{j=ws} = \frac{\pi}{4}\left[ \alpha_{d,O_j}\bar{c}_{O_j} C_{O_j} M_{O_j}\left(1-\Theta_{aq,i}-\Theta_{non-aq,i}\right)N_A d_{s,i}^2 + \right.$$

$$\left. \sum_k \sum_{j=ws} B_{ijk} n_{k,j}\left(\frac{d_{k,j}}{d_{s,i}}\right)^2 \left(1-\Theta_{aq,i}-\Theta_{non-aq,i}\right)M_{Oj,k} \right]$$ [2.2]

$$\left.\frac{dm_{Oj,i}}{dt}\right|_{j=ins} = \frac{\pi}{4}\left[ \alpha_{d,O_j}\bar{c}_{O_j} C_{O_j} M_{O_j}\left(1-\Theta_{aq,i}-\Theta_{non-aq,i}\right)N_A d_{s,i}^2 + \right.$$

$$\left. \sum_k \sum_{j=ws} B_{ijk} n_{k,j}\left(\frac{d_{k,j}}{d_{s,i}}\right)^2 \left(1-\Theta_{aq,i}-\Theta_{non-aq,i}\right)M_{Oj,k} \right]$$

where $M_S$, $M_{SO_3}$, and $M_{O_j}$ are the molecular weights of sulfuric acid, SO$_3$, and organic species $j$, and $M_{S,k}$ and $M_{Oj,k}$ are the molecular weights of homogeneous liquid droplets of sulfuric acid-water and organic species $j$ in the $k^{th}$ size bin, respectively.

### 2.3.1.2 Condensation Growth of Organic Vapors

In our model, condensation of volatile vapors can only occur on the activated parts of the soot surfaces. Our model also assumes that water-soluble species cannot condense on the hydrophobic part of the surface activated by water-insoluble organics, and vice versa. The total mass of sulfuric acid, water ($m_{W,i}$), and organic species $j$ on soot particles in the $i^{th}$ size bin due to condensation is calculated by:

$$\frac{dm_{S,i}}{dt} = 2\pi D_S d_{s,i} G_{S,i} \Theta_{aq,i} \left( \frac{P_S - \kappa_i a_S P_S^{sat}}{RT} \right) M_S$$

$$\frac{dm_{W,i}}{dt} = 2\pi D_W d_{s,i} G_{W,i} \Theta_{aq,i} \left( \frac{P_W - \kappa_i a_W P_W^{sat}}{RT} \right) M_W$$

$$\left. \frac{dm_{Oj,i}}{dt} \right|_{j=ws} = 2\pi D_{O_j} d_{s,i} G_{O_j,i} \Theta_{aq,i} \left( \frac{P_{O_j} - \kappa_i a_{O_j} P_{O_j}^{sat}}{RT} \right) M_{O_j}$$

$$\left. \frac{dm_{Oj,i}}{dt} \right|_{j=ins} = 2\pi D_{O_j} d_{s,i} G_{O_j,i} \Theta_{non\text{-}aq,i} \left( \frac{P_{O_j} - \kappa_i a_{O_j} P_{O_j}^{sat}}{RT} \right) M_{O_j}$$

[2.3]

where $M_W$ is the molecular weight of water, $D_S$, $D_W$, and $D_{Oj}$ are the diffusivities of the vapor phase sulfuric acid, water, and organic species $j$ in air, $P_S$, $P_W$, and $P_{Oj}$ are the vapor pressure of sulfuric acid, water, and organic species $j$, $P_S^{sat}$, $P_w^{sat}$, and $P_{O_j}^{sat}$ are the saturation vapor pressure of sulfuric acid, water, and organic species $j$, $\kappa_i$ is the Kelvin factor of the soot particles in the $i^{th}$ size bin, $a_S$, $a_W$, and $a_{Oj}$ are the activity coefficients of sulfuric acid, water, and organic species $j$ in the soot coating liquid mixtures, and $G_{S,i}$, $G_{W,i}$, and $G_{O_j,i}$ are the correction factors for condensation of each species on soot particles in the $i^{th}$ size bin, calculated by (Pruppacher and Klett, 1997; Seinfeld and Pandis, 1998):

$$G_{j,i} = \left[ \frac{1}{1 + \frac{2\lambda}{d_{s,i}}} + \frac{2\lambda}{3\alpha_{w,j} d_{s,i}} \right]^{-1}$$

[2.4]

where $\lambda$ is the molecular mean free path in air, and $\alpha_{w,j}$ is the mass accommodation coefficient for the condensation of species $j$ on soot (referred to as wet accommodation coefficients), which describes the sticking probability of a vapor molecule on the activation fraction of a soot surface.

As described in the equations above, the rate of activation of soot surfaces is proportional to the values of dry accommodation coefficients (i.e., $\alpha_{d,S}$ and $\alpha_{d,O_j}$), and the rate of condensation of volatile vapors on soot increases with larger wet accommodation coefficients (i.e., $\alpha_{w,S}$ and $\alpha_{w,O_j}$). For sulfuric acid and $SO_3$, the dry accommodation coefficient was set to 0.018 and the wet accommodation coefficient was set to unity based on our previous study (Wong et al., 2008). For surrogate organic species, values of dry and wet accommodation coefficients are not typically available in the literature. As a result, a sensitivity study of our modeling results to these coefficients was performed in this work (discussed in Section 2.3.4.4). Experimental efforts to determine the values of dry and wet accommodation coefficients for selected organic surrogate species are described in Section 3.

In our previous model treatment, the water-soluble and water-insoluble surface coverage would only increase due to surface activation and would not change because of vapor condensation on soot. This treatment may lead to unrealistic liquid layers piled up on an activated soot surface. In this present study, we revised our model treatment by assuming that the contact angle of a coated soot particle remains constant and vapor condensation on soot can

cause changes in the soot surface coverage. Using the geometry of a cap-shaped droplet on a partially activated surface, rate of change of soot surface coverage ($\Theta$) can be related to rate of change of condensation mass ($m$) on soot surfaces, as described in Equation 2.5, where a proportionality function $f(\Theta, \rho, \theta_{cont}, d_{c,i})$ containing surface coverage ($\Theta$), density of the condensed liquid ($\rho$), the contact angle ($\theta_{cont}$), and the core soot diameter ($d_{c,i}$) can be derived:

$$\left.\frac{d\Theta}{dt}\right|_{condensation} = \left.\frac{dm}{dt}\right|_{condensation} \cdot f(\Theta, \rho, \theta_{cont}, d_{c,i}) \tag{2.5}$$

The derivation of $f(\Theta, \rho, \theta_{cont}, d_{c,i})$ is outlined below.

Consider an idealized geometry of a droplet (blue) condensed on soot surface (grey) illustrated in Figure 2.1.
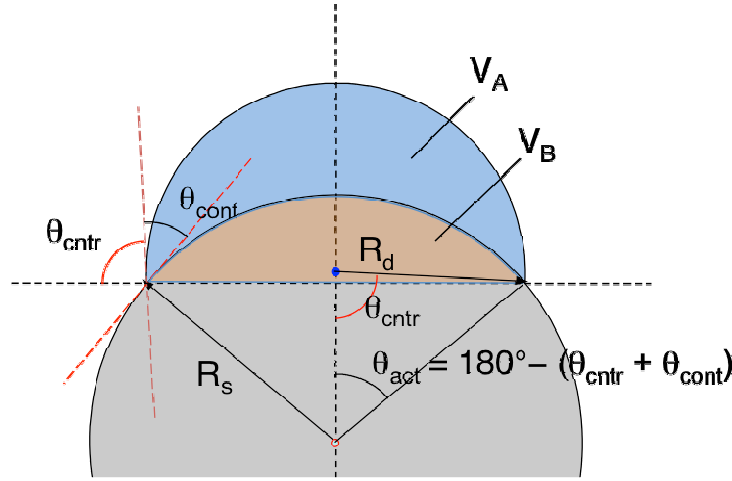


**Figure 2.1 Idealized geometry of a droplet condensed on soot surface.**

First, surface area fraction ($\Theta$) covered by a spherical cap-shaped droplet can be expressed with half of the apex angle ($\theta_{act}$) of the corresponding cone as:

$$\Theta = \frac{2\pi Rs^2(1-cos\,\theta_{act})}{4\pi Rs^2} = \frac{1-cos\,\theta_{act}}{2} \tag{2.6}$$

$$cos\,\theta_{act} = 1-2\Theta$$
$$sin\,\theta_{act} = 2(\Theta-\Theta^2)^{1/2}$$

$$\left.\frac{d\Theta}{dt}\right|_{condensation} = \left.\frac{sin\,\theta_{act}}{2}\frac{d\theta_{act}}{dt}\right|_{condensation} \tag{2.7}$$

The volume of the liquid droplet ($V_A$) can be calculated from the geometry arguments as:

$$V_A = (V_A + V_B) - V_B$$

$$= \left\{ \frac{\pi}{3} [R_d (1 + \cos\theta_{cntr})]^2 [3R_d - R_d(1 + \cos\theta_{cntr})] \right\} -$$

$$\left\{ \frac{\pi}{3} [R_s (1 - \cos\theta_{act})]^2 [3R_s - R_s(1 - \cos\theta_{act})] \right\} \qquad [2.8]$$

$$V_A = \frac{\pi}{3} R_s^{\ 3} \left\{ \left( \frac{\sin^3\theta_{act}}{\sin^3(\theta_{act} + \theta_{cont})} \right) (1 - \cos(\theta_{act} + \theta_{cont}))^2 (2 + \cos(\theta_{act} + \theta_{cont})) - \right.$$
$$\left. ((1 - \cos\theta_{act})^2 (2 + \cos\theta_{act})) \right\}$$

where $R_d$ is the radius of curvature of the liquid droplet, and $R_s$ is the radius of soot core. Combining Equation 2.8 with Equation 2.6 yields:

$$V_A = \frac{\pi}{3} R_s^{\ 3} [f_1(\Theta,\theta_{cont}) \cdot f_2(\Theta,\theta_{cont}) \cdot f_3(\Theta,\theta_{cont}) + f_4(\Theta,\theta_{cont})] \qquad [2.9]$$

where

$$f_1(\Theta,\theta_{cont}) = \frac{8(\Theta - \Theta^2)^{3/2}}{(\sin\theta_{cont} - 2\Theta\sin\theta_{cont} + 2(\Theta - \Theta^2)^{1/2}\cos\theta_{cont})^3}$$

$$f_2(\Theta,\theta_{cont}) = 1 + (1 - 2\Theta)\{(1 - 2\Theta)\cos^2\theta_{cont} - 2\cos\theta_{cont}\} +$$
$$4(\Theta - \Theta^2)^{1/2}\{(\Theta - \Theta^2)^{1/2}\sin^2\theta_{cont} + \sin\theta_{cont}\} -$$
$$4(1 - 2\Theta)(\Theta - \Theta^2)^{1/2}\sin\theta_{cont}\cos\theta_{cont}$$

$$f_3(\Theta,\theta_{cont}) = (2 + \cos\theta_{cont}) - 2\Theta\cos\theta_{cont} - 2(\Theta - \Theta^2)^{1/2}\sin\theta_{cont}$$

$$f_4(\Theta,\theta_{cont}) = 8\Theta^3 - 12\Theta^2$$

Differentiating Equation 2.9 with respect to time and rearranging the equation yields:

$$\frac{dV_A}{dt}\bigg|_{\text{condensation}} = \frac{\pi}{3} R_s^{\ 3} [f'_1 \cdot f_2 \cdot f_3 + f_1 \cdot f'_2 \cdot f_3 + f_1 \cdot f_2 \cdot f'_3 + f'_4] \cdot \frac{d\Theta}{dt}\bigg|_{\text{condensation}}$$

$$\frac{dV_A}{dt}\bigg|_{\text{condensation}} = \frac{\pi}{3} R_s^{\ 3} \cdot f_n(\Theta,\theta_{cont}) \cdot \frac{d\Theta}{dt}\bigg|_{\text{condensation}} \qquad [2.10]$$

$$\frac{d\Theta}{dt}\bigg|_{\text{condensation}} = \frac{3}{\pi R_s^{\ 3} \cdot f_n(\Theta,\theta_{cont})} \cdot \frac{dV_A}{dt}\bigg|_{\text{condensation}} = \frac{3}{\rho\pi R_s^{\ 3} \cdot f_n(\Theta,\theta_{cont})} \cdot \frac{dm}{dt}\bigg|_{\text{condensation}}$$

where $f_n(\Theta,\theta_{cont}) = f'_1 \cdot f_2 \cdot f_3 + f_1 \cdot f'_2 \cdot f_3 + f_1 \cdot f_2 \cdot f'_3 + f'_4$.

Therefore, $f(\Theta,\rho,\theta_{\text{cont}},d_{c,i})$ in Equation 2.5 can be expressed as:

$$f(\Theta,\rho,\theta_{\text{cont}},d_{c,i}) = \frac{3}{\rho\pi R_s^{\ 3} \cdot f_n(\Theta,\theta_{cont})} = \frac{24}{\rho\pi d_{c,i}^{\ 3} \cdot f_n(\Theta,\theta_{cont})} \qquad [2.11]$$

Typical contact angles of water on soot surfaces are reported in the range of 60°−80° (Persiantseva et al., 2004), and contact angle of $H_2SO_4$-$H_2O$ droplets was measured as 64±2° on regular graphite surfaces and 55±2° on OH-treated graphite surfaces (Kärcher et al., 1996). In this work, a contact angle of 60° was used for vapor condensation on aviation soot particles.

### 2.3.2 Organic Surrogate Species

Since a wide variety of organic species are emitted from aircraft gas turbine engines, it is impractical to include every single organic species emitted into our model simulations. Recent field measurements identified organic emissions as large as methylnaphthalene in the gas phase at idle (Knighton et al., 2007; Yelvington et al., 2007). Heavier, less volatile organic species that can be partitioning into the aerosol phase, however, were not easily identified due to their low concentration in the gas phase. In this work, we selected several organic surrogate species to efficiently simulate interactions of volatile organics and aircraft emitted soot particles. Our selection of organic surrogates was based on the saturation vapor pressure in the typical range of organic saturation concentrations at room temperature between 0.01 and $10^6$ $\mu$g/m$^3$. To be in line with the uniform basis set of saturation vapor pressure framework (Donahue et al., 2006; Robinson et al., 2007), we selected one water insoluble species for every two saturation concentration bins in this range, except for the most volatile bin where two species, one water soluble and one water insoluble, were selected. Surrogate species in the low volatility bins were assumed to be water insoluble because typical organic species directly emitted from aircraft engines in this volatility range are not oxygenated enough to be considered as water soluble. A list of organic surrogate species selected for our modeling work is provided in Table 2.1.

**Table 2.1 Organic surrogate species selected in this work**

| Surrogate species | Saturation vapor pressure at 300°C, C* ($\mu$g/m$^3$) | C* bin ($\mu$g/m$^3$) |
|---|---|---|
| Pentanoic acid ($C_5H_{10}O_2$) | $1.552 \times 10^6$ | $10^6$ |
| Naphthalene ($C_{10}H_8$) | $1.845 \times 10^6$ | $10^6$ |
| Anthracene ($C_{14}H_{10}$) | $1.469 \times 10^4$ | $10^4$ |
| Pyrene ($C_{16}H_{10}$) | $3.226 \times 10^2$ | $10^2$ |
| Perylene ($C_{20}H_{12}$) | $8.018 \times 10^{-1}$ | $10^0$ |
| Anthanthrene ($C_{22}H_{12}$) | $2.164 \times 10^{-2}$ | $10^{-2}$ |

### 2.3.3 Properties of Liquid Organic Mixtures

To include these organic surrogate species in our microphysical model, approaches of estimating species' physical and thermodynamical properties were implemented into the model. Boiling points and critical properties (*i.e.* critical temperature, pressure, volume, and compressibility factor) of the pure organic surrogate species are necessary for this estimation. In this work, experimentally measured boiling points and critical properties are used if they are available. The group contribution method by Nannoolal et al. (Nannoolal et al., 2004; Nannoolal

et al., 2007) was used otherwise. The density of a liquid mixture of sulfuric acid, water, and water-soluble organics or a liquid mixture of water-insoluble organics was estimated by the Rackett equation with the Li mixing rule (Poling et al., 2001). The empirical relationship developed by Brock and Bird was used to calculate surface tension of a pure organic surrogate species (Poling et al., 2001). Surface tension of a liquid soot coating was assumed to be the molar averaged surface tension of all the species in the mixture. The activity coefficients of sulfuric acid, water, and organic surrogates in a liquid mixture were estimated using the model developed by Clegg and Seinfeld (Clegg and Seinfeld, 2006), which calculates activity coefficients by dividing the liquid mixtures into three independent components (aqueous sulfuric acid solution, aqueous organic solution, and non-aqueous organic solution), with the assumption that the interactions between sulfuric acid and water-soluble organic species in the aqueous mixture are negligible. The modified UNIversal Functional Activity Coefficient (UNIFAC) group contribution model (Larsen et al., 1987) was used for calculating activity coefficients of organic species in aqueous and non-aqueous organic solutions, and the empirical relationship developed by Taleb et al. (Taleb et al., 1996) was used for calculating activity coefficients of sulfuric acid and water in an aqueous sulfuric acid solution. Finally, experimental saturation vapor pressure of an organic surrogate species expressed as the Antoine Equation was used if available. For heavier organic species without experimental saturation vapor pressure, the group contribution method developed by Nannoolal et al. (Nannoolal et al., 2008) for estimating vapor pressure of organic species was used due to its good agreements with measurement data for both water-soluble and water-insoluble organic species over a wide range of temperatures, compared to other group contribution methods (Jensen et al., 1981; Asher and Pankow, 2006; Pankow and Asher, 2008).

### 2.3.4   Results and Discussion

To apply our model to understand the growth of liquid soot coatings in aircraft exhaust plumes in the presence of organic emissions, we selected to simulate the CFM56-2C1 engine studied in the Aircraft Particle Emissions eXperiment (APEX) at idle (7%) power (Wey et al., 2007). Soot emissions at the engine exit plane were set to the measurement values during APEX, which assumes a log-normal distribution with a geometric mean diameter of 16 nm, a total concentration of $8.5 \times 10^6$ cm$^{-3}$, and a standard deviation of 1.3. A total of 8 log-normally distributed bins between 6 nm to 80 nm in diameter were used to simulate this soot particle size distribution.

In our simulations, the ambient temperature was varied in between 275 and 285 K. The ambient relative humidity was varied in between 40 and 80%. The total concentration of organic emissions at the engine exit plane was varied in between 200 and 600 ppb. To merely study soot microphysics, binary nucleation of sulfuric acid and water was not considered in the simulations. As discussed earlier, understanding of the exact amount of organic emissions and speciation distribution remains limited, and this range was set to be as the best guess according to experimental measurements (Yelvington et al., 2007). The sensitivity of soot growth to ambient temperature, ambient relative humidity levels, organic concentration at the engine exit plane, and mass accommodation coefficients used in the model was further investigated in the parametric study discussed in this section.

### 2.3.4.1 Representative Modeling Results

To examine our model performance, a microphysical simulation following an exhaust centerline plume up to 1000 m downstream of a CFM56-2C1 engine operated at idle (7%) power was performed. In this simulation, the ambient temperature was set to 280 K, and ambient relative humidity was set to 60%. Total organic emissions at the engine exit plane were set at 400 ppb, and molar fraction of each surrogate species was set to the distribution shown in Figure 2.2. The dry mass accommodation coefficients for sulfuric acid and organic species in Equations 2.1 and 2.2 were set to 0.01, and the wet mass accommodation coefficients for sulfuric acid and organic species in Equation 2.4 were set to unity.
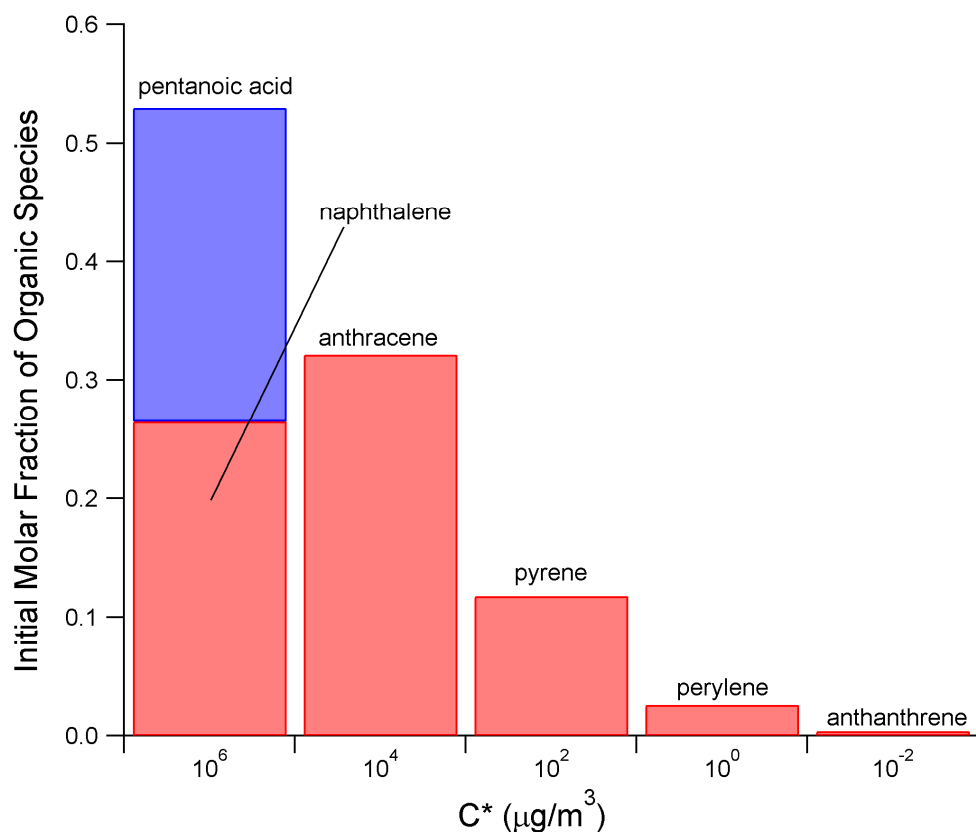


**Figure 2.2 Modeled molar fraction of organic emissions at the engine exit plane.**

Figure 2.3 shows the results from this simulation. The composition of soot coatings as a function of downstream distance from the engine is shown in Figure 2.3a in terms of mass fraction of each species. Our simulation predicted that soot coatings are organic-rich within the first 10 meters downstream of the engine. Organic species with higher initial concentrations in the more volatile vapor pressure bins are the major components. This suggests that activation of soot surfaces via adsorption of volatile vapors dominates over the vapor condensation route in this region, since the exhaust plume is still warm and most species still have not reached the saturation limit to condense. Note that although pentanoic acid, naphthalene, and anthracene are responsible for more than half of the soot coating mass in this region, total soot coating mass is still very small (Figure 2.3d). As the plume cools in the atmosphere, less volatile species, such as

sulfuric acid, perylene, and anthanthrene begin to condense on soot surfaces and become the major components in soot coatings even though their initial concentrations are lower than the more volatile species. In summary, our simulation results suggest that activation of soot surfaces, whose rates are proportional to the species' vapor phase concentrations, is more important immediately after the engine exit plane, whereas condensation of volatile vapors, whose rates are dependent on species' saturation vapor pressure, is more important further downstream. Consequently, for sampling locations of more than 10 m downstream of an engine, soot coatings are likely to consist of sulfuric acid, water and emitted organic species with low volatility (with a C* lower than 1 µg/m$^3$).

The size of emitted soot particles at the engine exit plane also has an impact on the composition of soot coatings. Figure 2.3b shows predicted hydrophilic and hydrophobic soot surface coverage at 1000 m downstream of the engine as a function of initial soot (core) sizes. As illustrated in the figure, larger soot cores result in smaller overall surface coverage (i.e., larger empty surface fractions). This can be explained by Equation 2.5, where the quantity

$\left.\dfrac{d\Theta}{dt}\right|_{condensation}$ is roughly inversely proportional to soot core diameter squared (because

$\left.\dfrac{dm}{dt}\right|_{condensation}$ is proportional to soot core diameter, as described in Equation 2.3, and

$f\left(\Theta, \theta_{cont}, d_{c,i}\right)$ is inversely proportional to soot core diameter cubed, as described in Equation 2.11). Since sulfuric acid condenses earlier than any other species due to its low volatility (Figure 2.3a), the change in surface coverage starts with the hydrophilic fraction first. As a result, larger soot cores present more available soot surfaces for water insoluble organic species to condense on, causing soot surfaces to be more hydrophobic on larger soot particles at 1000 m downstream (Figure 2.3b). This difference in soot surface coverage also causes decreased sulfuric acid mass fraction (and consequently decreased acidity) and increased organic mass fraction with increasing soot particle core size at 1000 m downstream of the engine, as depicted in Figure 2.3c.

The growth of soot coatings can be illustrated with size distributions, as shown in Figure 2.3d. As depicted in the figure, the majority of the particle growth took place in between 100 to 750 m downstream of the engine. This suggests that the exhaust plume in this region has sufficiently low temperature to facilitate condensation before plume dilution becomes more important further downstream, which favors evaporation. The final mean diameter of soot particles reached about 30 nm at 1000 m downstream. This can be viewed as an upper bound of soot growth at this condition, since binary homogeneous nucleation of sulfuric acid and water was not considered in this simulation and a fraction of the soot coating mass is supposed to be in the homogeneous nucleation mode particles if this pathway is considered.

(a)



(b)



14

(c)



(d)
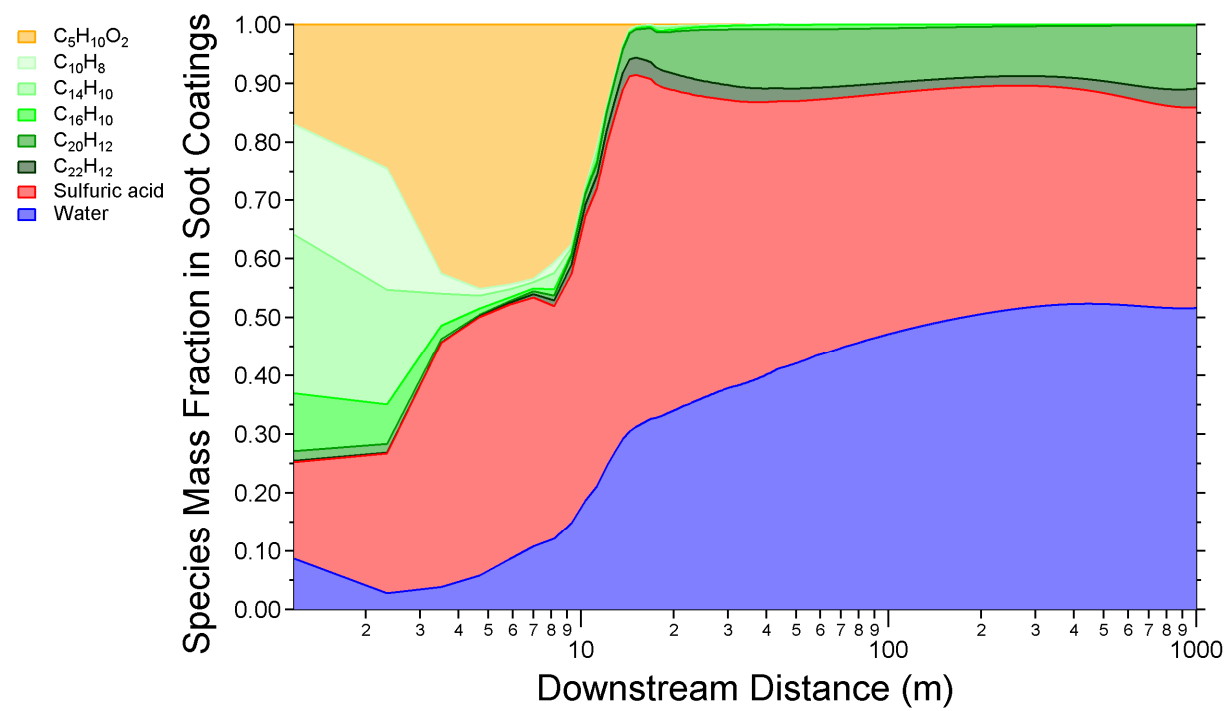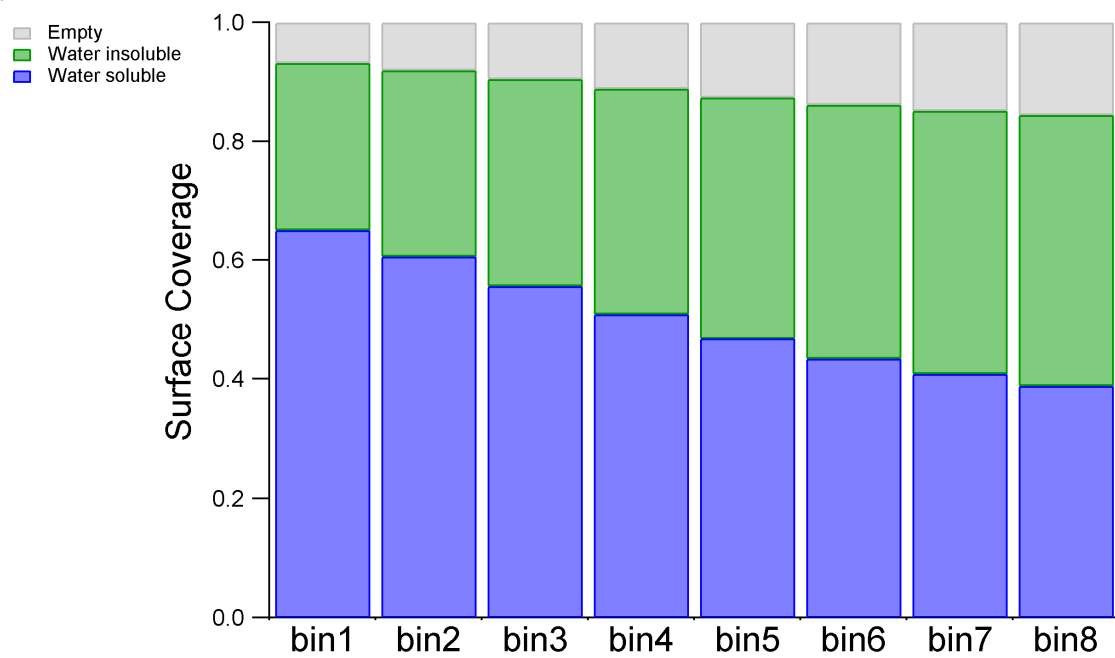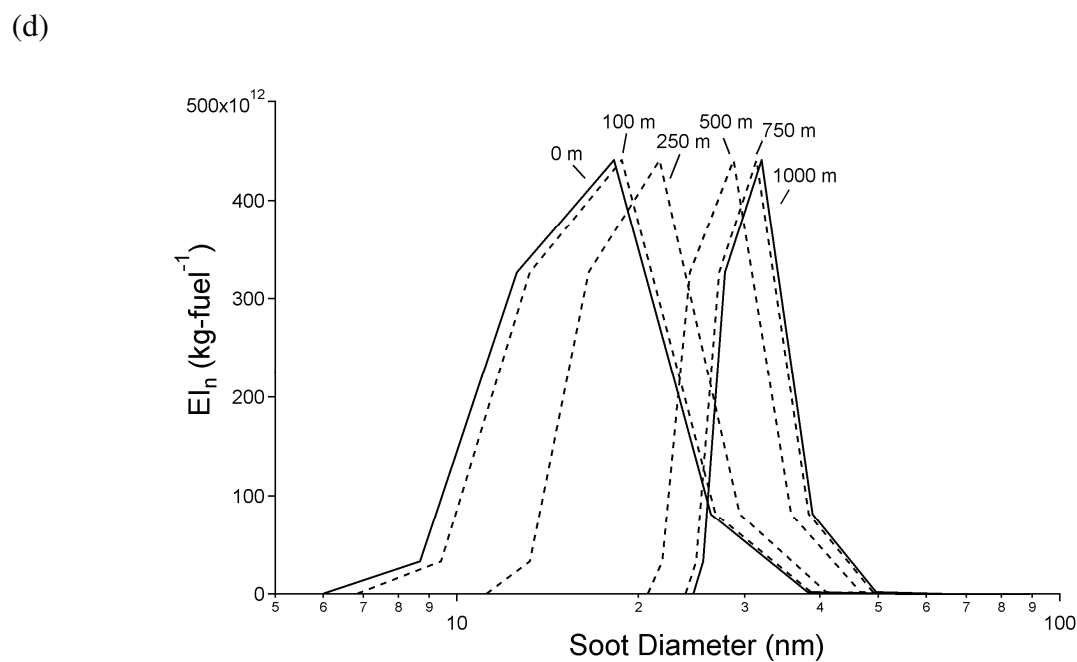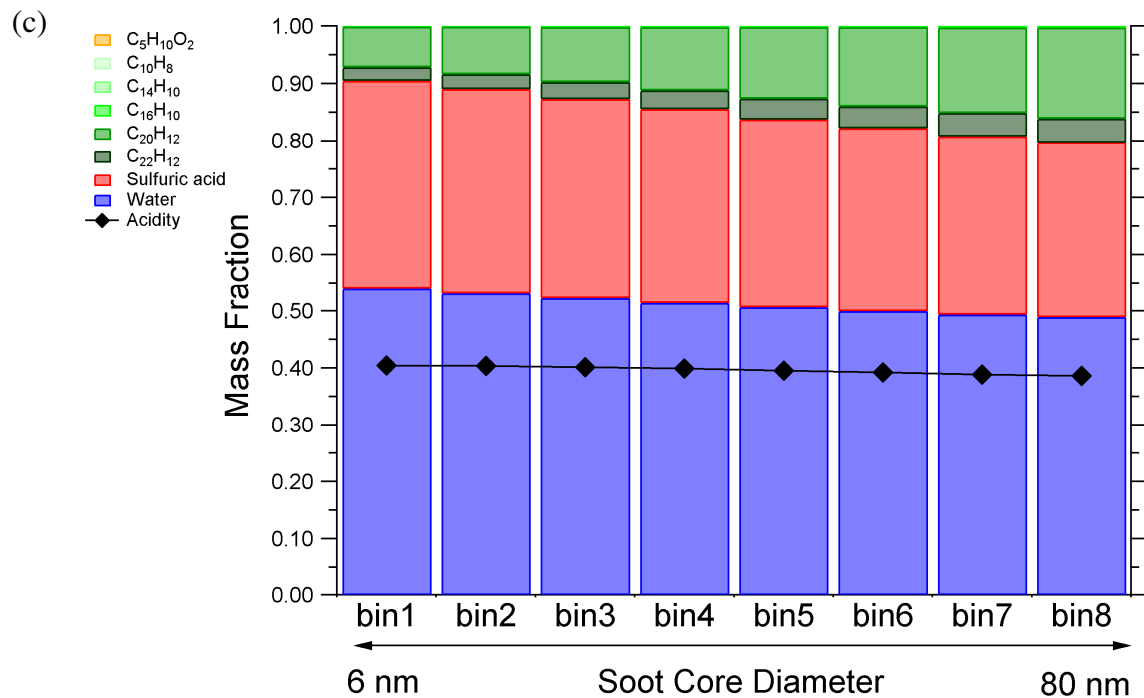


**Figure 2.3 Representative modeling results following plume centerline trajectory up to 1000 m downstream: (a) soot coating composition as a function of downstream distance; (b) size-dependent surface coverage at 1000 m downstream; (c) size-resolved composition of soot coatings at 1000 m downstream; (d) size evolution of soot particles.**

## 2.3.4.2 Effects of Ambient Conditions

Ambient temperature and relative humidity levels were found to be important in PM formation microphysics in our previous modeling work when organic species were not included

(Wong et al., 2008). To examine the sensitivity of soot microphysics to ambient conditions in the presence of organic species, several model simulations were performed using the same assumptions described in Section 2.3.4.1 but with different ambient temperature or relative humidity levels.

Our simulation results suggest that higher ambient temperature suppresses soot microphysics since smaller soot coatings and less organic mass on soot particles were predicted at 1000 m downstream of the engine, as depicted in Figure 2.4a; this effect arises from the temperature dependence of the species vapor pressures. This suppression is more marked for organic species than sulfuric acid, since organic to sulfuric acid mass ratio and organic mass fraction on soot both decrease with increasing ambient temperature, also illustrated in Figure 2.4a.

The effect of ambient relative humidity levels is more complex, as shown in Figure 2.4b. On one hand, higher relative humidity level slightly promotes the growth of soot coatings. This promotion is more marked for organic species than for sulfuric acid, since increased organic mass and organic to sulfuric acid mass ratio on soot particles were predicted at 1000 m downstream of the engine. However, organic mass fraction on soot decreases with increasing relative humidity levels. This suggests even more water condenses on the activated fraction of soot surfaces at higher ambient relative humidity levels, and most of the difference in soot particle size resulted from ambient relative humidity levels is due to condensation of ambient water vapors.

Overall, our simulations considering organic soot microphysics give the same trend that lower ambient temperature and higher ambient relative humidity would promote the formation of soot coatings. It was also observed from our runs that organic species are more sensitive to ambient conditions than sulfuric acid.
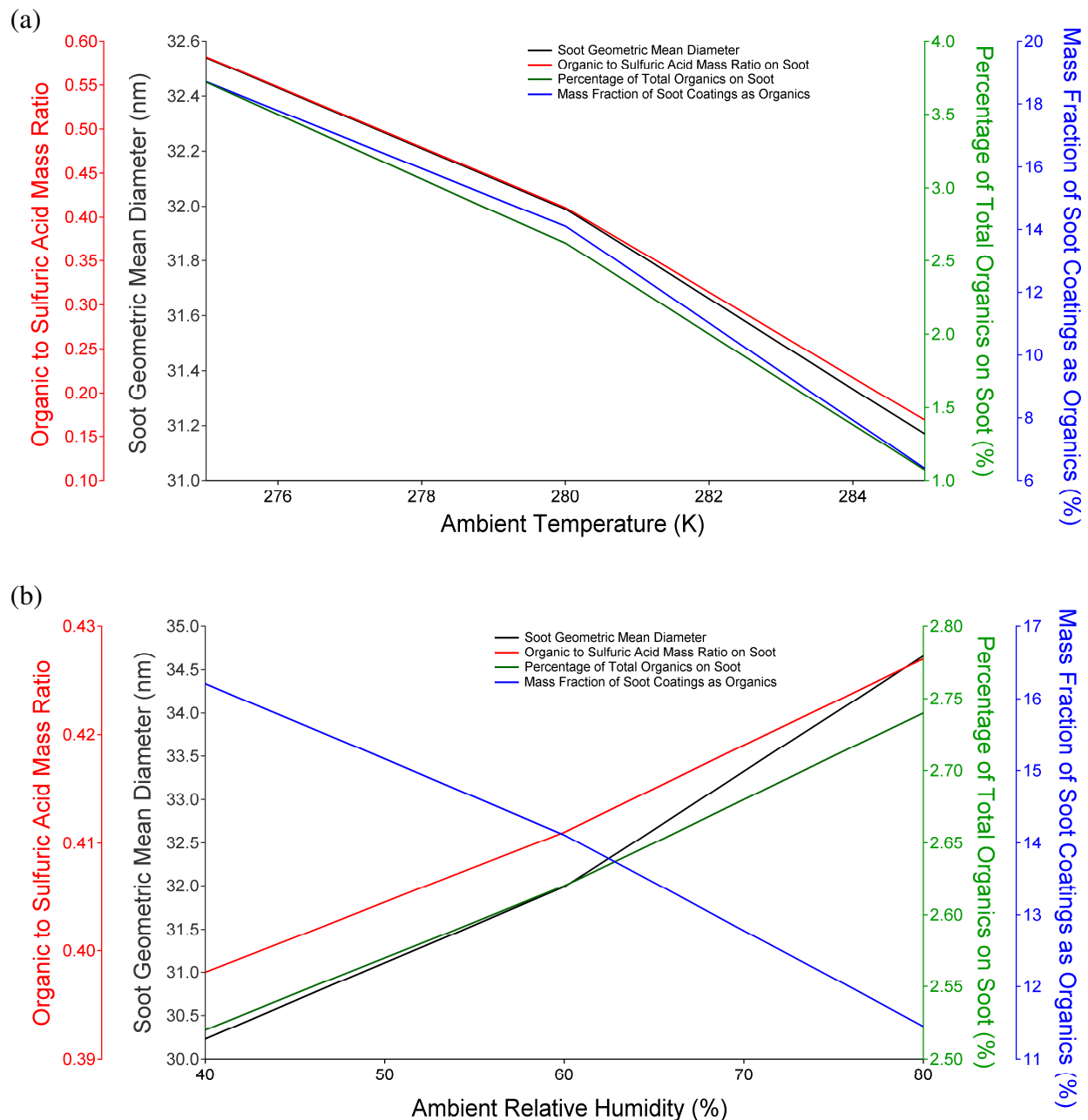
**Figure 2.4 Effect of (a) ambient temperature and (b) ambient relative humidity levels on the soot properties at 1000 m downstream of the engine.**

### 2.3.4.3 Effects of Initial Organic Concentrations

Since the exact amount of organic emissions and speciation distribution at the engine exit plane remains uncertain, a sensitivity study focusing on the effect of initial organic concentration will help determine uncertainties incurred in our simulations. Our first exercise was to vary total initial organic concentrations, between 200 to 600 ppb. As expected, higher organic emissions (i.e., higher initial organic concentration at the engine exit plane) resulted in larger soot coatings and more organic mass on soot at 1000 m downstream of the engine, as shown in Figure 2.5. The

organic to sulfuric acid mass ratio and organic mass fraction on soot also increase linearly with increasing organic emissions. Compared to Figure 2.4b, however, the increase in soot particle size at higher initial organic concentrations is mostly due to condensation of semi-volatile organic vapors, as opposed to ambient water vapors. The distribution of organic emissions at the engine exit plane may also play a role. Besides the baseline distribution we studied in Figure 2.2, we examined four additional distributions of organic emissions at the engine exit plane, as shown in Figure 2.6. Compared to the baseline case in Figure 2.2, these distributions were either more water soluble (*i.e.*, containing more pentanoic acid, Figure 2.6a), more water insoluble (containing less pentanoic acid, Figure 2.6b), more volatile (having more organics distributed in the higher C* bins, Figure 2.6c), or less volatile (having more organics distributed in the lower C* bins, Figure 2.6d). The total organic concentration, however, was set to be the same at 400 ppb for all five distributions for comparison consistency.

The predicted soot properties with different starting distributions of organic concentrations are shown in Figure 2.7. It can be clearly seen that volatility is the more critical factor affecting soot microphysics, and an initial concentration distribution with more organic molar fraction in the low volatility bins (i.e., Figure 2.6d) gives significantly thicker soot coatings (Figure 2.6a) and more condensed organic mass (Figure 2.7b). The composition of soot coatings at 1000 m downstream is also more organic rich, where the organic to sulfuric acid mass ratio in the coatings is about 1.5 (Figure 2.7c) and the mass fraction of soot coatings as organics exceeds 35% (Figure 2.7d). On the other hand, the effect of water solubility of the organic emissions at the engine exit plane is very minor. Our simulation results in Figure 2.7 suggest that higher fraction of water insoluble organics in the first C* bin (i.e., Figure 2.6b) only slightly promotes organic condensation on soot (Figure 2.7b, Figure 2.7c, and Figure 2.7d), whereas the final soot particle size at 1000 m downstream remains similar for the three cases with varied water solubility (Figure 2.7a). In summary, our parametric study on initial organic concentration suggests that the amount of organics in the low volatility bins, with a C* value lower than 1 $\mu g/m^3$, is the most determining factor affecting soot mode PM growth in near-field aircraft plumes.
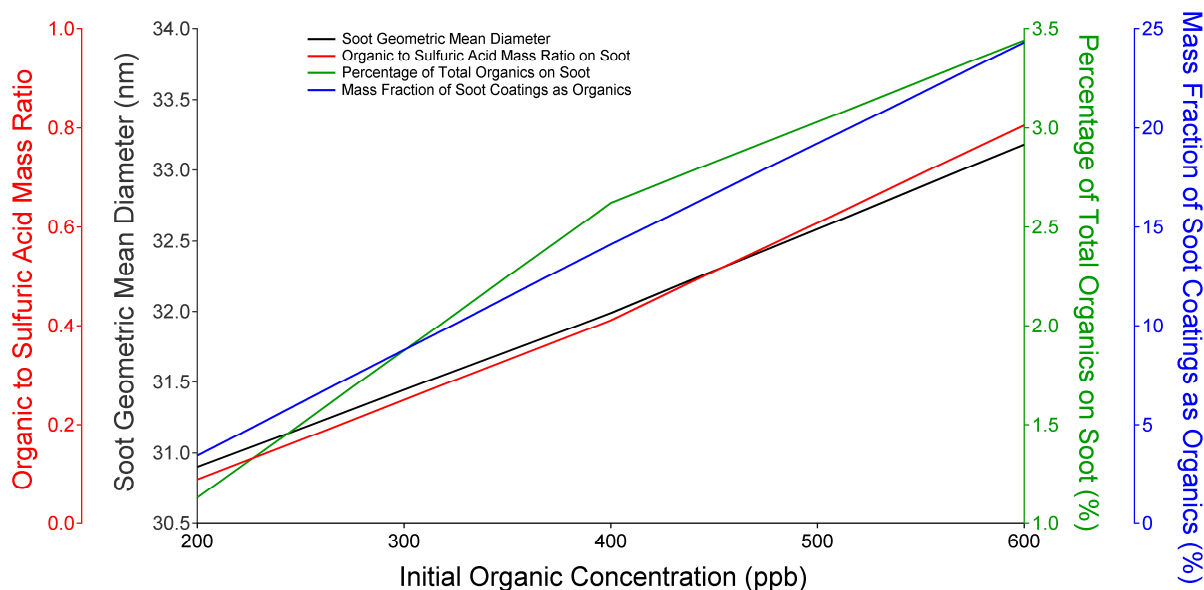


**Figure 2.5 Effect of initial organic concentration in the vapor phase on the soot properties at 1000 m downstream of the engine.**
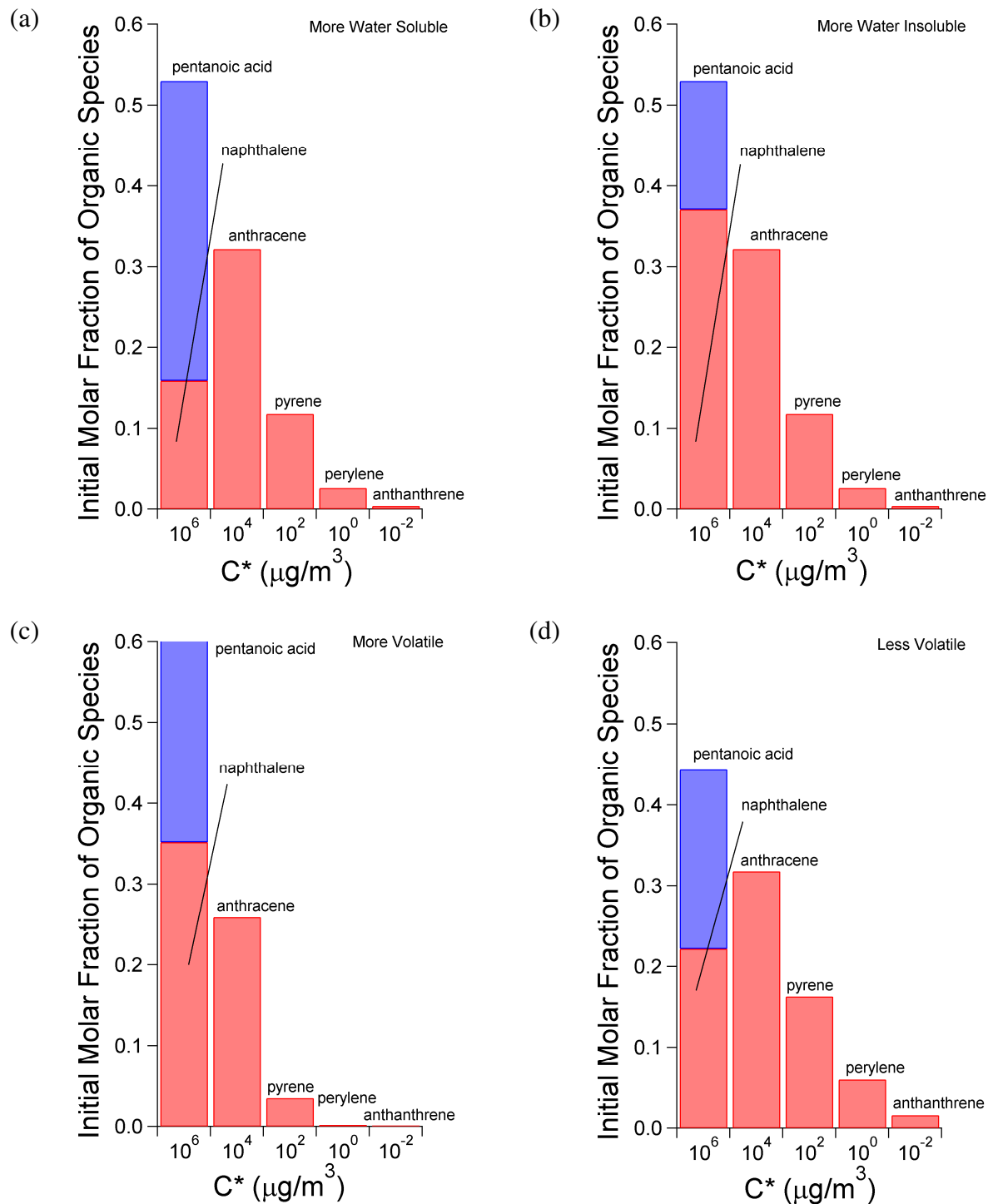
**Figure 2.6 Additional distributions of organic concentrations at the engine exit plane selected for our parametric study for the effect of initial organic concentration.**

(a)

(b)

(c)

(d)
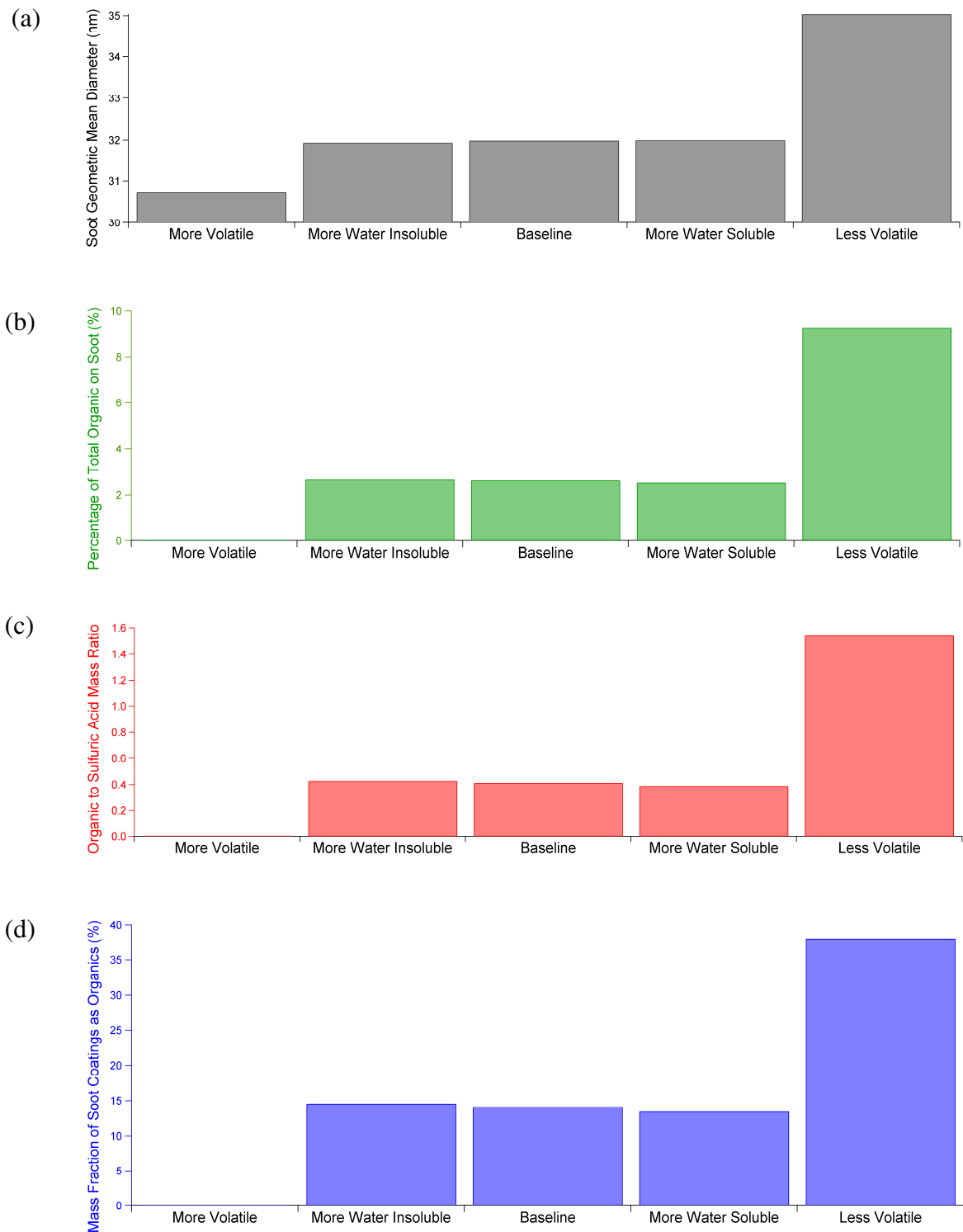
**Figure 2.7 Effect of organic distribution at the engine exit plane on the soot properties at 1000 m downstream of the engine.**

**2.3.4.4 Effects of Mass Accommodation Coefficients**

        Mass accommodation coefficients used in our model play a critical role in determining rates of interactions between organic species and soot surfaces. Estimating the values of mass accommodation coefficients for the surrogate organic species, however, is a very challenging task since only limited information is available in the literature. Our model simulations used certain default values for mass accommodation coefficients, reflecting our best guesses based on literature data. To examine the sensitivity of our assumptions, a parametric study on the effect of mass accommodation coefficients was performed.

        Two different types of mass accommodation coefficients exist in our model formulation: "dry" mass accommodation coefficient that is responsible for the surface activation process (Equations 2.1 and 2.2), and "wet" mass accommodation coefficient that is responsible for the volatile vapor condensation process (Equations 2.3 and 2.4). Each mass accommodation coefficient type can also be applied to either water soluble or water insoluble organic species, making a total of four variations. In our parametric study, mass accommodation coefficients of different species with the same type was set to the same value and varied within a reasonable range to understand their potential effects.

        Figure 2.8 and Figure 2.9 depict predicted soot properties at 1000 m downstream of the engine when different values of mass accommodation coefficients were used in the model. As discussed earlier, the activation of soot surfaces by vapor molecules is directly affected by dry mass accommodation coefficients. Larger dry mass accommodation coefficients would result in more activated soot surfaces, allowing further vapor condensation. This explains why thicker soot coatings were predicted from our model when dry mass accommodation coefficients for both water soluble and water insoluble organic species were increased, as shown in Figure 2.8. The effect of dry accommodation coefficients on soot compositions, however, is different between water soluble and water insoluble organic species. Increased dry mass accommodation coefficients for water soluble species promotes more water soluble vapors, including sulfuric acid and water itself, to condense on soot surfaces, resulting decreases in organic to sulfuric acid mass ratio on soot, percentage of total organic on soot, and mass fraction of soot coatings as organics at 1000 m downstream of the engine (Figure 2.8a). For water insoluble organic species, increased dry accommodation coefficients causes an opposite effect, since condensation of water insoluble organic species is in turn promoted. This promotion, as shown in Figure 2.8b, appears to be most rapid in the region where dry mass accommodation coefficients are less than 0.1, and variation of dry mass accommodation coefficients for water insoluble organic species above this value will not have significant impact on soot properties at 1000 m downstream of the engine.

        Since our model only considers water soluble organic species in the most volatile bin (with a C* value of $10^6$ μg/m$^3$), condensation of water soluble organic species is negligible in our model simulations. The effect of wet mass accommodation coefficients for water soluble organic species is therefore insignificant, as illustrated in Figure 2.8a. For water insoluble organic species, increased wet mass accommodation coefficients increases the condensation rates of organic vapors on soot surfaces. This results in thicker and more organic-rich soot coatings, as depicted in Figure 2.9b.

        In summary, our parametric study on mass accommodation coefficients suggests that increased dry mass accommodation coefficients for both water soluble and water insoluble organic species promotes growth of soot coatings. Larger dry mass accommodation coefficients for water soluble organic species favors condensation of other water soluble species, such as sulfuric acid and water itself, whereas larger dry mass accommodation coefficients for water

insoluble organic species favors condensation of water insoluble organic species and coatings to be more organic-rich. For wet mass accommodation coefficients, no significant effect was predicted for water soluble organic species since they are too volatile to condense. For water insoluble species, increased wet mass accommodation coefficients promotes condensation and increases soot coating size and organic mass on soot. Our calculation results were more sensitive to dry and wet mass accommodation coefficients for water insoluble organic species compared to those for water soluble organic species.
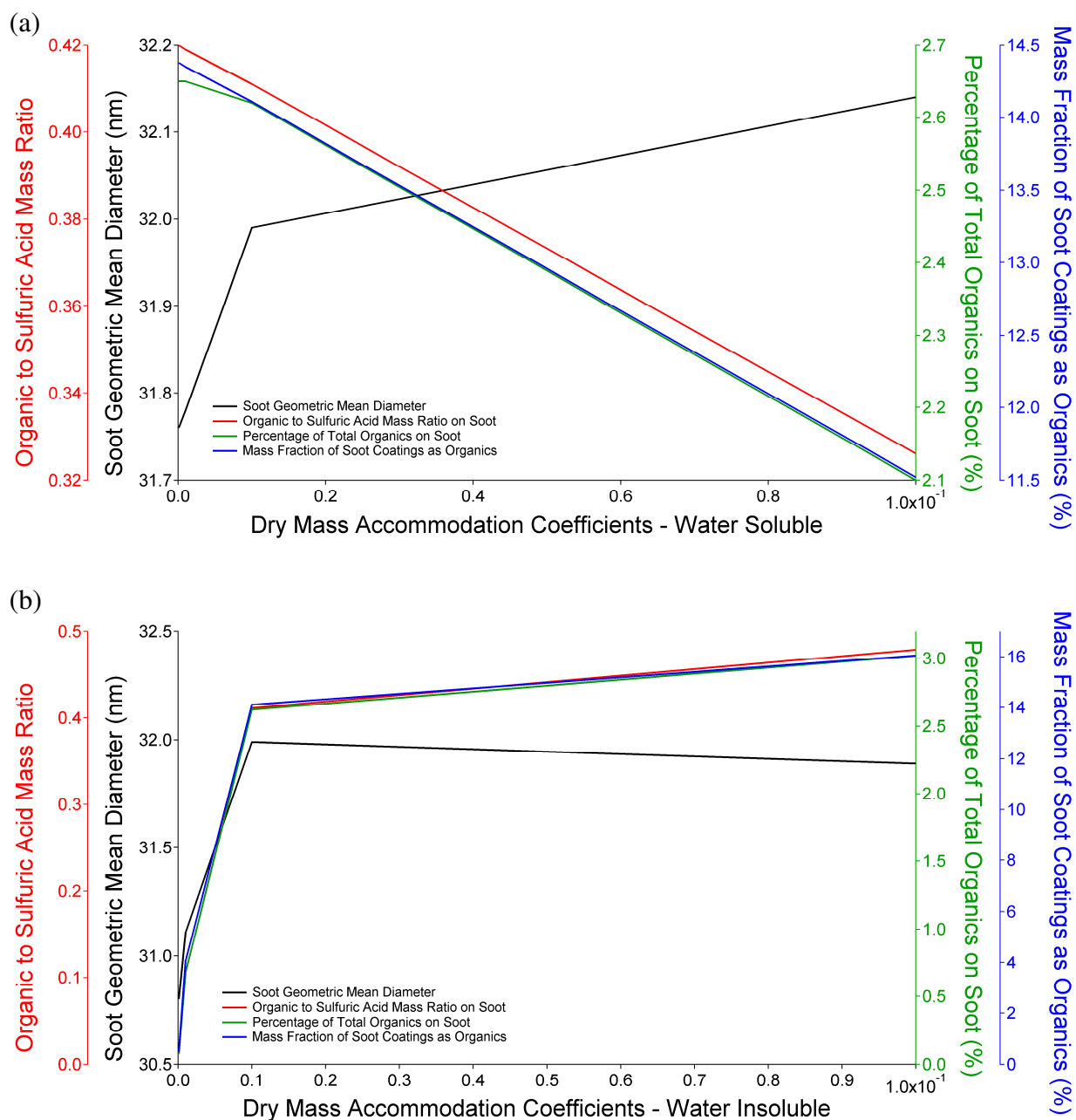


**Figure 2.8 Effect of dry mass accommodation coefficients for (a) water soluble organic species and (b) water insoluble organic species on the soot properties at 1000 m downstream of the engine.**
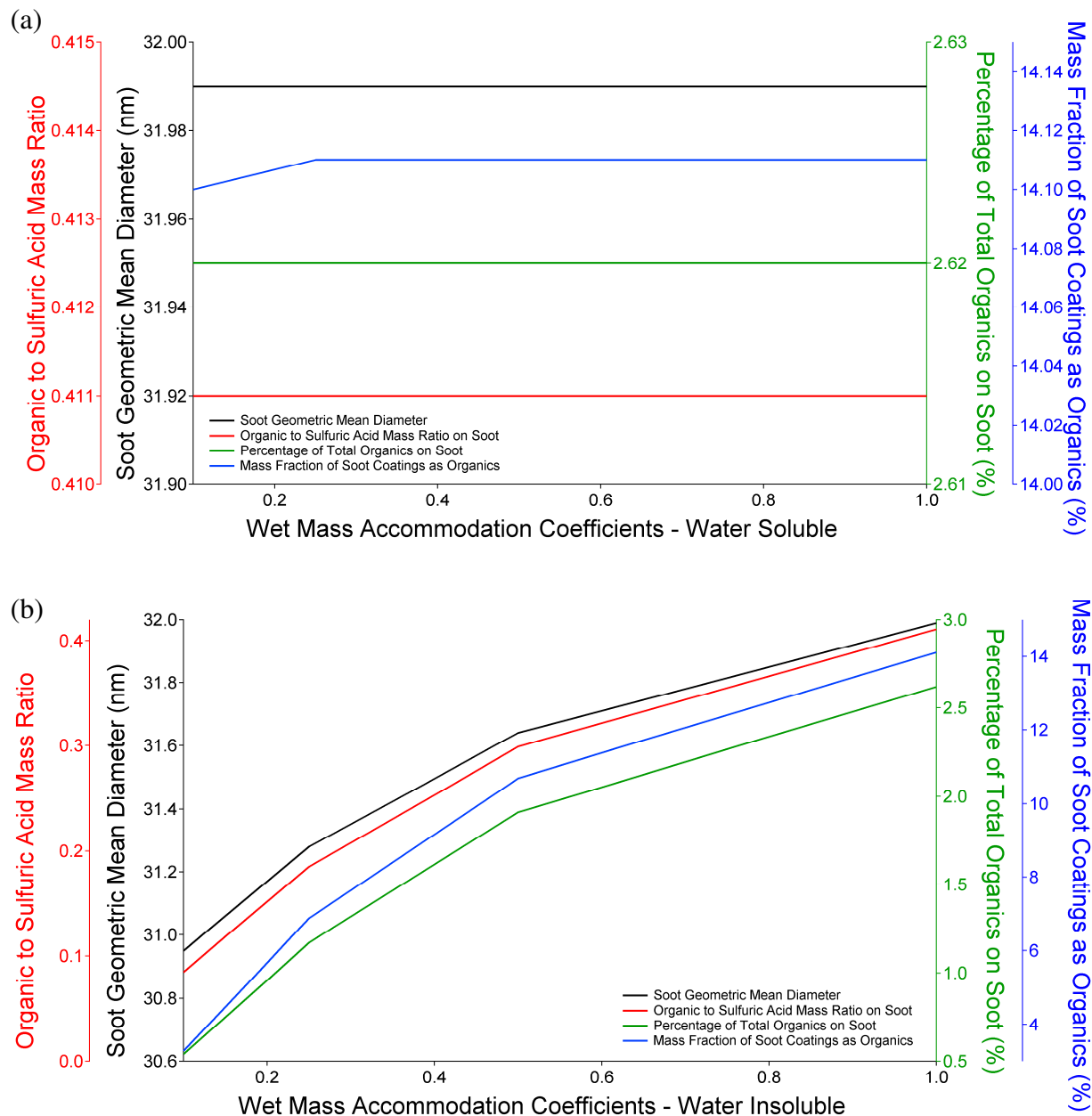
**Figure 2.9 Effect of wet mass accommodation coefficients for (a) water soluble organic species and (b) water insoluble organic species on the soot properties at 1000 m downstream of the engine.**

### 2.3.5   Summary

A detailed microphysical model previously developed to study PM evolution in near-field aircraft emitted plumes was extended to study soot microphysics in the presence of organic emissions. Our new formulation considers the activation and condensation processes of organic species, and several organic surrogate species mimicking organic emissions from modern gas turbine engines were selected for our modeling study. Methodologies were also developed for

estimating chemical and physical properties of the aerosols containing complex mixtures of sulfuric acid, water, and various organic molecules. A parametric study on ambient conditions, organic emissions levels, and mass accommodation coefficient values was also performed to understand critical factors in volatile PM evolution in near-field aircraft emitted plumes. Our simulation results suggest the following key findings:

- Activation of soot surfaces is more important immediately after the engine exit plane, whereas condensation of volatile vapors is more important further downstream. For sampling locations of more than 10 m downstream of an engine, soot coatings are likely to consist of sulfuric acid, water and emitted organic species with low volatility.
- Sizes of soot cores have an effect on soot coating composition, and coatings on larger soot cores are more organic-rich with larger hydrophobic (water insoluble) surface coverage even though the overall fractional surface coverage (hydrophilic plus hydrophobic) is smaller.
- At the conditions considered, the majority of soot coating growth takes place 100 to 750 meters downstream of the engine.
- Higher ambient temperature suppresses soot microphysics, and this suppression is more marked for organic species than sulfuric acid.
- Higher ambient relative humidity promotes the growth of soot coatings, increasing the amount of emitted organic and ambient water condensation on soot particles.
- For the effect of initial organic concentrations at the engine exit plane, our simulations suggest that the amount of organic emissions with a C* value lower than 1 $\mu g/m^3$ is most critical to soot mode PM growth in near-field aircraft plumes.
- For the effect of mass accommodation coefficients, our simulations suggest that increased dry mass accommodation coefficients for both water soluble and water insoluble organic species promote growth of soot coatings. For wet mass accommodation coefficients, no significant effect was predicted for water soluble organic species, whereas increased wet mass accommodation coefficients for water insoluble organic species promotes condensation that increases soot coating size and organic mass on soot.

## 2.4   Liquid Particle Microphysics

### 2.4.1   Introduction

Previously, aerosol growth by activation and condensation was discussed, focusing on interaction with solid particles directly emitted from aircraft engine. There are also microphysical processes forming new liquid particles from gas, such as nucleation and coagulation.

Nucleation processes are classified with the following four types in general (Seinfeld and Padnis, 2006):

- Homogeneous-homomolecular: nucleation of one species without foreign nuclei.

- Homogeneous-heteromolecular: nucleation of more than one species without foreign nuclei.

- Heterogeneous-homomolecular: nucleation of one species on foreign surfaces.

- Heterogeneous-heteromolecular: nucleation of more than one species on foreign surfaces.

While this identification of nucleation types includes heterogeneous nucleation processes, this work focuses on the homogeneous nucleation.

Water is very unlikely to form nuclei by itself at typical ambient conditions or even at supersaturated condition. However, the existence of sulfuric acid can induce aqueous binary nucleation at a subsaturated conditions experienced in an exhaust plume. However, the presence of sulfuric acid can induce aqueous binary nucleation at even a subsaturated condition. Binary nucleation can occur if species are supersaturated with respect to their solution in a liquid droplet, even when both components are subsaturated with respect to their pure gas phase. If the nucleated clusters exceed their critical cluster size, the clusters are likely to grow to larger droplets due to larger growth rate. At the critical cluster the net nucleation rate becomes zero as evaporation rate and growth rate are equal. If clusters are smaller than the critical cluster, on the other hand, the clusters are prone to evaporate and decay.

Binary $H_2SO_4$-$H_2O$ nucleation is an important source forming liquid aerosols in aircraft plumes. A binary $H_2SO_4$-$H_2O$ nucleation model has been widely studied and enhanced for better predictions and modified to capture additional features in atmospheric nucleation (Kulmala *et al*., 2000, Seinfeld and Pandis, 2006, and Yu and Turco, 2001). A potential role of organic compounds in nucleation has also been studied (Kanakidou *et al*., 2005 and Zhang *et al*., 2004). However, incorporating more than one hydrocarbon species into a nucleation model is not a straightforward task since handling more than two components with the classical nucleation theory would be very time-consuming and impose a heavy computational burden. For example, finding minimum free energy configurations and tracking all possible combinations of cluster configurations will be very challenging as the number of species considered in the nucleation process at the same time is increased. Therefore, it will be more practical to apply a simplified model with adequate assumptions applicable to the system being considered (for example, aircraft plume conditions in fast equilibrium with water vapor). The following sections discuss several nucleation models which can be easily extended to a multi-component model.

### 2.4.2   Review of Nucleation Models

### 2.4.2.1 Quasi-unary nucleation model

The binary homogeneous nucleation of $H_2SO_4$-$H_2O$ can be simplified as a kinetic model simulating quasi-unary nucleation (QUN) of $H_2SO_4$ in equilibrium with water vapor in atmospheric conditions due to the presence of much higher concentration of water vapor (Yu 2005, Yu 2007). In these conditions, binary $H_2SO_4$-$H_2O$ clusters are controlled by collision or evaporation of $H_2SO_4$ molecules, and the amount of water vapor in the cluster reaches equilibrium very quickly due to excess available water vapor. The QUN model can be simulated kinetically with the mass balance equations in Equation 2.12:

$$\frac{dn_1}{dt} = 2\gamma_2 n_2 + \sum_{i=3}^{m} \gamma_i n_i - \sum_{1}^{m-1} \beta_i n_i \qquad (i=1)$$

$$\frac{dn_2}{dt} = \frac{1}{2}\beta_1 n_1 - \gamma_2 n_2 - \beta_2 n_2 + \gamma_3 n_3 \qquad (i=2) \qquad [2.12]$$

$$\frac{dn_i}{dt} = \beta_{i-1} n_{i-1} - \gamma_i n_i - \beta_i n_i + \gamma_{i+1} n_{i+1} \qquad (i>2)$$

The growth rate coefficient $\beta_i$, and the evaporation rate coefficient $\gamma_i$ are given with the kinetic theory of gases for collisions between $H_2SO_4$ monomers and $H_2SO_4$-$H_2O$ clusters,

$$\beta_i = \left(\frac{8\pi kT(m_1 + m_i)}{m_1 m_i}\right)^{1/2} (r_1 + r_i)^2 n_1$$

$$\gamma_i = \left(\frac{8\pi kT(m_1 + m_i)}{m_1 m_i}\right)^{1/2} (r_1 + r_i)^2 n_{a,sol}^{\infty} \exp\left(\frac{2M_a \sigma}{\rho_i RT r_i}\right)$$

[2.13]

where $m_1$ and $r_1$ are the mass and radius of $H_2SO_4$-$H_2O$ monomers, $m_i$ and $r_i$ are the mass and radius of $i$-mers, $n_1$ is the concentration of monomers, and $n_{a,sol}^{\infty}$ is the concentration of $H_2SO_4$ vapor above a flat surface of a solution having the same composition as the $i$-mers, $M_a$ is the molecular mass of $H_2SO_4$, $\sigma$ is the surface tension of the binary solution, $\rho_i$ is the density of $i$-mers, $R$ is the ideal gas constant, and $k$ is the Boltzmann constant. The kinetic QUN model shows better estimation than the classical binary nucleation model based on comparisons with experimental data. Additionally, the QUN model is applicable for conditions such as diluting engine exhaust where properties of gases change rapidly.

### 2.4.2.2 Multi-component nucleation models

There have been several studies that have used simplified nucleation models for a multi-component system. Some of them can be applicable with the QUN model for binary homogeneous nucleation of $H_2SO_4$-$H_2O$. Du and Yu (2009) developed a ternary nucleation model that extended binary $H_2SO_4$-$H_2O$ equations. An unknown third species participates in the ternary nucleation equations by reducing the Gibbs free energy from that of binary $H_2SO_4$-$H_2O$ nucleation. Like the binary nucleation case, sulfuric acid controls the growth and evaporation rate of clusters by colliding with and evaporating from clusters and water influences the composition of the clusters and the evaporation coefficient of sulfuric acid clusters. Du and Yu assumed that the third species plays a similar role as water. The reduction of Gibbs free energy by the third species decreases evaporation coefficients of binary clusters and increases stability as a result. The change in Gibbs free energy was expressed as a function of the number of molecules of the third species and empirical parameters by assuming the Gibbs free energy difference between binary and ternary nucleation increases with decreasing cluster size and diminishes to zero with sufficiently large clusters as:

$$\gamma_i = \beta_{i-1} \exp\left(\frac{\Delta G_{i-1,i}}{kT}\right)$$

$$\Delta G_{i-1,i}^{ternary} = \Delta G_{i-1,i}^{binary} - dG(i)$$

[2.14]

$$dG(i) = a + \frac{b}{i^c}$$

where $\gamma_i$ is the evaporation rate of $i$-mers, $\beta_{i-1}$ is the collision rate of $(i-1)$-mers to grow to $i$-mers, $\Delta G_{i-1,i}$ is the Gibbs free energy associated with $(i-1)$-mers and $i$-mers, and $a$, $b$, and $c$ are empirical parameters.

Gorbunov (2001) suggested that in the embryos formed from multi-component nucleation, two main species will be dominant in concentration with the remining species being insignificant. They modeled the multi-component nucleation with two separate steps extended from binary nucleation: 1) the binary nucleation process with two dominant species, and 2) the

26

subsequent transformation process of minor species. The Gibbs free energy of the embryo formation can be calculated with the sum of the Gibbs free energy for the corresponding steps:

$$\Delta G\left(N_w, N_{sa}, N_1, N_2, ..., N_{N-2}\right) = \Delta G\left(N_w, N_{sa}\right) + \Delta G\left(N_1, N_2, \cdots, N_{N-2}\right)$$

$$= \Delta G_{binary} - RT\sum_{i=1}^{N-2}\left[\ln\left(\frac{P_i}{k_i X_i}\right) + 1\right]N_i + \sigma_{e2}\sum_{i=1}^{N-2}\Delta S_i \qquad [2.15]$$

where $N_w$ is moles of water and $N_{sa}$ is moles of sulfuric acid transferred from gas phase to embryo. $P_i$ is the partial pressure of species $i$, $K_i$ is the Henry's law constant, $v_i$ is the molar volume of species $i$, $r_e$ is the radius of the embryo, $\sigma_{e2}$ is the interfacial free energy for the embryo formation in the second step, and $\Delta S_i$ is the change of the embryo surface area due to transfer molecules at the second step.

The composition of minor species forming diluted solution in sulfuric acid and water solution is calculated thermodynamically using Henry's law with respect to the composition of binary major species:

$$N_i = \left(N_w + N_{sa}\right)\frac{P_i}{K_i}\exp\left(-2\frac{\sigma_e v_i}{RTr_e}\right) \qquad [2.16]$$

where radius of embryo, $r_i$, can be replaced with the radius of embryo in the first step:

$$r_{e1} = \left(\frac{3m_{e1}}{4\pi\rho_{e2}}\right)^{1/3} \qquad [2.17]$$

With known mole fraction of all species, coefficients for growth rate and evaporation rate can be calculated as:

$$\beta_{e1} = \left[\frac{8\pi k_B T\left(m_1 + m_{e1}\right)}{m_1 m_{e1}}\right]^{1/2}\left(r_1 + r_{e1}\right)^2 n_1 \qquad [2.18]$$

$$r_{e2} = \left(\frac{3m_{e2}}{4\pi\rho_{e2}}\right)^{1/3}$$

$$\beta_{e2} = \left[\frac{8\pi k_B T\left(m_1 + m_{e2}\right)}{m_1 m_{e2}}\right]^{1/2}\left(r_1 + r_{e2}\right)^2 n_1 \qquad [2.19]$$

$$\gamma_{e2} = \beta_{e2}\frac{n_{a,sol}^\infty}{n_1}\exp\left(\frac{2M_a\sigma_{e2}}{\rho_{e2}k_B Tr_{e2}}\right)$$

where $\sigma_{e2}$ is the interfacial free energy for the embryo formation in the second step but can be replaced with that in the first step since it can be assumed that it depends only on concentration of the dominant species.

Du and Yu's parametric model is applicable to a kinetic nucleation model simply with one additional step, but it is not useful when the values of the empirical parameters are not available. While Gorbunov's approach is more general and applicable to systems with more than three species, it is only applicable to a system controlled by two major species and limited to the equilibrium calculation of other insignificant species. In this work, Gorbunov's approach was used to test multi-component nucleation among one of possible nucleation pathways for hydrocarbons in a sulfuric acid and water system.

### 2.4.3   Microphysical Model for Hydrocarbon in Nucleation Process

This section provides the modeling approach of hydrocarbon nucleation applicable according to their solubility. Nucleation of water-insoluble hydrocarbons was modeled independently from $H_2SO_4$-$H_2O$ nucleation because water-insoluble hydrocarbons are not expected to participate in forming aqueous clusters via a nucleation process. Nucleation of water-soluble hydrocarbons was examined among possible pathways, including multi-component nucleation extended from binary sulfuric acid-water nucleation, binary hydrocarbon and water nucleation as well as separate unary nucleation. Clusters formed via nucleation can subsequently grow to larger particles via coagulation with other aqueous clusters or hydrocarbon clusters. Coagulation is described in Section 2.4.4 in detail.

### 2.4.3.1 Nucleation of water-insoluble hydrocarbons

In this work, it was assumed that water-insoluble hydrocarbons have no direct effect on the nucleation of aqueous clusters. Therefore, sulfuric acid and water participate in the nucleation process the same way as the previously-implemented binary nucleation case, regardless of presence of water-insoluble hydrocarbons. Water-insoluble hydrocarbons are assumed to be involved in the new particle formation via homogeneous nucleation of separate water-insoluble clusters from aqueous nuclei. Water-insoluble hydrocarbon clusters are allowed to contribute to the growth of aqueous embryos or droplets by coagulation afterward.

In contrast to the aqueous cluster formation process, in which clusters grow by gaining or losing hydrated sulfuric acid monomers ($H_2SO_4$-$(H_2O)_n$ would form with abundant water molecules), water-insoluble hydrocarbon molecules nucleate by collisions with molecules of its own kind or other hydrocarbon species. In this work, rather than considering multi-component nucleation of hydrocarbon species, nucleation of water-insoluble hydrocarbons was modeled as unary nucleation.  This approach, while not strictly reflecting reality, is a reasonable way of modeling water-insoluble hydrocarbon nucleation in aircraft emissions. This is because nucleation of hydrocarbons is not a favorable pathway to grow to critical clusters compared to binary nucleation of sulfuric acid and water. $H_2SO_4$-$H_2O$ aerosols are most abundant in aircraft plume, and thus, tracking coagulation between hydrocarbon clusters may not be critical because these collisions are rare compared to those between hydrocarbon clusters and $H_2SO_4$-$H_2O$ clusters under the conditions of our interest.
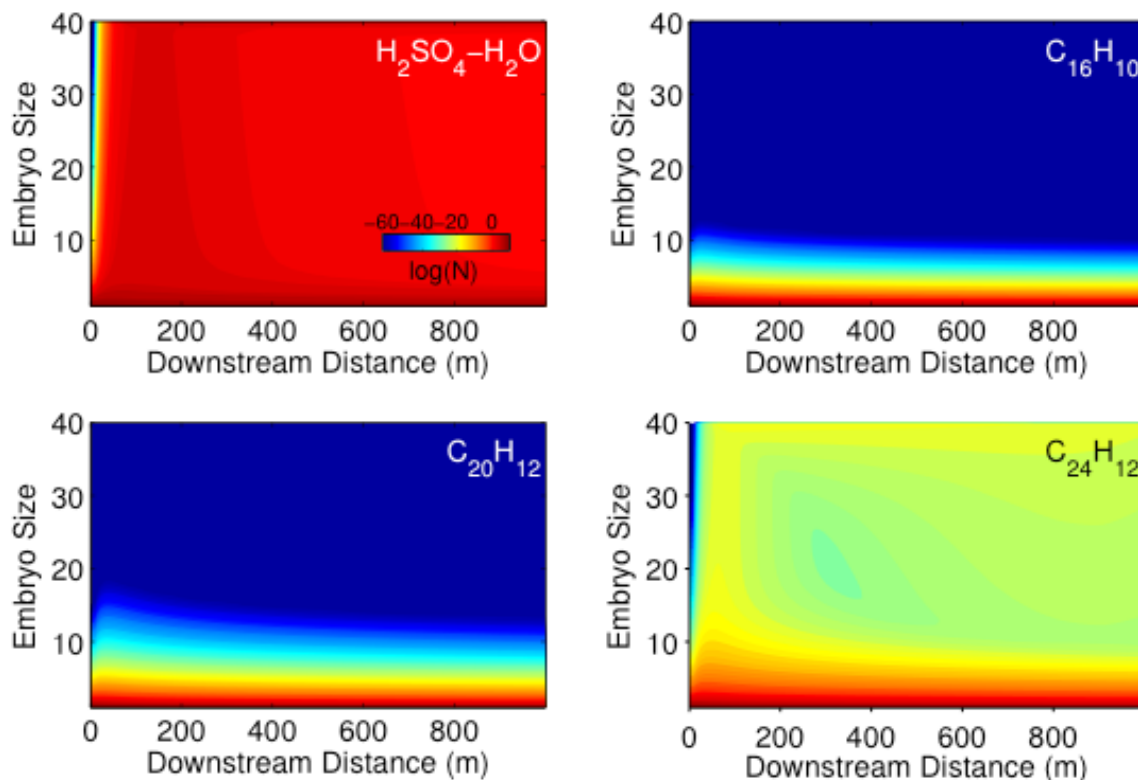
**Figure 2.10 Concentrations for binary H₂SO₄-H₂O embryos and unary water-insoluble hydrocarbon embryos**

Concentrations of water-insoluble hydrocarbon embryos and $H_2SO_4$-$H_2O$ embryos are compared in Figure 2.10. While $H_2SO_4$-$H_2O$ embryos tend to grow and form larger homogeneous droplets, water-insoluble hydrocarbons remain in the gas phase or form low concentrations of oligomers smaller than the critical cluster size via unary nucleation. We thus conclude that under the conditions of aviation emissions, $H_2SO_4$-$H_2O$ nucleation determines the population of homogeneous aerosols in general, and the contribution of water-insoluble hydrocarbon nucleation to the aerosol number density is negligible. It is likely, though, that water-insoluble hydrocarbons can contribute to other processes such as particle growth by coagulation and condensation on $H_2SO_4$-$H_2O$ clusters to form aerosols composed of hydrocarbons as well as sulfuric acid and water.

### 2.4.3.2 Nucleation of water-soluble hydrocarbons

For water-soluble hydrocarbons, the possibility of binary or multi-component nucleation of hydrocarbons with sulfuric acid and water should be considered in contrast to unary nucleation of water-insoluble hydrocarbons.

Nucleation mechanisms for water-soluble hydrocarbons examined in this work are:

- Multi-component clusters with sulfuric acid and water. Hydrocarbons may change stability of aqueous clusters and their lifetime. Following Gorbunov's approach of modeling multi-component nucleation with two subsequent nucleation steps, the composition of binary clusters with sulfuric acid and water is calculated first by quasi-unary nucleation approach. Transfer of water-soluble hydrocarbons from gas to aqueous clusters is then calculated thermodynamically in terms of the composition of sulfuric acid and water. This calculation is based on the assumption that additional species in the

second nucleation step are relatively insignificant compared to the two species participating in the main nucleation process. This assumption (of very small fractions of hydrocarbons in embryos compared to those of sulfuric acid and water) is acceptable in considering conditions for near-field aircraft emissions with highly volatile water-soluble hydrocarbon species.

- Binary nucleation of water-soluble hydrocarbons and water in addition to binary nucleation of sulfuric acid and water. In this approach, water-soluble hydrocarbons are assumed to play a similar role to sulfuric acid in the binary nucleation; that is, they control the growth and evaporation of clusters.

- Unary nucleation of water-soluble hydrocarbons (similar to the unary nucleation of water-insoluble hydrocarbons). This approach would be acceptable if the number of water molecules attracted by hydrocarbon clusters is very small.

- Negligible contribution of water-soluble hydrocarbons to the nucleation process because of their high volatility. This assumption would be valid if there is no effect of water-soluble hydrocarbons on mass composition and nucleation rate of liquid particles regardless of approaches applied for water-soluble hydrocarbon nucleation.

Comparisons of different cluster formation mechanisms for water-soluble hydrocarbons are shown in Figure 2.11. Interaction between water-soluble hydrocarbons and sulfuric acid - water clusters in the nucleation process has a minor contribution to the earliest formation of clusters, as shown in the first (top) panel of Figure 2.11 (showing the difference of embryo concentration between binary $H_2SO_4$-$H_2O$ nucleation and multi-component nucleation of $H_2SO_4$-$H_2O$-ws HCs). However, as the residence time increases, multi-component nucleation does not significantly affect binary nucleation of sulfuric acid and water because light hydrocarbons having high Henry's coefficients tend to remain in the gas phase rather than nucleating with sulfuric acid and water. Also, the hydrocarbon cluster concentration shown in Figure 2.11 suggests that neither binary nucleation of water-soluble hydrocarbons with water nor unary nucleation of water-soluble hydrocarbons is an efficient pathway to grow to larger liquid particles. For binary nucleation of water-soluble hydrocarbons and water, only small number of water molecules is attracted to hydrocarbon clusters due to the high activity coefficient of water in water-soluble hydrocarbon solutions (which is much smaller than that in water-insoluble hydrocarbon solutions but still significantly higher than that in sulfuric acid solutions). This result indicates that binary nucleation of water-soluble hydrocarbon and water is close to unary nucleation of hydrocarbons. Both nucleation models for water-soluble hydrocarbon clusters predict that formation of new particles is difficult to initiate due to high volatility of water-soluble hydrocarbons. These species re-evaporate to the vapor phase quickly due to their high vapor pressure, such that the evaporation rates of clusters are much greater than the growth rates. The analysis of nucleation pathways of water-soluble hydrocarbons presented in this section shows that their contribution to aerosol formation, under the conditions of interest in this work, may be negligible without foreign nuclei, similar to our observation with water-insoluble hydrocarbons. Therefore we conclude that hydrocarbon oligomers evolved in aircraft plume are unlikely to grow bigger than the critical size of clusters.
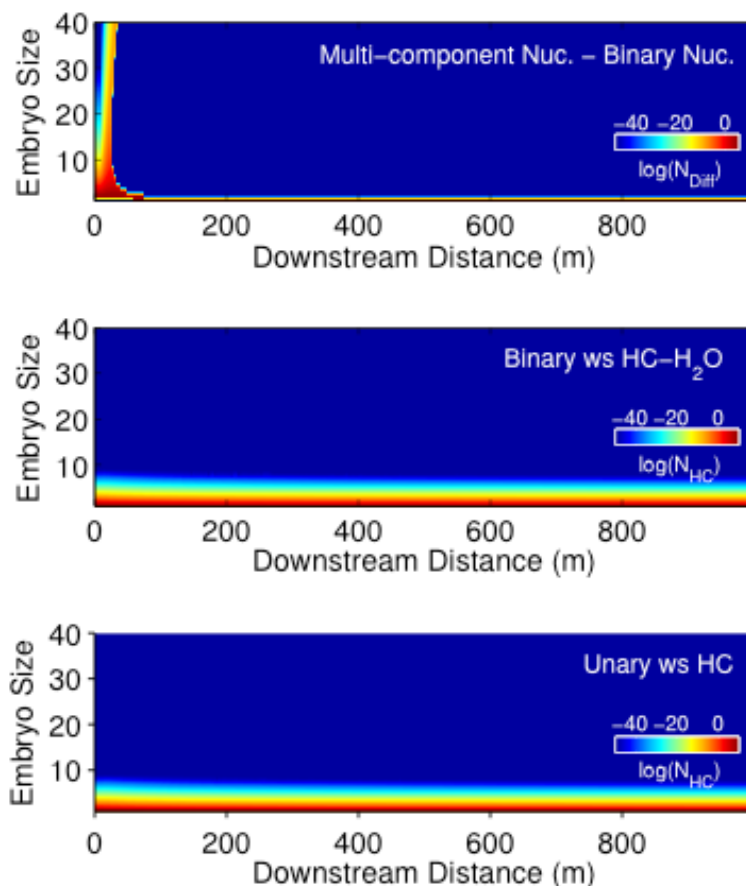
**Figure 2.11 Calculated difference in embryo concentrations between binary H$_2$SO$_4$-H$_2$O nucleation and multi-component nucleation of water-soluble hydrocarbon molecules**

### 2.4.4   Multi-component Coagulation Model

As discussed in the previous section, nucleation of hydrocarbons in aircraft emissions is not an efficient means to promote new particle formation from gaseous molecules and most of the hydrocarbon mass remains in the gas phase or in the form of small oligomers. However, this conclusion does not necessary mean that their involvement in the evolution of homogeneous aerosols is insignificant. A considerable organic fraction has been measured in aircraft-emitted volatile particles during recent field missions (Onasch *et al*., 2009, Timko *et al*., 2010b), and several studies have shown that aerosol particles contain an aqueous core with hydrocarbon surface layers forming hydrophobic organic coatings due to their negligible water solubility (Ellison *et al*., 1999, Gilman *et al*., 2006, Tervahattu *et al*., 2005).

Figure 2.12 illustrates mechanisms of forming liquid coatings on a solid core or on a liquid aqueous core considered in this work. On a partially-wetted solid surface, liquid films tend to aggregate with liquid of the same type of solubility; with an aqueous core, however, hydrophobic liquid films tend to spread on the aqueous liquid surface. If collisions occur between water-insoluble hydrocarbon clusters and H$_2$SO$_4$-H$_2$O clusters, hydrocarbon mass starts to have uptake on H$_2$SO$_4$-H$_2$O clusters. As H$_2$SO$_4$-H$_2$O clusters grow to larger liquid particles via coagulation, aggregates of H$_2$SO$_4$-H$_2$O clusters and hydrocarbon clusters form multi-component aerosols having a hydrophobic film of hydrocarbons. Coagulation between unary-nucleated

clusters of different water-insoluble hydrocarbon species was not considered here, since this process is less likely compared to the collision between hydrocarbon clusters and much more abundant sulfuric acid-water clusters. The coagulation model for multi-component aerosols used here is based on the assumption that water-insoluble hydrocarbons form thin oily film on aqueous droplets; the film is assumed to spread uniformly and quickly after collisions and it is assumed that it does not affect the thermodynamics of the binary droplets and the compositions of the sulfuric acid-water core. While some studies have shown that the presence of organic films on aerosol particles can retard the uptake or evaporation of water from an aqueous core (Gill *et al*., 1983, and Xiong *et al*., 1998), Garland *et al.* (2005) suggested that the retardation effect is negligible with a thin hydrophobic film. Here, it is assumed that ignoring the effect of a thin hydrocarbon film on hygroscopic growth of nanometer-size particles would be acceptable for the rapidly growing particles in the aircraft plume.
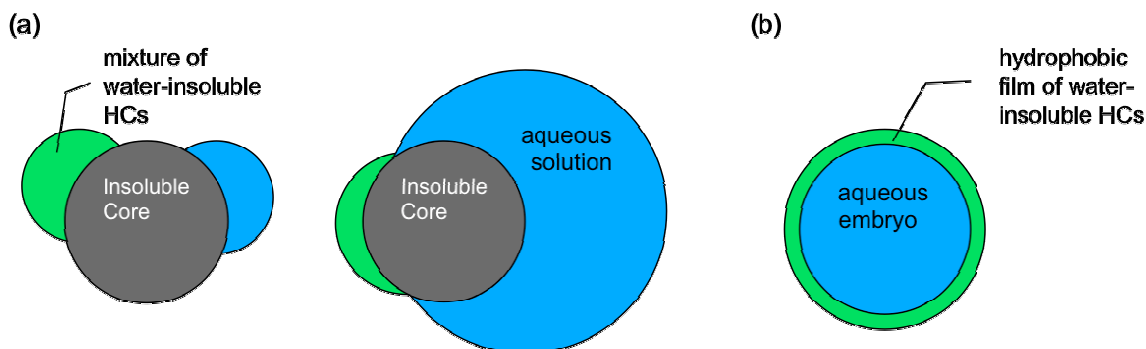


**Figure 2.12 Structure for coagulation on: (a) solid core, (b) aqueous core**

The coagulation model for the multi-component aerosols requires additional variables to simulate and track the growth of hydrophobic films, while the composition of binary droplets can be calculated by finding the composition of minimum free energy at the size of particles being considered. Since tracking all possible combinations of aqueous core sizes and hydrocarbon film volumes for volatile particles is impractical, a modified sectional bin approach was implemented in the simulation model to track the evolution of both the aqueous core and the hydrocarbon film.

For the original $H_2SO_4$-$H_2O$ binary model, Wong *et al.* (2008) used the fully stationary sectional bin approach for coagulated droplets bigger than the largest size of embryos, where embryos were tracked by the number of sulfuric acid molecules. The fully stationary bin approach, on the other hand, uses fixed size of bins, forcing all particles in a bin to have the same volume while allowing particles to move between bins if they grow or shrink. To conserve particle number and volume, a coagulated new particle whose volume falls between two neighboring sectional bins is partitioned into these two bins based on the fraction of volume of the new particle and values of the bins' volumes. The composition of binary droplets can be calculated by finding the composition of minimum free energy at the size of the sectional bins. The stationary sectional bin approach is generally practical for simulating coagulation of particles. However, the approach may cause numerical issues when particles grow via condensational and evaporation (Jacobson and Turco, 1995) and it is difficult to track particles having components in separate phases (e.g. aqueous core with hydrophobic coatings). Jacobson and Turco (1995) suggested a hybrid model combining the stationary bin approach and the fully moving bin approach. The hybrid bin approach tracks core and non-core components separately, which applies fixed size bins for the core fraction and allows non-core fraction to grow to its

exact size. If a particle is moved to a new bin, its averaged non-core volume in that bin will also be moved along with the particle.

      With the hybrid bin approach, the aqueous cores are tracked with the stationary bin approach and the growth of hydrophobic film is tracked to its exact size, where the size of each stantionary bin becomes a lower limit of the mean size of whole particles, as illustrated in Figure 2.13. If two particles having an aqueous core and hydrophobic film coagulate [in the case of Figure 2.13b], the coagulated particle is partitioned based on the volume of aqueous core into two adjacent bins using the stationary bin approach, whereas the mass of the hydrophobic film on the particles is fractionated into both bins according to how the core is distributed. The hydrocarbon mass composing the hydrophobic film on partitioned particles entered into bins is averaged with the hydrocarbon mass of the existing particles in those bins. This approach also allows the condensational growth of hydrophobic film via coagulation of hydrocarbon clusters and sulfuric-acid water droplets as shown in Figure 2.13c. Detailed calculations are shown in Table 2.2 and Figure 2.14.
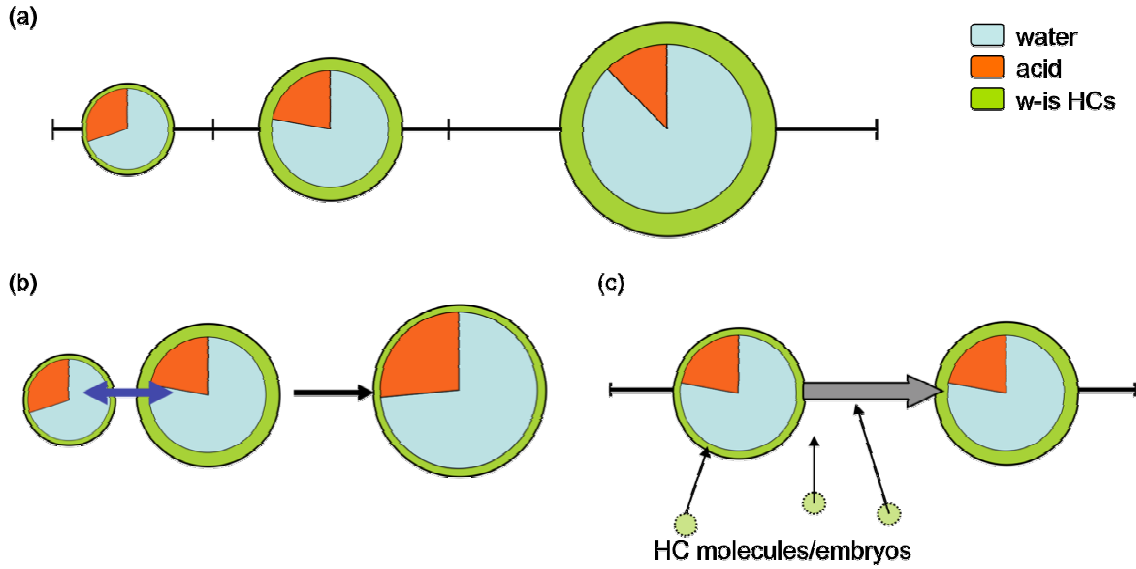


**Figure 2.13 Outline for modeling coagulation with the hybrid bin approach (a), applicable to coagulation of sulfuric acid-water droplets having hydrophobic film (b) and coagulation of sulfuric acid-water droplets and hydrocarbon clusters (c)**

**Table 2.2 Calculation for tracking coagulation with the hybird bin appraoch**

Particle composition at time $t_1$: $m_w$, $m_{ac}$, $m_{hc}$ for mass of water, sulfuric acid, hydrocarbon

$$X_w = \frac{m_w}{m_w + m_{ac}}, \qquad X_{ac} = \frac{m_{ac}}{m_w + m_{ac}}, \qquad X_{hc} = \frac{m_{hc}}{m_w + m_{ac} + m_{hc}}$$

Coagulation of particle in bin $i$ and particle in bin $j$

step i. calculate properties of the new particle:

$$m_{ac,new} = m_{ac,i} + m_{ac,j} \qquad m_{hc,new} = m_{hc,i} + m_{hc,j}$$

find *bin k* and *bin k+1* satisfying $m_{ac,k} \le m_{ac,new} < m_{ac,k+1}$

$$X_{ac,new} = (1 - f_{ac}) \cdot X_{ac,k} + f_{ac} \cdot X_{ac,k+1} \qquad where \quad f_{ac} = \frac{m_{ac,new} - m_{ac,k}}{m_{ac,k+1} - m_{ac,k}}$$

$$m_{ac,new} + m_{w,new} = m_{aq,new} = \frac{m_{ac,new}}{X_{ac,new}}$$

step ii. find *bin l* and *bin l+1* satisfying $m_{aq,l} \leq m_{aq,new} < m_{aq,l+1}$ where $f_{aq} = \dfrac{m_{aq,new} - m_{aq,l}}{m_{aq,l+1} - m_{aq,l}}$

step iii. calculate properties of partitioned particles:
$n_{new}$ = the number of coagulated particles
$\Delta n_l$ = the number of partitioned particles entering into *bin l* = $n_{new}(1\text{-}f_{aq})$
$\Delta n_{l+1}$ = the number of partitioned particles entering into *bin l+1* = $n_{new}f_{aq}$
step iv. update averaged properties of particles in *bin l* and *bin l+1* after coagulation

$$n_{l,new} = n_{l,t_1} + n_{new}\left(1 - f_{aq}\right)$$

$$m_{aq,l,new} = m_{aq,l,t_1}$$

$$m_{hc,l,new} = \frac{n_{l,t_1} m_{hc,l,t_1} + n_{new}\left(1 - f_{aq}\right)m_{hc,new}}{n_{l,t_1} + n_{new}\left(1 - f_{aq}\right)}$$

$$n_{l+1,new} = n_{l+1,t_1} + n_{new}f_{aq}$$

$$m_{aq,l+1,new} = m_{aq,l+1,t_1}$$

$$m_{hc,l+1,new} = \frac{n_{l+1,t_1} m_{hc,l+1,t_1} + n_{new}f_{aq}m_{hc,new}}{n_{l+1,t_1} + n_{new}f_{aq}}$$
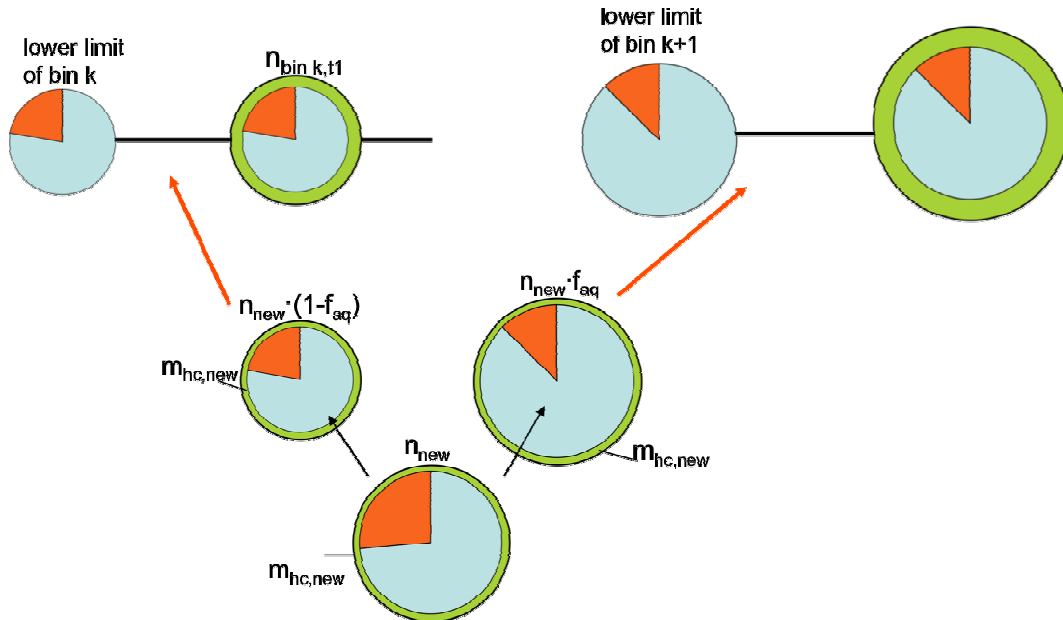


**Figure 2.14 Details of the combined bin approach**

### 2.4.5 Summary of pathways for new particle formation

This section summarizes possible interactions and mechanisms of the nucleation and coagulation processes and compares their contributions to the formation of hydrocarbon-containing aerosols. Figure 2.15 shows a schematic of new liquid particle formation pathways via nucleation (indicated as alphabet letters) or coagulation (indicated as Roman numerals) processes. Table 2.3 lists five different approaches of including different particle formation pathways discussed in Section 2.4.3. Figure 2.16 shows simulated liquid particle size distributions at 1 km downstream of a CFM56-2C1 engine at 80 % ambient relative humidity and 286 K ambient temperature using the approaches in Table 2.4. Coagulation between water-insoluble hydrocarbon clusters and aqueous clusters forms hydrocarbon films on aqueous cores, like the particle shown with green coating in Figure 2.15. Our analysis shows that the coagulation between water insoluble hydrocarbon clusters and sulfuric acid-water particles (process iii) is the most critical pathway. The growth of hydrophobic organic films increased aerosol size by about 1.5 (mode size) to 2.5 (min size) times compared to aerosols formed merely from binary nucleation of sulfuric acid and water without hydrocarbons (i.e., Approach 5). The contribution of water-soluble hydrocarbons, on the other hand, is insignificant (see the comparison between Approach 4 and Approach 1 or 3 in Figure 2.16) since they remain mostly in the gas phase as shown in Table 2.4. The predicted particle size distributions from Approaches 1 and 3 are almost identical, suggesting that the interaction between water-soluble hydrocarbon and water (process b) is insignificant. While the interaction between water-soluble hydrocarbons with $H_2SO_4$-$H_2O$ clusters via coagulation (process i) is identified as an inefficient pathway to change aerosol size distribution, the interaction between water-soluble hydrocarbon molecules and $H_2SO_4$-$H_2O$ nuclei in the nucleation step (process e) contributes slightly to aerosol growth by decreasing evaporation rate (via reduction of surface tension).
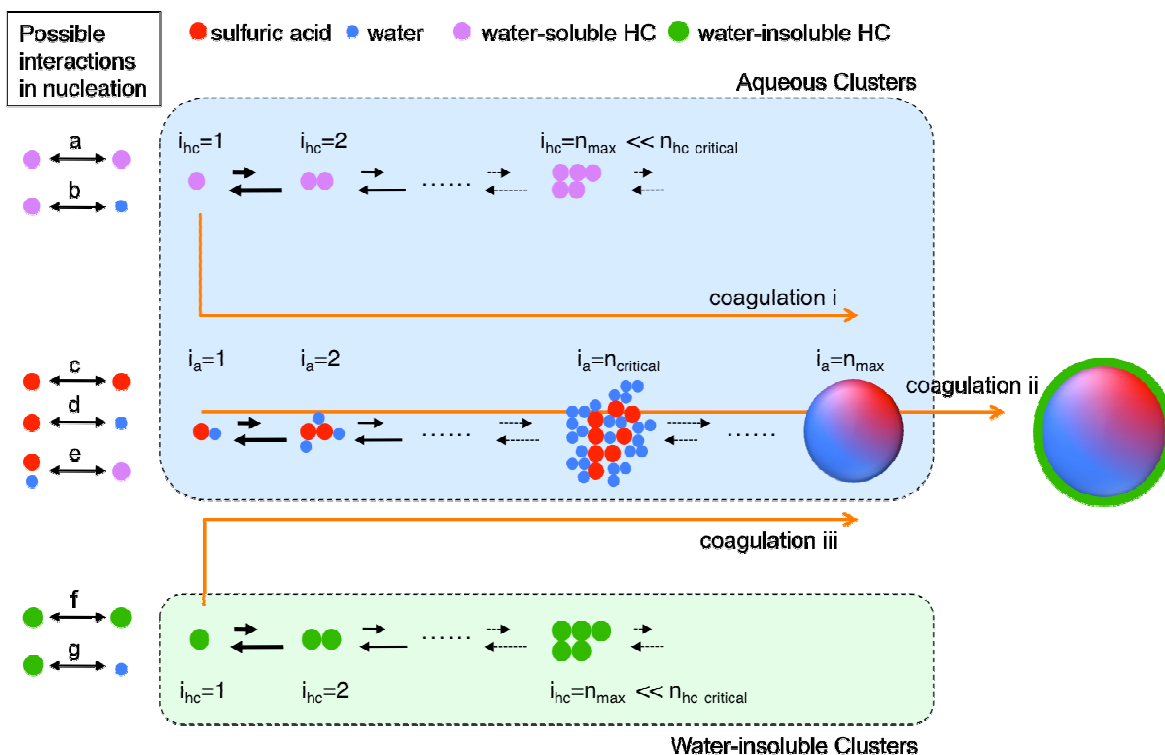


**Figure 2.15 Interaction and pathways for new particle formation**

35

**Table 2.3 Nucleation and coagulation approaches for new particle formation**

| | Binary nucleation of $H_2SO_4$-$H_2O$ | Multi-component nucleation of $H_2SO_4$-$H_2O$-water soluble Hydrocarbons (HCs) | Binary nucleation of w-s HCs | Unary nucleation of w-s HCs | Negligible effect of nucleation of w-s HCs | Unary Nucleation of water insoluble HCs |
|---|---|---|---|---|---|---|
| included interactions | c,d,ii | c,d,e,ii | a,b,i | a,i | - | f,iii |
| Approach 1<br>a, b, c, d, f, i, ii, iii | v | | v | | | v |
| Approach 2<br>c, d, e, f, ii, iii | | v | | | | v |
| Approach 3<br>a, c, d, f, i, ii, iii | v | | | v | | v |
| Approach 4<br>c, d, f, ii, iii | v | | | | v | v |
| Approach 5<br>c, d, ii | v | | | | | |



**Figure 2.16 Comparison of predicted particle size distributions of liquid aerosols at 1 km downstream of a CFM56-2C1 engine by involved different interactions in nucleation and coagulation processes**

**Table 2.4 Comparison of mass fraction transferred to the nucleation mode**

| | Mass fraction (%) of species in nucleation mode | | |
|---|---|---|---|
| | Sulfur | Water-insoluble HCs | Water-soluble HCs |
| Approach 1 | 100 | 99.8 | 0.007 |
| Approach 2 | 100 | 99.7 | 0 |
| Approach 3 | 100 | 99.8 | 0.36 |
| Approach 4 | 100 | 99.7 | - |
| Approach 5 | 99 | - | - |

### 2.4.6 Results and Discussion

### 2.4.6.1 Simulation Results

This section provides simulation results for the evolution of aviation PM emissions at ground level with all microphysical processes considered. The role of hydrocarbons in the particle growth is also discussed. Ambient conditions were set to a temperature of 286 K and 80% relative humidity. Also, 100 ppb of three water-insoluble hydrocarbons, $C_{16}H_{10}$, $C_{20}H_{12}$, $C_{24}H_{12}$, and 100 ppb of three water-soluble hydrocarbon oxygenates, $C_3H_6O$, $C_3H_6O_2$, $C_4H_8O_2$, were used as hydrocarbon surrogates in the exhaust plume, and initial gas concentrations (mole fractions) were determined using the following equations:

$$\sum X_{w\text{-soluble}} = 100 \text{ ppb}; \qquad X_{w\text{-soluble},i}M_{w\text{-soluble},i} = X_{w\text{-soluble},j}M_{w\text{-soluble},j}$$

$$[2.20]$$

$$\sum X_{w\text{-insoluble}} = 100 \text{ ppb}; \qquad X_{w\text{-insoluble},i}M_{w\text{-insoluble},i} = X_{w\text{-insoluble},j}M_{w\text{-insoluble},j}$$

$H_2SO_4$-$H_2O$ clusters were tracked as embryos that are no larger than 40 sulfuric acid molecules, and larger particles having more than 40 acid molecules were tracked using 10 bins that were initially log-normally distributed between 3 nm to 250 nm. Hydrocarbon clusters were tracked up to a size of 5 monomer units since larger embryos are present in negligible concentration as shown previously in Figure 2.10. Monodisperse soot particles were employed with an initial diameter of 16 nm and an initial concentration of $9.75 \times 10^6$ cm$^{-3}$, which represents the emitted soot surface area of a CFM56-2C1 engine at low power, which was examined during the APEX measurement campaign.

Figure 2.17 compares the evolution of particle size distribution of homogeneous nucleation mode particles formed from two mechanisms: (a) binary homogeneous $H_2SO_4$-$H_2O$ particles without hydrocarbons and (b) multi-component liquid particles with $H_2SO_4$-$H_2O$ cores and hydrophobic film coatings of hydrocarbons. For both cases, the particle number densities evolved similarly. Small embryos were formed via binary $H_2SO_4$-$H_2O$ nucleation and grew to larger liquid particles via coagulation. At around 500 m downstream of the engine, liquid particles reached equilibrium size and then their concentrations started to decrease because of mixing with ambient air. Under the exhaust conditions where sufficient amounts of condensable hydrocarbons are present, the particle growth also had contributions from water-insoluble hydrocarbon coagulation even though the formation of liquid particles is primarily driven by binary $H_2SO_4$-$H_2O$ nucleation. Due to coagulation with water-insoluble hydrocarbons, small particles had hydrophobic film coatings as thick as the radii of their aqueous cores at 1 km downstream. The mean radius of liquid particle distribution increased from 5.4 nm to 10.5 nm when hydrocarbons were included in the model.

Figure 2.18 and Figure 2.19 show evolution of mass compositions of liquid particles and soot coatings predicted from the model, respectively. The predicted mass composition of soot coatings is not significantly different from that of the soot coating without nucleation and coagulation modes; however, the soot particle growth is suppressed significantly as a result of decreasing total soot coating mass. About 80% of the total sulfate mass and about 50% of water-insoluble hydrocarbon mass was found moving to the nucleation mode as compared to results from calculations where only soot mode microphysics were considered. The mass composition of liquid particles, on the other hand, demonstrated that aqueous liquid aerosols in the initial aircraft plume started to have a substantial amount of water-insoluble hydrocarbons as they grew downstream. Smaller liquid particles tend to obtain more hydrocarbon mass fractions, and these particles with small aqueous cores and thick hydrocarbon films could be considered as primarily organic aerosols. This suggests that organics constitute a significant mass fraction in very fine aerosols, where species with low volatility (e.g., $C_{20}H_{12}$ and $C_{24}H_{12}$) could account for a significant amount of organic mass. The contribution of water-soluble hydrocarbons is almost negligible in the nucleation and coagulation processes, but they still can contribute to the growth of soot particles by enhancing the hydrophilic fraction of the soot surfaces and consequently the hygroscopic growth of the soot particles.
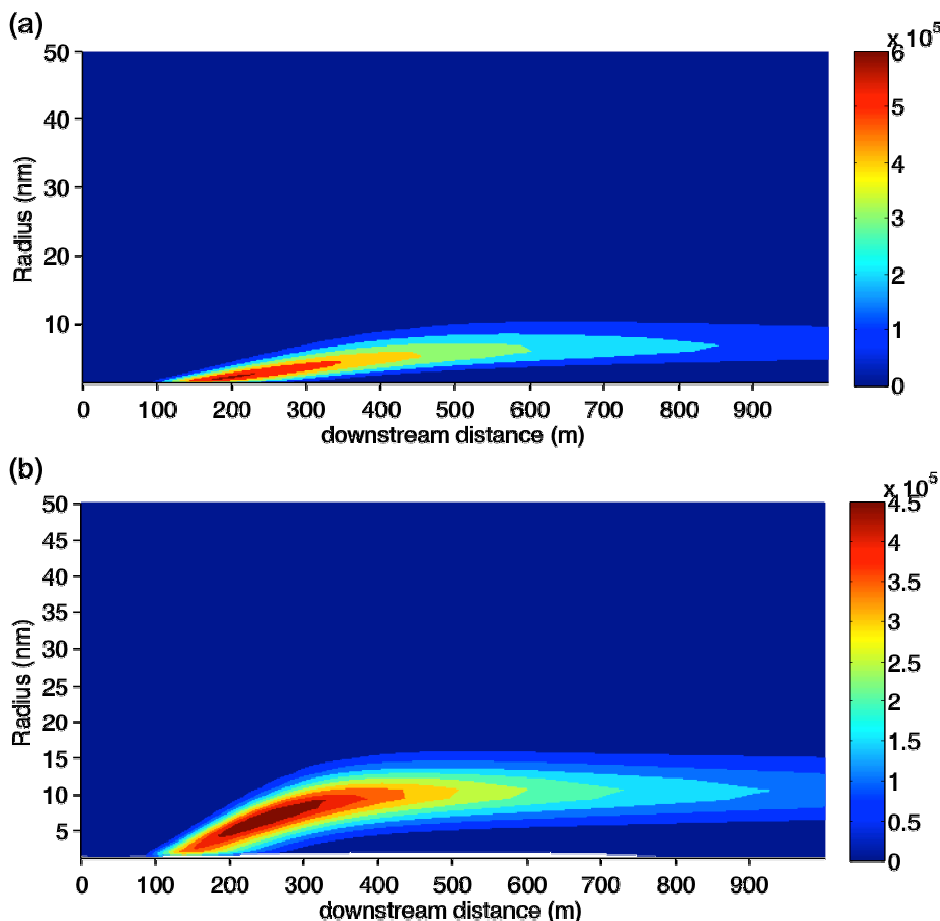


**Figure 2.17 Concentration and size evolution of liquid droplets predicted from the model with (a) only sulfuric acid and water binary nucleation, and (b) the presence of hydrocarbons in addition to sulfuric acid and water**
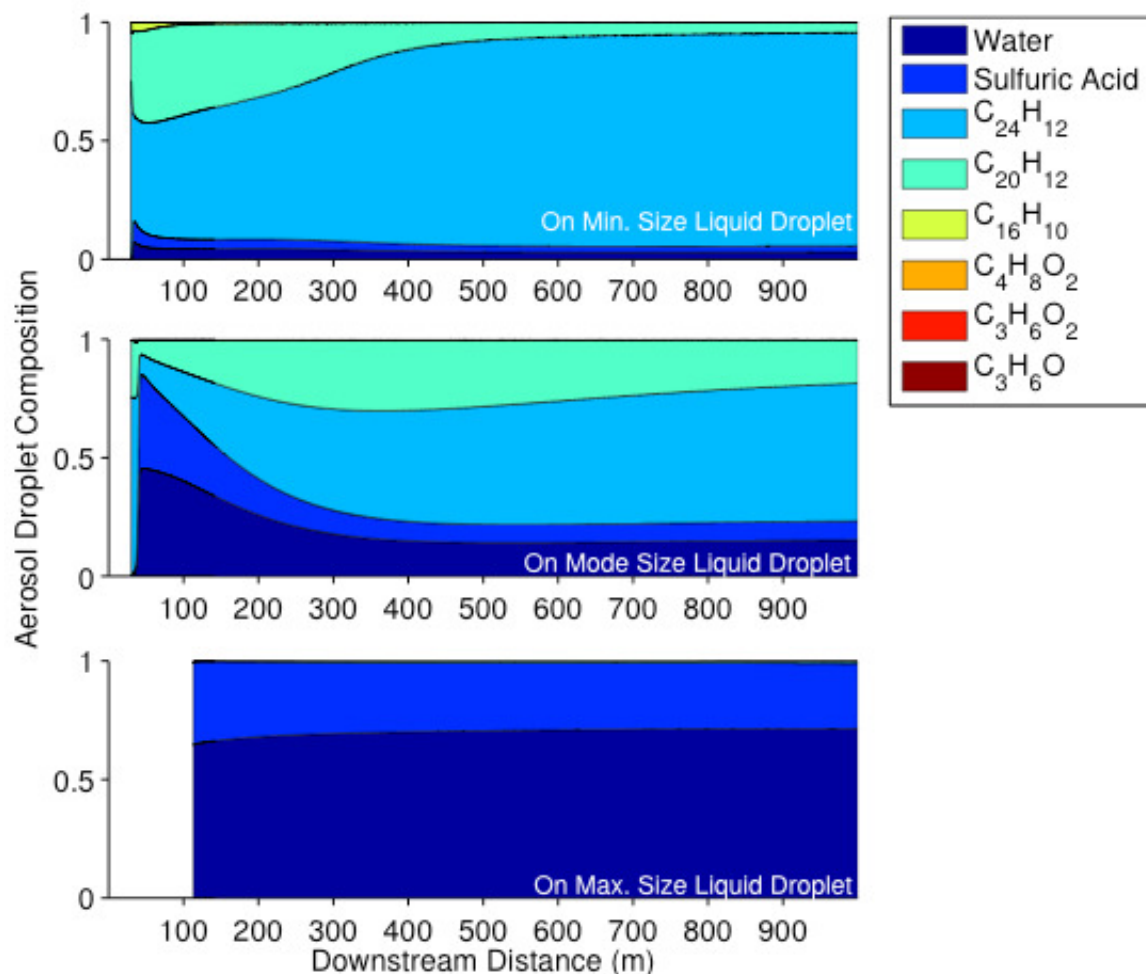
**Figure 2.18 Composition evolution of homogeneous particles in minimum, mode, maximum size**
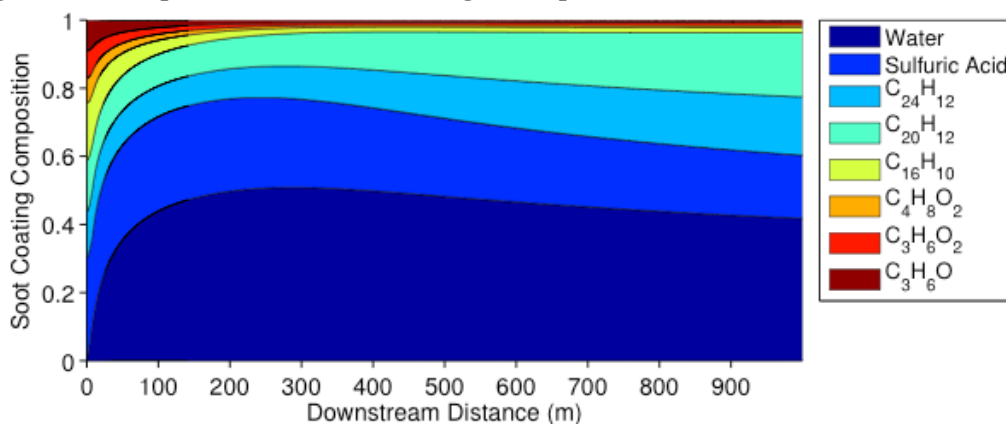


**Figure 2.19 Composition evolution of soot coatings**

In Figure 2.20, the mass budget for individual species is divided into three modes: 1) soot coatings due to activation and condensation, 2) liquid aerosol droplets and embryos formed via nucleation and coagulation, 3) vapor phase including monomers and gases. Under the same condition studied earlier, sulfate mass in aerosol droplets and soot coatings increased with downstream distance, and 100% of sulfate mass was transferred from vapor phase to liquid phase

at 1 km downstream. Under high ambient relative humidity levels (such as 80% in this case), binary $H_2SO_4$-$H_2O$ nucleation becomes a dominant process to transfer sulfate mass into aerosol droplets, even at a short distance downstream. This is significantly different than the prediction when the nucleation process is turned off in the simulation, where all sulfate mass condensed on soot coatings. Soot particle growth, however, continues after depletion of sulfuric acid gas via scavenging of liquid aerosols on soot particles. For condensable water-insoluble hydrocarbons, similar evolutions were observed: hydrocarbon mass in the vapor phase is transferred relatively quickly into homogeneous liquid aerosols via condensation on or coagulation with homogeneous $H_2SO_4$-$H_2O$ aerosols; this is followed by gradual coagulation of these particles with soot. Note, however, that benzopyrene ($C_{20}H_{12}$) mass fraction in the liquid droplets initially increases but starts to decrease at about 500 m downstream. Consequently, its mass fraction in the vapor phase increases because evaporation of the hydrocarbon species from smaller droplets occurs due to the Kelvin effect. This result implies that the nucleation mode is likely to be more sensitive to the volatility of species than the soot mode because much smaller clusters and droplets are involved in the process. Water-soluble hydrocarbons, on the other hand, are not favored to be partitioned into homogeneous liquid particles or soot particles because of their high vapor pressure.
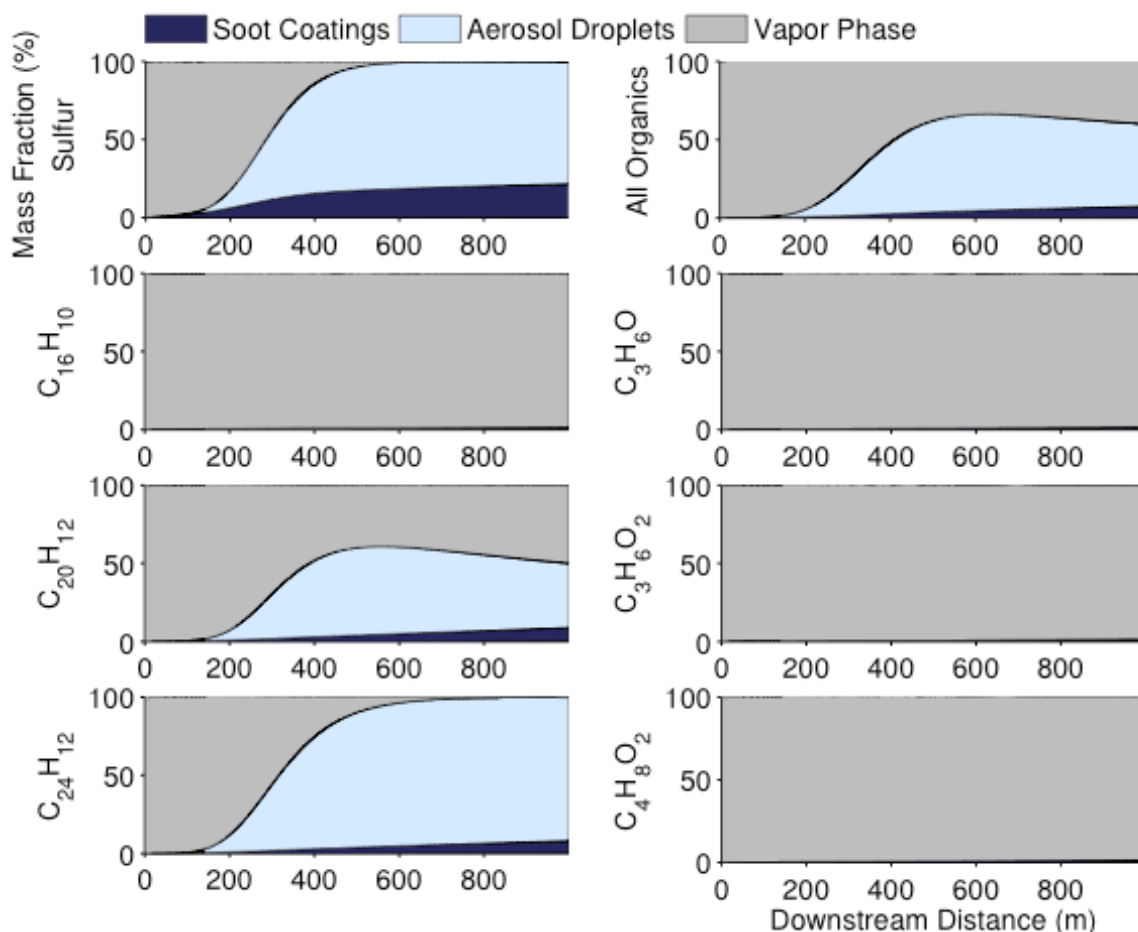


**Figure 2.20 Evolution of sulfate and hydrocarbon mass fractions under the conditions described in Section 2.4.6.1**

## 2.4.6.2 Effects of Composition and Ambient Conditions

### 2.4.6.2.1  Role of Hydrocarbons

The effect of hydrocarbons on aerosol formation is examined in this section. Three systems were studied and compared: binary (sulfuric acid-water) system without hydrocarbons, binary system with water-insoluble hydrocarbon species only, and binary system with all hydrocarbon species included. The contributions of the species to the size and mass growth of both types of particles can be seen in Figure 2.21. Incorporating water-insoluble hydrocarbons contributes to increased size of liquid aerosols while preventing the uptake of water-soluble species on soot coatings. The addition of water-soluble hydrocarbons on the other hand, improves the uptake of water and sulfuric acid on soot particles by competing with the hydrophobic effect of water-insoluble hydrocarbons on soot surfaces. It is important to note that hydrocarbons can contribute to the aerosol formation directly or indirectly via adding condensation mass directly and/or inducing competition between condensable species through microphysical processes.
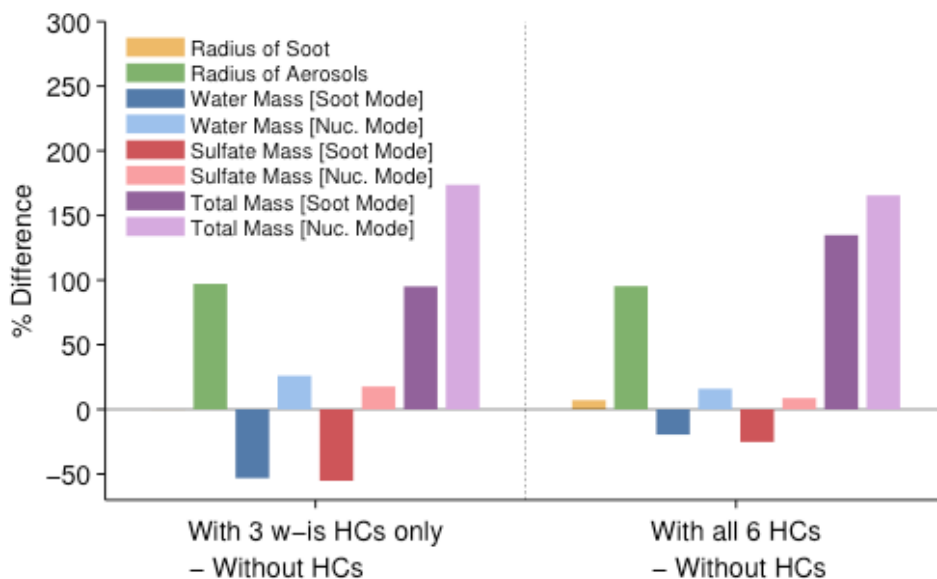


**Figure 2.21 Effect of hydrocarbons**

### 2.4.6.2.2  Competition Across Microphysical Modes

Nucleation is the most dominant microphysical process at high levels of ambient relative humidity. When ambient relative humidity was set to 80% in our simulations, the nucleation mode accounts for 80% of sulfate mass at 1 km downstream, whereas the soot mode was limited to the remaining 20% of sulfate mass. Consequently, the decreased contribution of nucleation mode at lower ambient relative humidity conditions can lead to increased sulfate mass budget in the soot mode. Figure 2.22 shows that the contribution of sulfate to the nucleation mode was completely suppressed when 20% ambient relative humidity was used in our simulation, whereas, the contribution of sulfate to the soot mode increased. It should be noted, however, that if the nucleation mode is turned off in the simulation, the trend is reversed and sulfate mass on soot mode *decreases* as the ambient RH is dropped. This indicates that competition between nucleation and soot modes is also important to the evolution of aerosols in addition to competition between exhaust species.

41
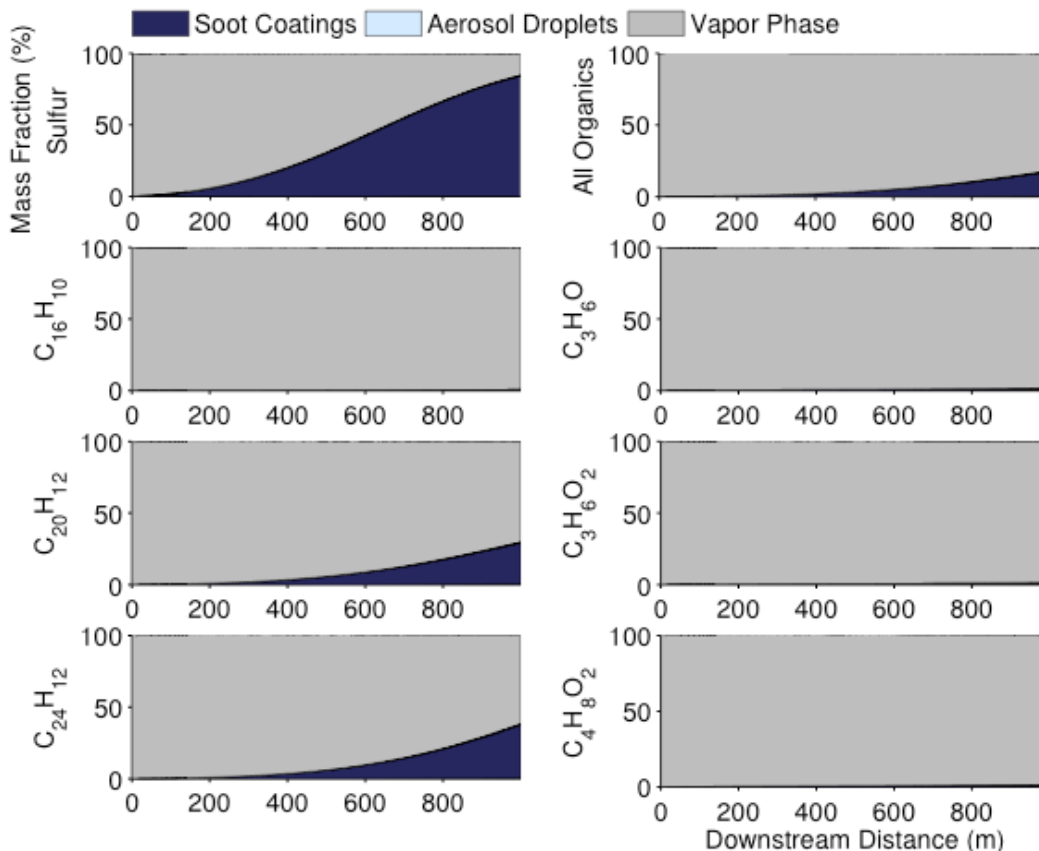
**Figure 2.22 Evolution of mass fraction at 20% RH**

The effect of RH on aerosol formation is examined with and without including hydrocarbons as shown in Figure 2.23a, and the effect of hydrocarbons is studied at different RH conditions as shown in Figure 2.23b. Regardless of the presence of hydrocarbons, decreasing RH restricted aerosol nucleation, and consequently sulfuric acid preferred to condense on soot coatings as opposed to liquid aerosols. The effect of RH on the soot mode is strengthened by the presence of hydrocarbons. At lower ambient RH levels, hydrocarbons have a stronger effect on soot particle growth. While water-insoluble hydrocarbons substantially contributed to soot particle growth via condensation, water-soluble hydrocarbons enhanced the uptake of water and sulfuric acid on soot coating by increasing hydrophilic surface area. At high ambient RH levels, competition between nucleation and soot modes and competition between hydrocarbons and sulfuric acid on soot surfaces occur at the same time. Delayed sulfuric acid adsorption on soot surfaces (due to competition with water-insoluble hydrocarbons during the initial activation process) allowed more mass transfer to nucleation mode. Consequently, water-insoluble hydrocarbons decreased the uptake of water and sulfuric acid in the soot mode.

42
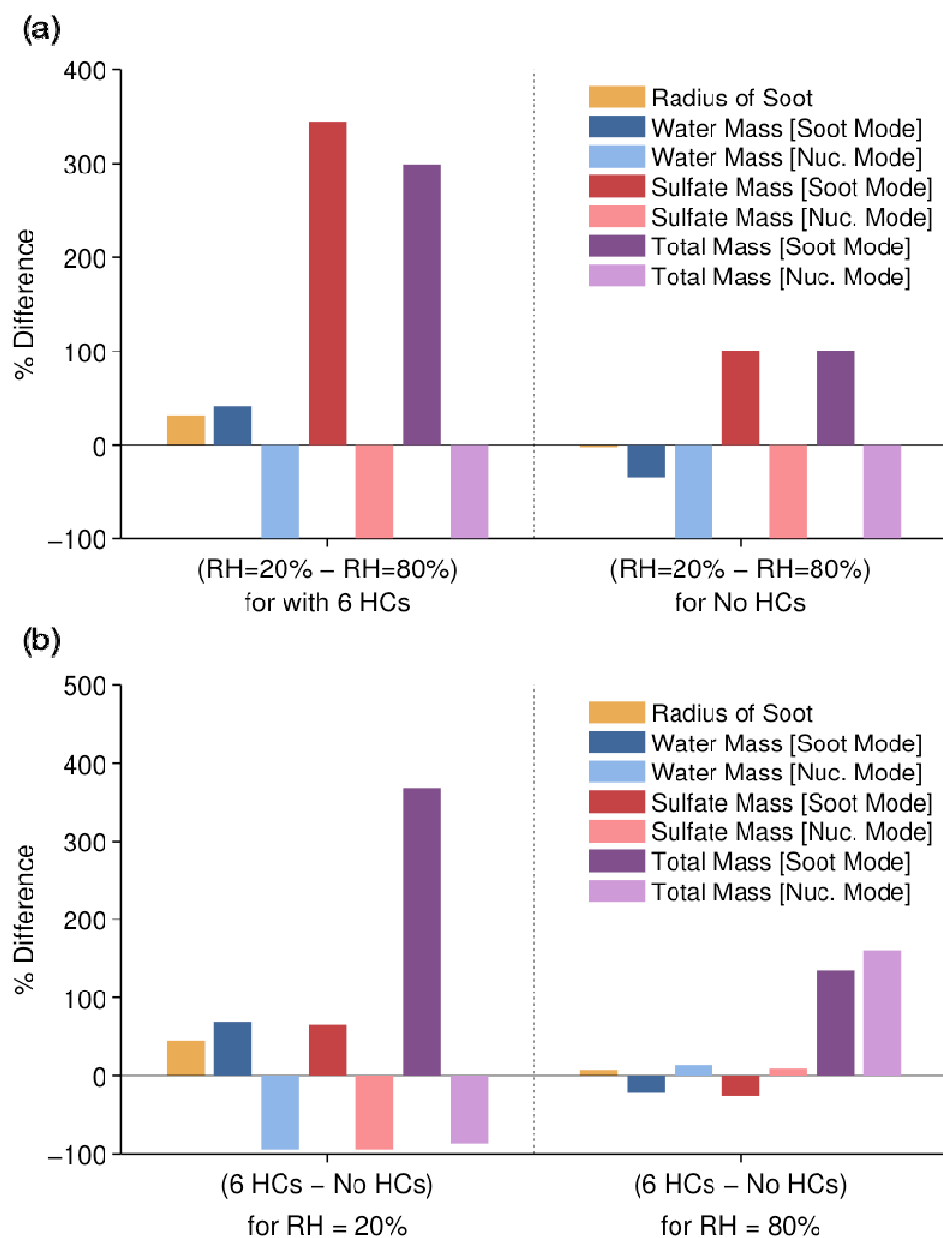
**Figure 2.23 Effect of RH and Hydrocarbons**

### 2.4.7 Summary

It is computationally expensive to simulate classical multi-component nucleation with increasing number of components. This section suggests nucleation approaches for hydrocarbons can be simplified by including only dominant effects, which would be acceptable for aircraft emissions, and Figure 2.24 shows simplified pathways for the formation of new particles in aircraft emissions. Depending on the solubility of species, possible interactions between nucleation and coagulation processes and proposed pathways for new particle formation are examined. These processes and pathways include independent unary nucleation of water-insoluble hydrocarbons and multi-component/binary/unary nucleation of water-soluble hydrocarbons. The results presented in this section demonstrate that homogeneous aerosol

43

formation is driven primarily by binary $H_2SO_4$-$H_2O$ nucleation, and the contribution of hydrocarbons is negligible to the rate of new particle formation.

Coagulation of water-insoluble hydrocarbon clusters with $H_2SO_4$-$H_2O$ clusters is assumed to form hydrophobic films on aqueous cores. While the contribution of water-soluble hydrocarbons is negligible in nucleation and coagulation processes, water-insoluble hydrocarbons significantly contribute to the size growth of liquid particles. Competition between nucleation and soot modes is discussed and compared with the competition between hydrophobic and hydrophilic species. In summary, the contribution of hydrocarbons is important for the growth of particles in both nucleation and soot modes through condensation and coagulation of water-insoluble hydrocarbons and competitions induced by both types of hydrocarbons.
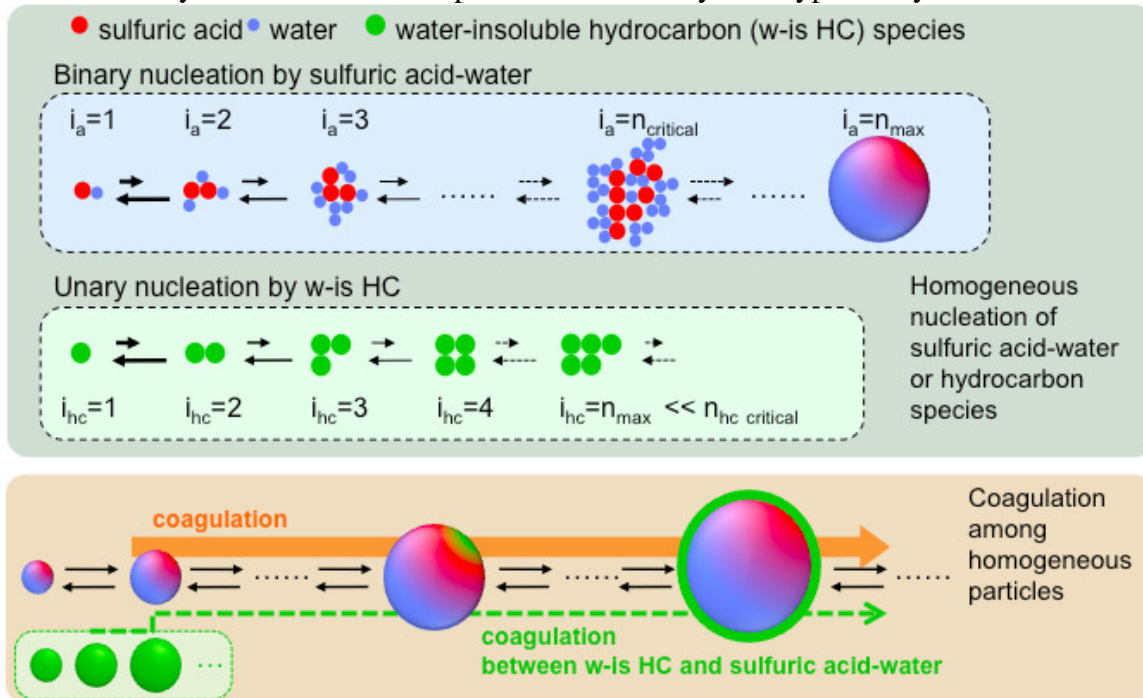


**Figure 2.24 Simplified pathways for the new particle formation in aircraft emissions**

## 2.5 References

Asher, W., and Pankow, J. (2006). Vapor Pressure Prediction for Alkenoic and Aromatic Organic Compounds by a Unifac-Based Group Contribution Method. *Atmos. Environ.*, 40:3588-3600.

Clegg, S. L., and Seinfeld, J. H. (2006). Thermodynamic Models of Aqueous Solutions Containing Inorganic Electrolytes and Dicarboxylic Acids at 298.15 K. 1. The Acids as Nondissociating Components. *J. Phys. Chem. A*, 110:5692-5717.

Donahue, N. M., Robinson, A. L., Stanier, C. O., and Pandis, S. N. (2006). Coupled Partitioning, Dilution, and Chemical Aging of Semivolatile Organics. *Environ. Sci. Technol.*, 40:2635-2643.

Du, H., and Yu, F. (2009). Kinetic modeling of nucleation experiments involving $SO_2$ and OH: new insights into the underlying nucleation mechanisms. *Atmos. Chem. Phys.*, 9:7913–7922.

Ellison, G. B., Tuck, A. F., and Vaida, V. (1999). Atmospheric processing of organic aerosols. *Journal of Geophysical Research*, 104(D9):11633–11641.

Garland, R. M., Wise, M. E., Beaver, M. R., DeWitt, H. L., Aiken, A. C., Jimenez,, J. L., and Tolbert, M. A. (2005). Impact of palmitic acid coating on the water uptake and loss of ammonium sulfate particles, *Atmospheric Chemistry and Physics*, 5:1951–1961.

Gill, P. S. and Graedel, T. E. (1983). Organic films on atmospheric aerosol particles, fog droplets, cloud droplets, raindrops, and snowflakes. *Reviews of Geophysics and Space Physica*, 21(4):903–920.

Gilman, J. B., Tervahattu, H., Vaida, V. (2006). Interfacial properties of mixed films of long-chain organics at the air-water interface, *Atmospheric Environment*, 40:6606–6614.

Gorbunov, B. (2001). From binary and ternary to multicomponent nucleation: Atmospheric aerosol formation. *Journal of Chemical Physics*, 115(6).

Jacobson, M. Z. and Turco, R. P. (1995). Simulating condensational growth, evaporation, and coagulation of aerosols using a combined moving and stationary size grid, *Aerosol Science and Technology*, 22:73–92.

Jensen, T., Fredenslund, A., and Rasmussen, P. (1981). Pure-Component Vapor Pressures Using Unifac Group Contribution. *Ind. Eng. Chem. Fundamen.*, 20:239-246.

Kanakidou, M., Seinfeld, J. H., Pandis, S. N., Barnes, I., Dentener, F. J., Facchini, M. C., Dingenen, R. V., Ervens, B., Nenes, A., Nielsen, C. J., Swietlicki, E., Putaud, J. P., Balkanski, Y., Fuzzi, S., Horth, J., Moortgat, G. K., Winterhalter, R., Myhre, C. E. L., Tsigaridis, K., Vignati, E., Stephanou, E. G., and Wilson, J. (2005). Organic Aerosol and Global Climate Modelling: A Review. *Atmos. Chem. Phys.*, 5:1053-1123.

Kärcher, B. (1998). Physicochemistry of Aircraft-Generated Liquid Aerosols, Soot, and Ice Particles. 1. Model Description. *J. Geophys. Res.-Atmospheres*, 103:17111-17128.

Kärcher, B., Peter, T., and Biermann, U. (1996). The Initial Composition of Jet Condensation Trails. *J. Atmos. Sci.*, 53:3066-3083.

Kärcher, B., and Yu, F. (2009). Role of Aircraft Soot Emissions in Contrail Formation. *Geophys. Res. Lett.*, 36:L01804, doi: 10.1029/2008GL036649.

Knighton, W. B., Rogers, T. M., Anderson, B. E., Herndon, S. C., Yelvington, P. E., and Miake-Lye, R. C. (2007). Quantification of Aircraft Engine Hydrocarbon Emissions Using Proton Transfer Reaction Mass Spectrometry. *J. Propul. Power*, 23:949-958.

Kulmala, M., Pirjola, L., and Mäkelä, J. M. (2000). Stable sulphate clusters as a source of new atmospheric particles. *Nature*, 404:66–69.

Kulmala, M., Kerminen, V.-M., Anttila, T., Laaksonen, A., and O'Dowd, C. D. (2004). Organic Aerosol Formation Via Sulphate Cluster Activation. *J. Geophys. Res.-Atmospheres*, 109:D04205, doi: 10.1029/2003JD003961.

Larsen, B., Rasmussen, P., and Fredenslund, A. (1987). A Modified Unifac Group-Contribution Model for Prediction of Phase Equilibria and Heats of Mixing. *Ind. Eng. Chem. Res.*, 26:2274-2286.

Nannoolal, Y., Rarey, J., and Ramjugernath, D. (2007). Estimation of Pure Component Properties Part 2. Estimation of Critical Property Data by Group Contribution. *Fluid Phase Equilibria*, 252:1-27.

Nannoolal, Y., Rarey, J., and Ramjugernath, D. (2008). Estimation of Pure Component Properties Part 3. Estimation of the Vapor Pressure of Non-Electrolyte Organic Compounds Via Group Contributions and Group Interactions. *Fluid Phase Equilibria*, 269:117-133.

Nannoolal, Y., Rarey, J., Ramjugernath, D., and Cordes, W. (2004). Estimation of Pure Component Properties Part 1. Estimation of the Normal Boiling Point of Non-Electrolyte Organic Compounds Via Group Contributions and Group Interactions. *Fluid Phase Equilibria*, 226:45-63.

Odum, J. R., Jungkamp, T. P. W., Griffin, R. J., Forstner, H. J. L., Flagan, R. C., and Seinfeld, J. H. (1997). Aromatics, Reformulated Gasoline, and Atmospheric Organic Aerosol Formation. *Environ. Sci. Technol.*, 31:1890-1897.

Onasch, T. B., Jayne, J. T., Herndon, S. C., Worsnop, D. R., Miake-Lye, R. C., Mortimer, I. P., and Anderson, B. E. (2009). Chemical Properties of Aircraft Engine Particulate Exhaust Emissions. *J. Propul. Power*, 25:1121-1137.

Pankow, J., and Asher, W. (2008). Simpol. 1: A Simple Group Contribution Method for Predicting Vapor Pressures and Enthalpies of Vaporization of Multifunctional Organic Compounds. *Atmos. Chem. Phys.*, 8:2773-2796.

Persiantseva, N., Popovicheva, O., and Shonija, N. (2004). Wetting and Hydration of Insoluble Soot Particles in the Upper Troposphere. *J. Environ. Monitoring*, 6:939-945.

Petzold, A., Gysel, M., Vancassel, X., Hitzenberger, R., Puxbaum, H., Vrochticky, S., Weingartner, E., Baltensperger, U., and Mirabel, P. (2005). On the Effects of Organic Matter and Sulphur-Containing Compounds on the Ccn Activation of Combustion Particles. *Atmos. Chem. Phys.*, 5:3187-3203.

Poling, B. E., Prausnitz, J. M., and O'Connell, J. P. (2001). *The Properties of Gases and Liquids*. McGraw-Hill, New York, NY.

Pope, C. A., and Dockery, D. (2006). Health Effects of Fine Particulate Air Pollution: Lines That Connect. *J. Air & Waste Manage. Assoc.*, 56:709-742.

Pruppacher, H. R., and Klett, J. D. (1997). *Microphysics of Clouds and Precipitation*. Kluwer Academic Publishers, Dordrecht, The Netherlands.

Robinson, A. L., Donahue, N. M., Shrivastava, M. K., Weitkamp, E. A., Sage, A. M., Grieshop, A. P., Lane, T. E., Pierce, J. R., and Pandis, S. N. (2007). Rethinking Organic Aerosols: Semivolatile Emissions and Photochemical Aging. *Science*, 315:1259-1262.

Schwarz, J. P., Spackman, J. R., Fahey, D. W., Gao, R. S., Lohmann, U., Stier, P., Watts, L. A., Thomson, D. S., Lack, D. A., Pfister, L., Mahoney, M. J., Baumgardner, D., Wilson, J. C., and Reeves, J. M. (2008). Coatings and Their Enhancement of Black Carbon Light Absorption in the Tropical Atmosphere. *J. Geophys. Res.-Atmospheres*, 113:D03203, doi: 10.1029/2007JD009042.

Seaton, A., Godden, D., MacNee, W., and Donaldson, K. (1995). Particulate Air Pollution and Acute Health Effects. *The Lancet*, 345:176-178.

Seinfeld, J. H., and Pandis, S. N. (2006). *Atmospheric Chemistry and Physics - from Air Pollution to Climate Change*. John Wiley & Sons, Inc., New York, NY.

Taleb, D., Ponche, J., and Mirabel, P. (1996). Vapor Pressures in the Ternary System Water-Nitric Acid-Sulfuric Acid at Low Temperature: A Reexamination *J. Geophys. Res.-Atmospheres*, 101:25967-25977.

Timko, M. T., Herndon, S. C., Wood, E. C., Onasch, T. B., Northway, M. J., Jayne, J. T., Canagaratna, M., Miake-Lye, R. C., and Knighton, W. B. (2010a). Gas Turbine Engine Emissions Part 1. Hydrocarbons and Nitrogen Oxides. *ASME J. Eng. Gas Turbines Power*, 132:061504/061501-061504/061514.

Timko, M. T., Onasch, T. B., Northway, M. J., Jayne, J. T., Canagaratna, M., Herndon, S. C., Wood, E. C., Miake-Lye, R. C., and Knighton, W. B. (2010b). Gas Turbine Engine Emissions Part 2. Chemical Properties of Particulate Matter. *ASME J. Eng. Gas Turbines Power*, 132:061505, doi: 10.1115/1.4000132.

Tervahattu, H., Juhanoja, J., Vaida, V., Tuck, A. F., Niemi, J. V., Kupiainen, K., Kulmala, M., and Vehkamäki, H. (2005). Fatty acids on continental sulfate aerosol particles, *Journal of Geophysical Research*, 110:D06207.

Wey, C. C., Anderson, B. E., Wey, C., Miake-Lye, R. C., Whitefield, P., and Howard, R. (2007). Overview on the Aircraft Particle Emissions Experiment. *J. Propul. Power*, 23:898-905.

Wong, H.-W., and Miake-Lye, R. C. (2010). Parametric Studies of Contrail Ice Particle Formation in Jet Regime Using Microphysical Parcel Modeling. *Atmos. Chem. Phys.*, 10:3261-3272.

Wong, H.-W., Yelvington, P. E., Timko, M. T., Onasch, T. B., Miake-Lye, R. C., Zhang, J., and Waitz, I. A. (2008). Microphysical Modeling of Ground-Level Aircraft-Emitted Aerosol Formation: Roles of Sulfur-Containing Species. *J. Propul. Power*, 24:590-602.

Wong, H.-W., Yu, Z., Timko, M. T., Herndon, S. C., de la Rosa Blanco, E., and Miake-Lye, R. C. (2011). Design Parameters for an Aircraft Engine Exit Plane Particle Sampling System. *ASME J. Eng. Gas Turbines Power*, 133:021501, doi: 10.1115/1.4001979.

Xiong, J. Q., Zhong, M., Fang, C., Chen, L. C., and Lippmann, M. (1998). Influence of organic films on the hygroscopicity of ultrafine sulfuric acid aerosol. *Environmental Science & Technology*, 32(22):3536–3541.

Yelvington, P. E., Herndon, S. C., Wormhoudt, J. C., Jayne, J. T., Miake-Lye, R. C., Knighton, W. B., and Wey, C. (2007). Chemical Speciation of Hydrocarbon Emissions from a Commercial Aircraft Engine. *J. Propul. Power*, 23:912-918.

Yu, F. and Turco, R. P. (2001). From molecular clusters to nanoparticles: role of ambient ionization in tropospheric aerosol formation. *Journal of Geophysical Research*, 106(5): 4797–4814.

Yu, F. (2005). Quasi-unary homogeneous nucleation of $H_2SO_4$-$H_2O$. *Journal of Chemical Physics*, 122(7):074501/1–074501/8.

Yu, F. (2007). Improved quasi-unary nucleation model for binary $H_2SO_4$-$H_2O$ homogenous nucleation. *Journal of Chemical Physics*, 127(5):054301/1–054301/8.

Zhang, R., Suh, I., Zhao, J., Zhang, D., Fortner, E. C., Tie, X., Molina, L. T., and Molina, M. J. (2004). *Atmospheric new particle formation enhanced by organic acids*. Science, 304: 1487–1490.

# 3 Laboratory measurements of soot interactions with organic species

## 3.1 Introduction

Particulate matter emissions from military aircraft engines can have significant environmental impacts (Finlayson-Pitts & Pitts 1997; Ramanathan et al. 2001). Accurate quantification is necessary for both the non-volatile black carbon soot emissions and the volatile contributions to particle mass. The scientific understanding of particle formation and growth is still evolving, and neither a complete predictive capability nor a standard measurement approach has been developed. The objective of this work is to develop fundamental understanding of microphysical processes of particle formation and growth by advancing microphysical modeling tools and by focused laboratory studies to characterize and quantify particulate matter emissions from military aircraft engines. As described in Section 2, a detailed microphysical model has been developed to include hydrocarbon species in addition to sulfuric acid. For the model to be quantitatively accurate, however, some parameters need to be determined for individual hydrocarbon species. Laboratory scale experiments were designed to measure the necessary parameters for the model. In this section, the microphysical model developed in Section 2 will be applied to a flow geometry representing the laboratory setup, and the relevant parameters will be optimized to best replicate the experimental measurements.

## 3.2 Compounds which influence the gas to particle evolution on the plume scale

In addition to the major gaseous species in the exhaust of a jet engine ($CO_2$, NO, $NO_2$, $H_2O$ and CO), trace amounts of volatile hydrocarbon species as well as sulfuric acid and nitric acid are found. Nitric acid, produced from combustor NOx, is present at lower levels than sulfuric acid, and nitrate aerosol is more volatile than sulfuric acid. Therefore, nitric acid is considered less important in the particle formation processes in the aircraft exhaust. As described in Section 2, the understanding of the contribution of sulfuric acid to the microphysical processes has been advanced significantly. Prior to this project and in literature sources the microphysical modeling and corroborating field measurements of sulfate aerosol are somewhat well developed. Assessments of the role of hydrocarbon species, however are still being developed. In particular, the fate of aromatic species or multifunctional hydrocarbons and other potential condensable species are important in determining atmospheric impact of jet exhaust. In this study, the condensation of hydrocarbons on soot is being measured, experimentally characterized and microphysically modeled. The experiment and modeling are complementary to each other because the experiment can provide necessary parameters for the model, and the model can help designing the experiment and interpreting the result thereof.

## 3.3 Experiment

This section describes the work undertaken in the laboratory phase of the project aimed at elucidating several key parameters for the microphysical model described in Section 2. The microphysical modeling of gas to particle processing (e.g. condensation) on soot particles requires knowledge of species volatility, initial concentration, and mass accommodation

coefficients on soot. The volatility and concentration establish the 'driving force' while the accommodation coefficient represents the efficiency of the gas-particle interaction. To investigate and understand the required parameters and compare to model predictions, controlled experiments were performed at UTRC with the help of ARI to determine uptake coefficients and condensational growth. The following conclusions were drawn from these experiments:

- Uptake coefficients of a variety of VOCs (including naphthalene and its derivatives, phenol, and water-soluble alcohols) by combustion soot were determined
- Condensational particle growth was not observed for species with vapor pressure below saturation limit
- Coating growth rates were relatively insensitive to temperature (over the tested range)
- A correlation between uptake coefficient and aqueous solubility was established
- Residence time and VOC concentration controlled coating growth rate
- Modeling simulations capture same trends for condensational growth of dicarboxylic acids on soot as observed in lab

### 3.3.1 Experiment Description

The combustion soot particles used in this study were produced by a miniCAST (Combustion Aerosol Standard, Model 5200); in this system, a miniature propane diffusion flame generates a steady stream of soot particles with a lognormal poly-disperse size distribution. Mean geometric soot size is controlled by adjusting flow parameters of the miniCAST according to the operation manual. As shown in Figure 3.1 and Figure 3.2, a secondary (external) dilution system was then applied at the exhaust of the miniCAST to control soot concentration and total flow rate. Particle size distribution in mobility diameter ($D_m$) was measured by a scanning mobility particle sizer (SMPS, Model 3936, TSI). The geometric mean diameter (GMD) of the generated soot particles was controlled by precisely setting the flame stoichiometry and dilution parameters provided by the designer of the miniCAST. The concentration and size distribution of the produced soot particles were repeatable over the investigation; however, a gradual decrease in particle concentration occurs over time requiring cleaning of the system. Both poly-disperse and mono-disperse distributions were used during the investigation.
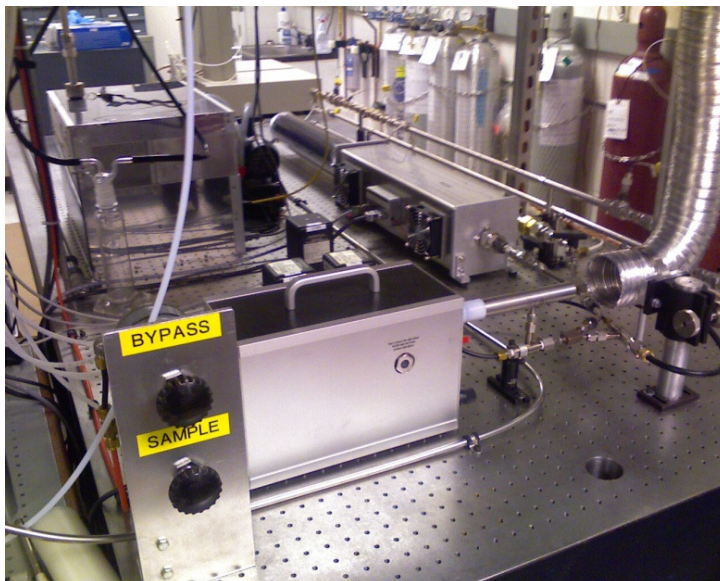


**Figure 3.1 MiniCAST soot generator and the secondary dilution apparatus**
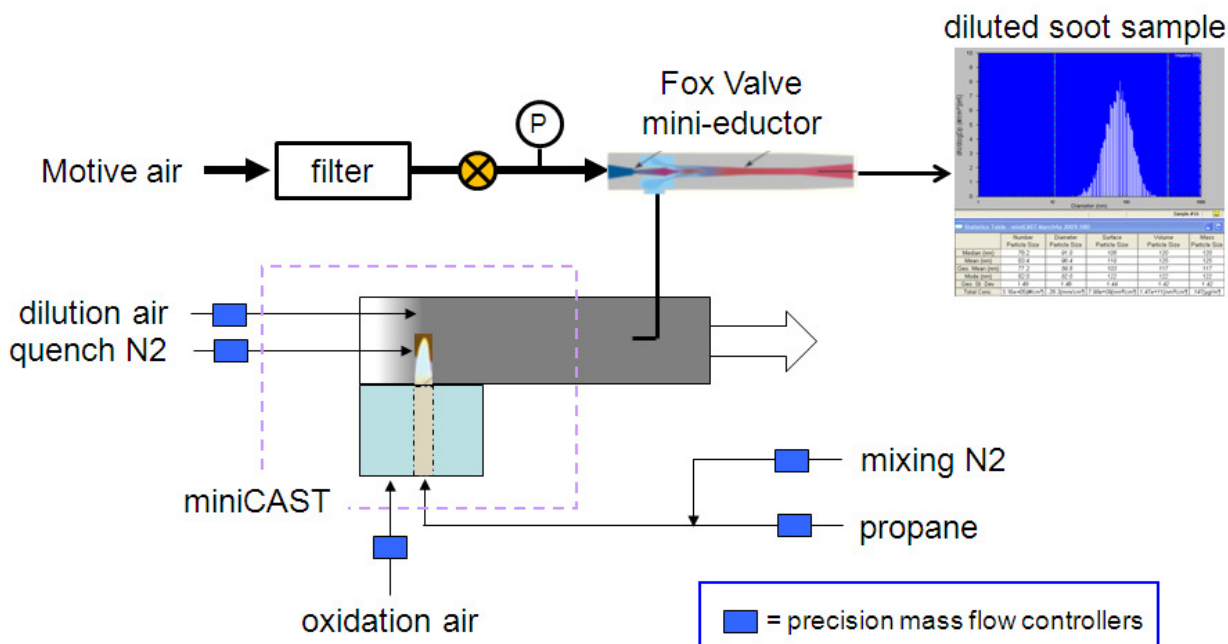
**Figure 3.2 Schematic of the flow configuration to utilize the miniCAST as a soot generator**

The VOC delivery system was heated stainless tubing with 15.9 mm outside diameter in junction with a constant nitrogen flow of 0.9 liter per minute (LPM). The gas-phase total carbon concentration was continuously monitored with a heated flame ionization detector (HFID). The HFID was constrained to a detection limit of approximately 1 part per million carbon (ppm C). The HFID was also limited by a sampling system which could only be heated to ~160 °C. The VOC vapor was produced in a heated tube from high-purity samples at ambient or a slightly higher temperature to generate a signal of 10-200 ppmC from HFID. The heating temperature was controlled by heating elements accurate to 2-3 °C. In all cases considered during this soot coating investigation, the resulting partial pressure of the introduced VOCs was below their saturation vapor pressure.

In addition, before mixing with the vaporized VOCs, the soot stream was passed through a thermal denuder (TD) at 150 °C to remove the volatile and semi-volatile components and ensure low organic coating on the soot particles (Huffman et al. 2008). As demonstrated in Figure 3.3 from the SMPS measurements, the timeline shows the response of a typical soot stream to conditioning by the TD. Soot particle concentration was constant while particle size decreased when the TD was on and increased when the TD was off.

Since the dry accommodation of VOC by the soot particles is usually small, the PM mass of VOC coated on the soot particles was measured by a compact Time-of-Flight Aerosol Mass Spectrometer (CToF-AMS), made by Aerodyne Research, Inc. At present it is the only available instrument capable of simultaneously providing quantitative size and chemical mass loading information in real-time for non-refractory sub-micron aerosol particles. The description of the AMS instrument has been provided in detail in previous publications (Jayne et al 2000). In brief, the AMS uses an aerodynamic lens to focus the particles into a narrow beam that is then introduced into a high vacuum chamber while the air is differentially pumped. Volatile and semi-volatile species in/on the particles are vaporized on a heated, roughened molybdenum surface under high vacuum ($10^{-7}$ Torr) at about 600°C. The vaporized species are then ionized by the impact of energetic electrons (70 eV). The ions formed are analyzed by a time-of-flight mass

spectrometer (Tofwerk, Thun, Switzerland). Particle aerodynamic size is determined via particle time-of-flight, with the starting time provided by the opening time of a rotating beam chopper and the arrival time by the chemical detection. It offers detailed information of both particle size distribution in volume domain and volatile chemical compositions of lubricant oil PM emissions by monitoring size-dependent characteristic mass spectrum of semi-volatile PM.

To produce a reasonable signal-to-noise ratio for the AMS measurement, we use a high concentration of poly-disperse soot particles to investigate the dry accommodation of a number of semi-volatile compounds. To study the condensational growth of soot particles exposed to dicarboxylic acids, we use a mono-disperse distribution since the soot particles grow so dramatically that they can be easily measured with the SMPS. To generate mono-disperse soot particles, the denuded soot stream went through a TSI 3081 differential mobility analyzer (DMA), set at 50, 90, 120, and 160 nm for this study. We also let the soot flow bypass the DMA to investigate VOC condensation on the poly-disperse soot particles.
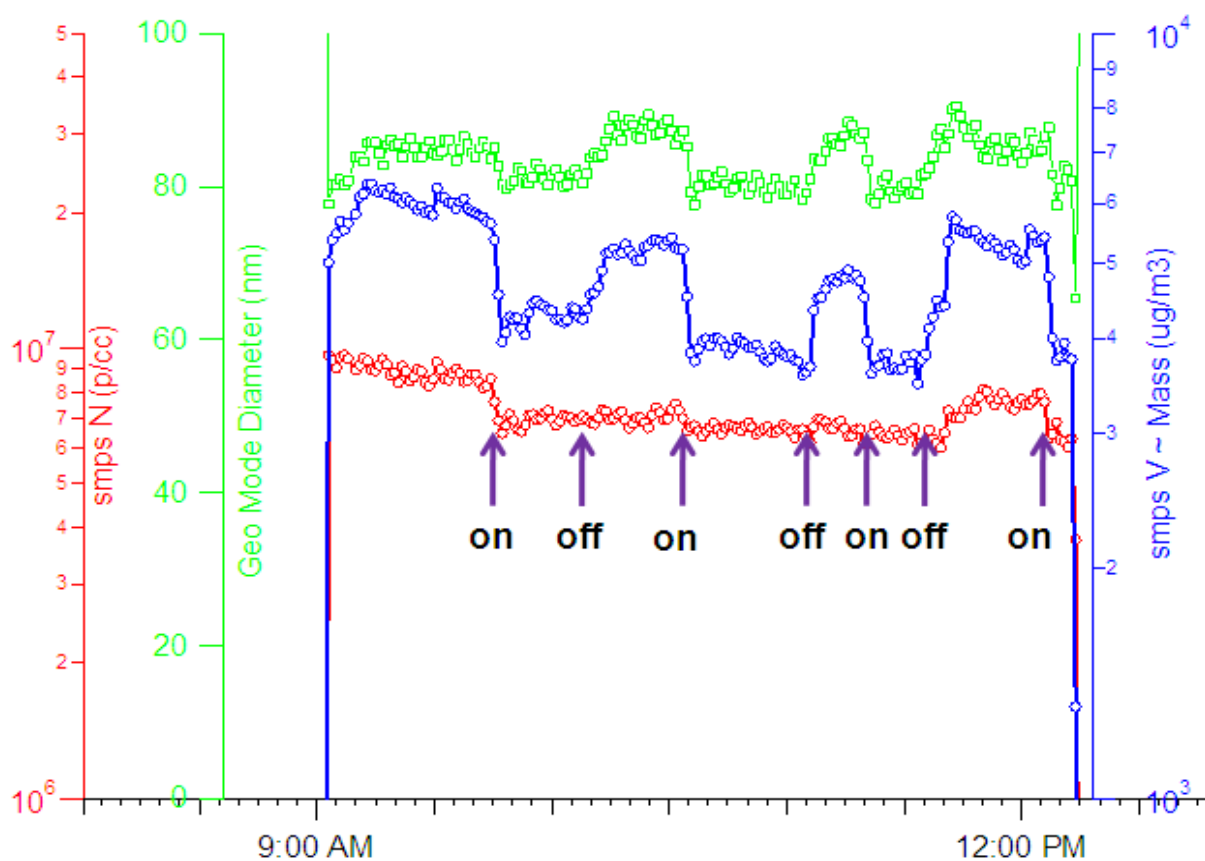


**Figure 3.3 The timeline showing the response of a typical soot stream to conditioning by the TD**

As shown in the schematic of the entire experimental configuration (Figure 3.4), the particle sampling occurs along the mixing tube. The coated soot sample was measured using SMPS and AMS. The SMPS measures particle size in mobility diameter and concentration while the AMS determines particle size in aerodynamic diameter and semi-volatile composition coated on soot particles.
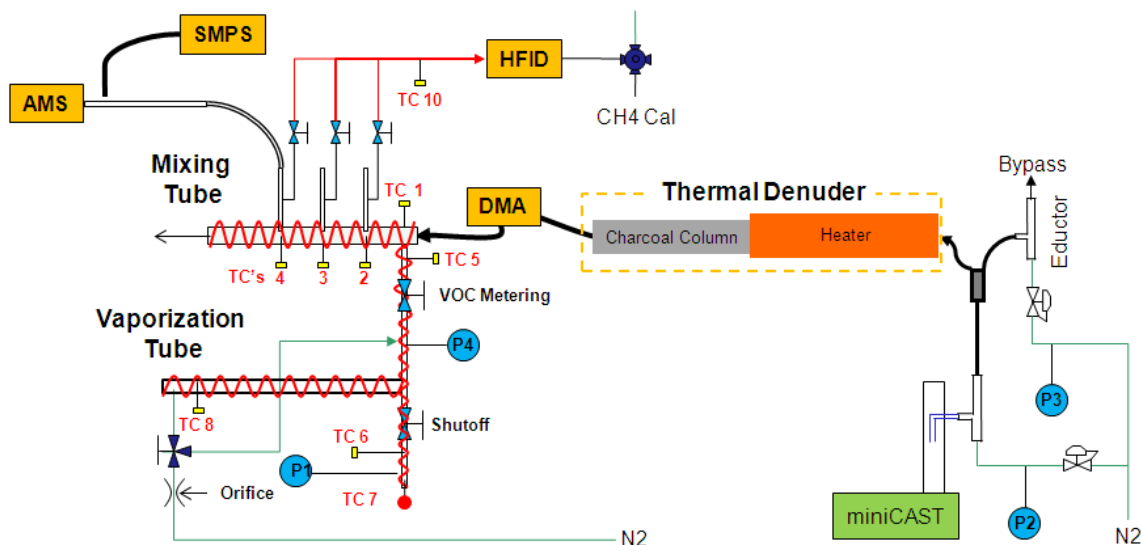


**Figure 3.4 Schematic of Laboratory Experiment to Measure VOC Condensation**
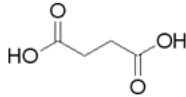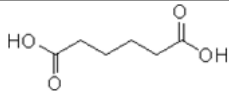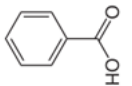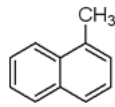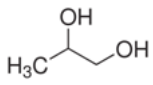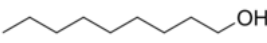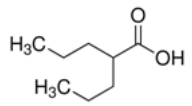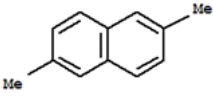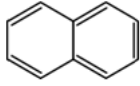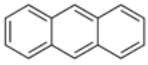
### 3.3.2    Reference Compounds

A number of hydrocarbons, including aromatics such as naphthalene ($C_{10}H_8$) and its derivatives, alkanes like tetradecane ($C_{14}H_{30}$), and water soluble organics such as phenol ($C_6H_6O$) and adipic acid ($C_6H_{10}O_4$), were utilized in this study to investigate the mass accommodation and condensation characteristics of hydrocarbons on combustion soot particles. Among the selected hydrocarbons, naphthalene, alkanes, and phenol have been detected by proton transfer reaction mass spectrometer (PTR-MS) in real-time from commercial aircraft engine exhausts in past field investigations sponsored by EPA and FAA (Spicer *et al.* 1992 and Knighton *et al.* 2007).

Literature value of vapor pressure measurements indicate that some of them are highly volatile while others are not (see Table 3.1).  Significant variation in chemical properties and vapor pressure enables us to evaluate the contribution of these properties to volatile condensation and subsequent growth of the soot particles.

Vapor pressure of 1-methylnaphthalene is 6.8 Pa at ambient temperature, compared to less than 1 ppm or 0.1 Pa for sulfuric acid; this suggests that 1-methylnaphthalene is quite volatile relative to sulfuric acid. In this study, the mixing ratio of 1-methylnaphthalene at the point of mixing with the soot flow was controlled at approximately 10 ppm, which is comparable to composition in the combustion emission exhaust of modern aircraft engines.

**Table 3.1 List of the Measured Volatile Organic Compounds**

| name | formula | MW | MP | BP | Vapor Pressure at 25C | Density at 20C | |
|---|---|---|---|---|---|---|---|
| | | (g/mol) | (deg C) | (deg C) | (atm) | (g/ml) | |
| n-dodecane | C12H26 | 170.3 | -9.6 | 216 | 3.95E-04 | 0.75 | CH3(CH2)10CH3 |
| n-tetradecane | C14H30 | 198.4 | 5.5 | 253 | 3.75E-05 | 0.763 | CH3(CH2)12CH3 |
| n-hexadecane | C16H34 | 226.5 | 18 | 287 | 6.58E-07 | 0.773 | CH3(CH2)14CH3 |
| n-docosane | C22H46 | 311.0 | 42 | 369 | | 0.78 | CH3(CH2)20CH3 |
| succinic acid | C4H6O4 | 118.0 | 186 | 235 | 2.24E-05 | 1.56 | |
| adipic acid | C6H10O4 | 146.0 | 152 | 338 | 1.00E-06 | 1.36 | |
| Benzoic acid | C6H5COOH | 122.0 | 122 | 249 | 7.00E-07 | | |
| 1-methylnaphthalene | C11H10 | 142.2 | -22 | 240 | 8.91E-05 | 1.00 | |
| propylene glycol | C3H8O2 | 76.1 | -59 | 188 | 1.97E-04 | 1.04 | |
| 1-nonanol | CH3(CH2)7CH2OH | 144.2 | -6 | 214 | 2.99E-05 | 0.83 | |
| valproic acid | (CH3CH2CH2)2CHCO2H | 144.2 | | 220 | 6.05E-05 | 0.9 | |
| 2,6-dimethylnaphthalene | C10H6(CH3)2 | 156.2 | 106 | 264 | 2.09E-05 | 1 | |
| naphthalene | C10H8 | 128 | 80 | 218 | 1.26E-05 | 1.1 | |
| phenol | C6H5OH | 94 | 43 | 182 | 4.60E-04 | 1.07 | |
| anthracene | C14H10 | 178.2 | 217 | 342 | 1.73E-06 | 1.28 | |

In this study, semi-volatile species like naphthalene and phenol were controlled at room temperature so the mixed VOC vapor was below their saturation vapor pressures. The coating mechanism of the VOC on the soot particles was mainly dry accommodation. On the other hand, low-volatility compounds such as adipic acid were heated and then introduced into the mixing tube at a much lower temperature. Therefore the vapor of such species was super-saturated. In these cases, coating on the soot particles was dominated by wet accommodation process.

### 3.3.3 Model of the apparatus

The objective of this experiment was to obtain the values of critical parameters (e.g. mass accommodation coefficients) in the microphysical model. Such parameters were determined by fundamental analysis of the experimental results and by comparing the experimental values with the microphysical modeling. The test setup was modeled to consist of a condensation tube and a sample transfer line.

Figure 3.5 shows a schematic of the model representation of the experimental setup. The condensation tube was 1/2" in diameter and 10 cm in length. The sample transfer line was 1/4" diameter with a length of 90 cm. The mixture of streams, one having soot particles and the other containing hydrocarbon vapor, enters the condensation tube. During experiments studying condensation of dicarboxylic acids on soot particles, the soot concentration was typically about $1\times10^5$ cm$^{-3}$ for monodisperse cases, and the total flow rate was 0.6 LPM. The initial temperature of the reactant was about 60$^o$C.
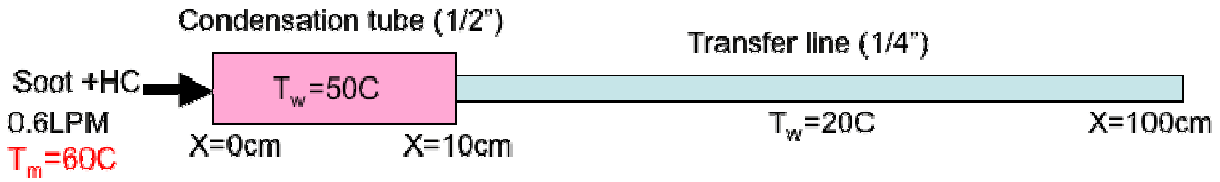


**Figure 3.5 Model Representation Scheme for Laboratory Experimental Data Evaluation**

We had the capability of actively controlling the wall temperature of the condensation tube, so the model assumed that the condensation tube wall was kept at 50$^o$C. The transfer line was exposed to the room temperature, so it was modeled to have a constant wall temperature of 20$^o$C. Based on these wall temperatures, the mean temperature profile of the sample can be estimated using a heat transfer model.

The Reynolds number was always smaller than 150 for the flow conditions of interest, and the thermal entry length is under 3 cm both for the condensation tube and the transfer line. Therefore, it is reasonable to use a fully-developed laminar flow model with constant wall temperature boundary conditions (for each section), the governing equation of which is:

$$\frac{T_m(x) - T_w}{T_m(0) - T_w} = exp\left(-\frac{\pi D \bar{h}}{\dot{m}C_p}x\right)$$

[3.1]

Figure 3.6 shows the temperature profile of the baseline case, calculated by Equation (1). Figure 3.6 indicates that the reactant spends about 1.5 seconds in the condensation tube, and another 3 seconds in the sample transfer line. The temperature is about 20$^o$C for more than half of its residence time.

55
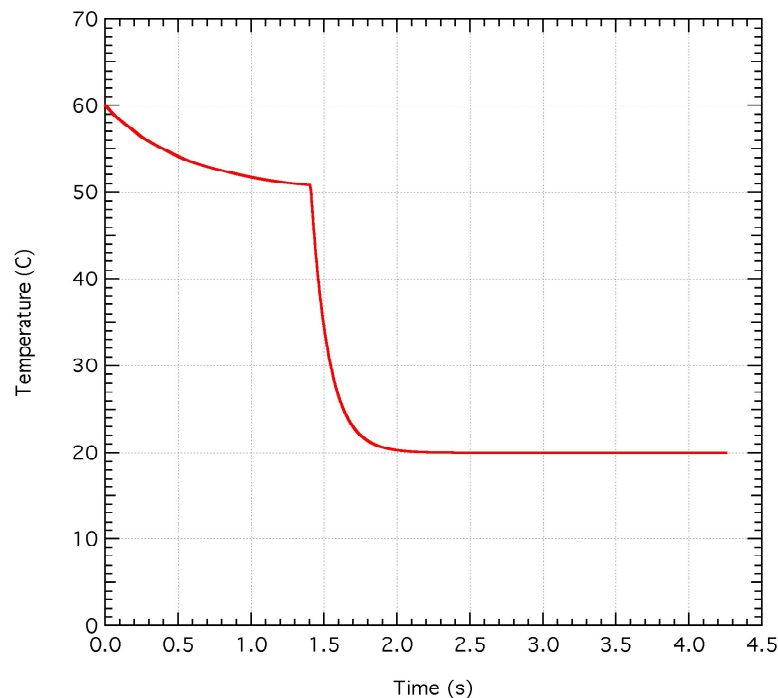
**Figure 3.6 Temperature profile for baseline model simulation**

Parametric studies were performed using this model.  The first study was to see the effect of saturation vapor pressures of different hydrocarbon species.  For this, the initial VOC concentration was varied using three different species: adipic acid, anthracene, and 1-methylnaphthalene, and the results are shown in Figure 3.7.  Soot particles were modeled to have an initial monodisperse diameter of 90 nm with a concentration of $1\times10^5$ cm$^{-3}$.  The simulation result indicates that condensational growth of soot particles requires supersaturation of the hydrocarbon vapor.  It also shows that there exists a threshold concentration for significant particle growth, and the threshold concentration depends on the saturation vapor pressure of each species.  Through the modeling, it is anticipated that particle growth would be observed for adipic acid with an initial concentration of ~1 ppm, but not with anthracene or 1-methylnaphthalene with a similar initial concentration.  Particle growth would be observed for anthracene with a higher initial concentration (~10 ppm), but species with higher saturation vapor pressure (e.g. toluene, naphthalene, and methyl- naphthalene) would never show significant particle growth experimentally.  As will be discussed in the next section, the simulation result is consistent with the experimental result.
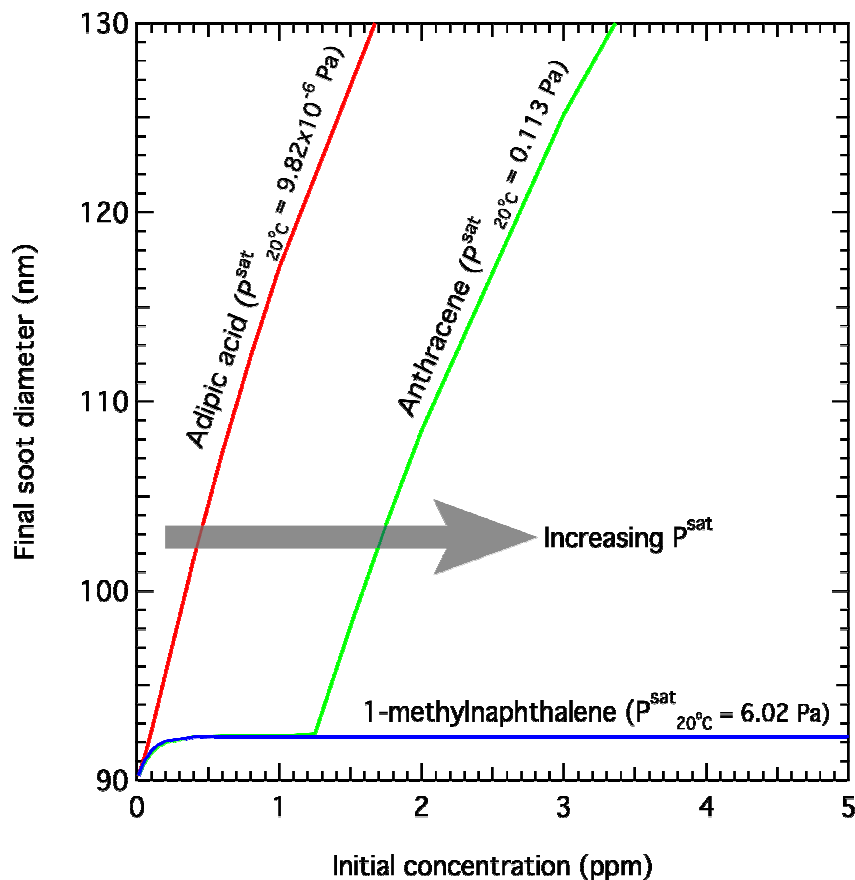
**Figure 3.7 Model simulation for adipic acid, anthracene and methyl-naphthalene**

We also explored the impact of mass accommodation coefficients using anthracene as a demonstration. Figures 3.8 and 3.9 show the model sensitivity to wet and dry mass accommodation coefficients, respectively. The results indicate that the wet mass accommodation coefficient ($\alpha_w$) determines the slope of the condensational growth when the initial hydrocarbon concentration is higher than its threshold concentration (Figure 3.8). On the other hand, Figure 3.9 shows that the dry mass accommodation coefficient ($\alpha_d$) determines the final soot diameter if the supersaturation of the hydrocarbon vapor is not reached (i.e. initial concentration is lower than the threshold concentration). If the vapor is supersaturated and $\alpha_d$ is higher than a certain value (0.001 in this case), it has no impact on the final soot diameter because the surface is fully activated before the condensational growth occurs. The threshold concentration is not affected by the mass accommodation coefficients, but affected only by the saturation vapor pressure of the species. These simulation results provide a couple of insights to guide experimental studies:

*1) To determine the wet mass accommodation coefficient of a hydrocarbon species, we need to vary the concentration above the threshold concentration, and see the size response in the SMPS.*

*2) To determine the dry mass accommodation coefficient, we need to vary the concentration below the threshold concentration. The SMPS is likely not able to detect the size change, so we need to see the coating mass on the AMS.*

57
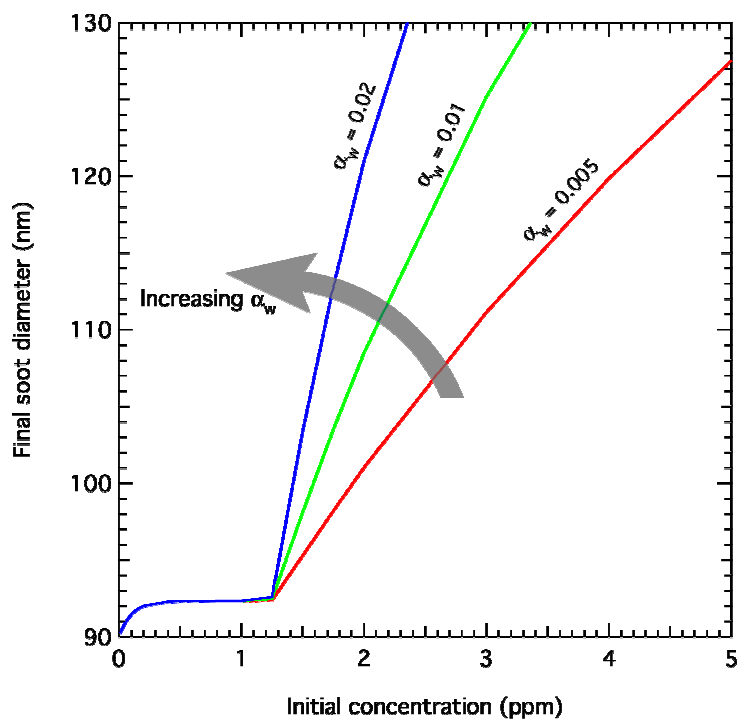
**Figure 3.8 Model simulations for different wet mass accommodation coefficients (using anthracene as a demonstration)**
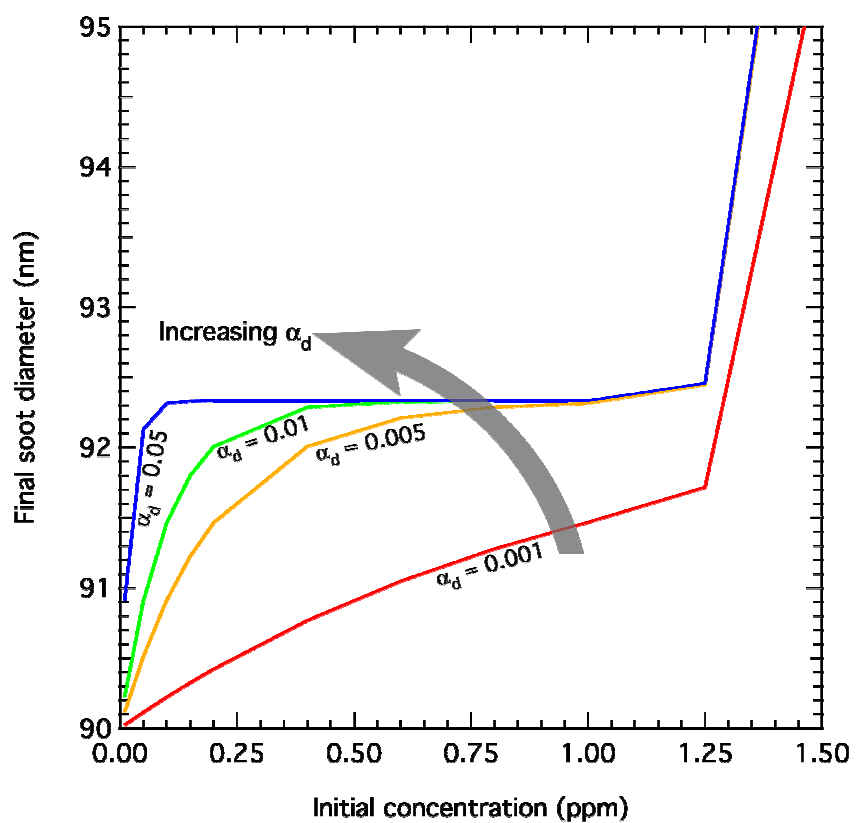


**Figure 3.9 Model simulations with varying dry accommodation (anthracene)**

### 3.3.4 Analysis of Experimental Data

### 3.3.4.1 Naphthalene

### 3.3.4.1.1 Determination of Effective Uptake Coefficient

To derive physical information of the dry accommodation process directly from the experimental measurements in this study, we define the effective uptake coefficient, $\gamma_{obs}$, as the probability of a gaseous VOC molecule sticking on the soot surface, according to the gas uptake model developed by Worsnop and coworkers (Davidovits et al 1995; Worsnop et al. 1989). The uptake coefficient ($\gamma$) can be expressed as:

$$\frac{1}{\gamma} = \frac{1}{\Gamma_{diff}} + \frac{1}{\alpha} + \frac{1}{\Gamma_{sat} + \Gamma_{rxn}} \qquad [3.2]$$

The model description of uptake of gaseous species by particulate matter without condensation includes the following kinetic processes: gas-phase diffusion resistance ($\Gamma_{diff}$), mass accommodation ($\alpha$), the resistance due to liquid-phase saturation limitation ($\Gamma_{sat}$), and the liquid-phase reaction ($\Gamma_{rxn}$). In cases where there is no significant reactive loss, Equation 3.1 reduces to:

$$\frac{1}{\gamma} = \frac{1}{\Gamma_{diff}} + \frac{1}{\alpha} + \frac{1}{\Gamma_{sat}} \qquad [3.3]$$

In this study, all the applied organic compounds are chemically stable under the experimental conditions. Even with the heating of VOC, the mixing area between soot particles and VOC vapors was set to be kept at a temperature of only 60°C. There should be no chemical reaction between the applied VOC and the soot particles. In addition, for uptake on the soot surface, we will neglect the resistance due to liquid-phase saturation limitation, $\Gamma_{sat}$.

In the atmosphere, for typical submicron-sized aerosol particles, gas-phase diffusion does not usually limit uptake coefficients unless the uptake coefficient is large. For example, for 0.1 $\mu$m diameter droplets at 1 atm, $Kn$ = 1.5 (assuming a gas-phase diffusion coefficient, $D_g$ of 0.1 atm cm$^2$ s$^{-1}$ and $c$ = 4×10$^4$ cm s$^{-1}$), giving $1/\Gamma_{diff}$ = 0.3. If $\alpha$ is less than 0.1, the gas-phase diffusion contribution is trivial. Typically, $\gamma$ has been found to be between $10^{-5}$ and $10^{-3}$ such that $1/\gamma$ is between $10^3$ and $10^5$. The geometric mean diameter (GMD) of the generated soot particles is around 120 nm in mobility diameter. Based on the above argument, we believe that in this experiment, the gas-phase contribution to naphthalene uptake by soot particles is negligible.

Combustion soot particles are usually a combination of elementary carbon (EC) and organic carbon (OC). The OC composition varies with the formation condition of the soot particles. To emphasize the uptake of VOC by ideal soot surface, the majority of organic coating on the soot particles initially generated from the miniCAST was removed through a thermal denude. The uptake of VOC by the soot particles becomes a pure interaction between gas species and solid surface. Thus the liquid-phase saturation effect also becomes negligible. Therefore the $\gamma_{obs}$ obtained through this experiment can be considered as the mass accommodation coefficient:

$$\frac{1}{\gamma_{obs}} \approx \frac{1}{\alpha} \qquad [3.4]$$

The effective uptake coefficient, $\gamma_{obs}$, can be experimentally determined by the measurements on uptake of VOC and collisions with soot per molecule as the following:

$$\frac{\Delta n}{n} = \gamma_{obs} \frac{c A_d N}{4 F_g} \qquad [3.5]$$

where $\Delta n$ is the VOC mass coated on soot particles and measured by the CToF-AMS; $n$ is the concentration of the VOC vapor measured by the HFID; $c$ is the mean thermal velocity of VOC vapor, which equals $\sqrt{\dfrac{8RT}{\pi M}}$ ; $N$ is the total number of soot particles determined from the SMPS measurement; $A_d$ is the surface area of soot particle; and $F_g$ is the system flow rate. The determination of $A_d$ is described in the next section. A portion of the AMS and HFID measurements on uptake of naphthalene by poly-disperse soot particles is presented in Figure 3.10. Here $\Delta n / n$ represents the uptake of VOC vapor by soot surface while $cA_d N / (4F_g)$ is the collisions per molecule. The total PM organic mass shows immediate response to the introduction of naphthalene vapor, which is monitored by the HFID. The baseline drift from the AMS measurement is due to the variation in mixing ratio between the VOC and soot flows.
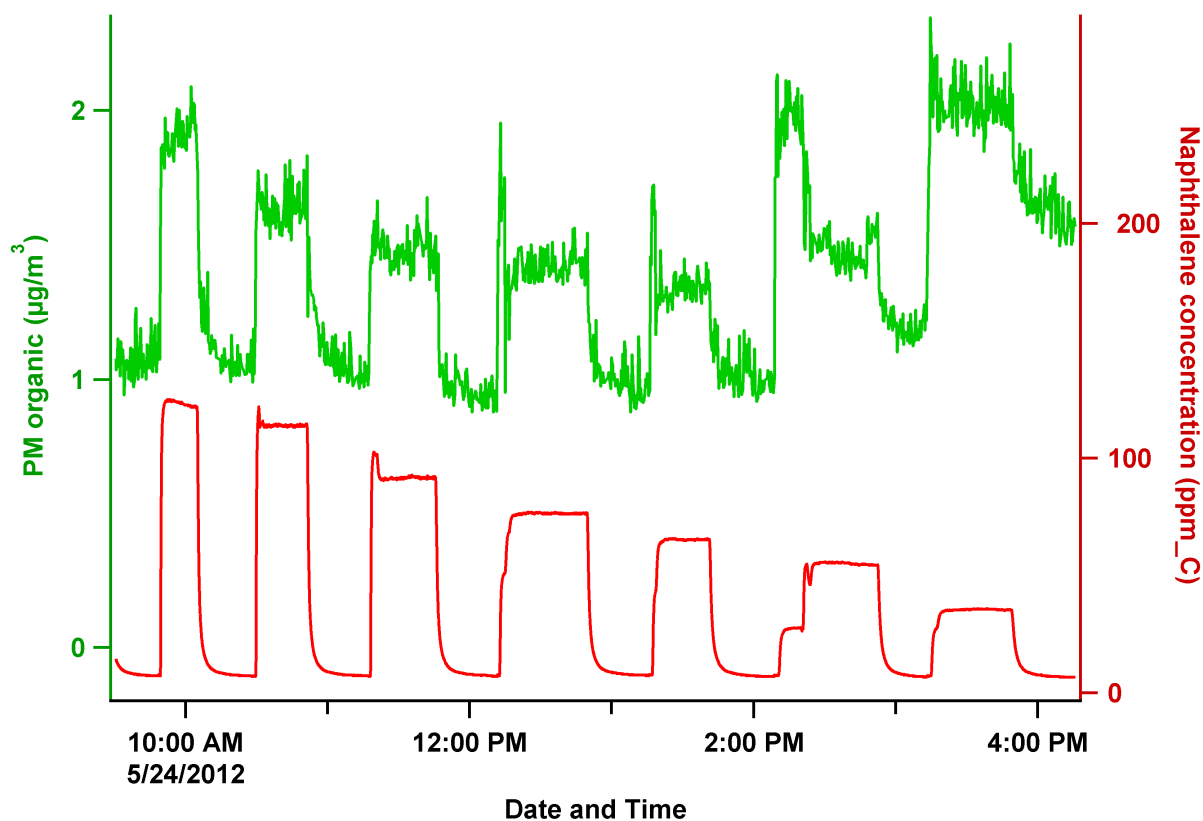


**Figure 3.10 A portion of AMS and HFID measurements on naphthalene**

### 3.3.4.1.2  Estimate of Surface Area

Combustion soot particles are fractal dimensional aggregates in nature. Since the properties of fractal aggregates, such as mass and surface area, do not dimensionally scale according to the mathematics of Euclidean geometry, conventional particle size measurement cannot lead to the determination of particle surface area. In this study, we applied a phenomenological approach to determine particle surface area based on simultaneous SMPS and AMS measures (Cross et al. 2010). This method has been discussed in detail in the previously published papers (DeCarlo et al. 2004; Slowik et al. 2004). In brief, the SMPS measures particle

60

size distribution in mobility diameter ($D_m$) while the AMS measures in vacuum aerodynamic diameter ($D_{va}$). Based on the measured $D_{va}$, $D_m$, and chemical composition of the particles, a method was developed by Slowik and coworkers to determine volumetric equivalent diameter ($D_{ve}$) from the AMS-SMPS measurements. The relationship between the determined $D_m$ and $D_{va}$ for mono-dispersed soot particles are plotted in Figure 3.11. It is consistent with the observation of Type I soot by Cross and coworkers during the Boston College Soot Investigation. The estimated surface area was then calculated from the obtained $D_{ve}$ with the assumption of spherical particles.
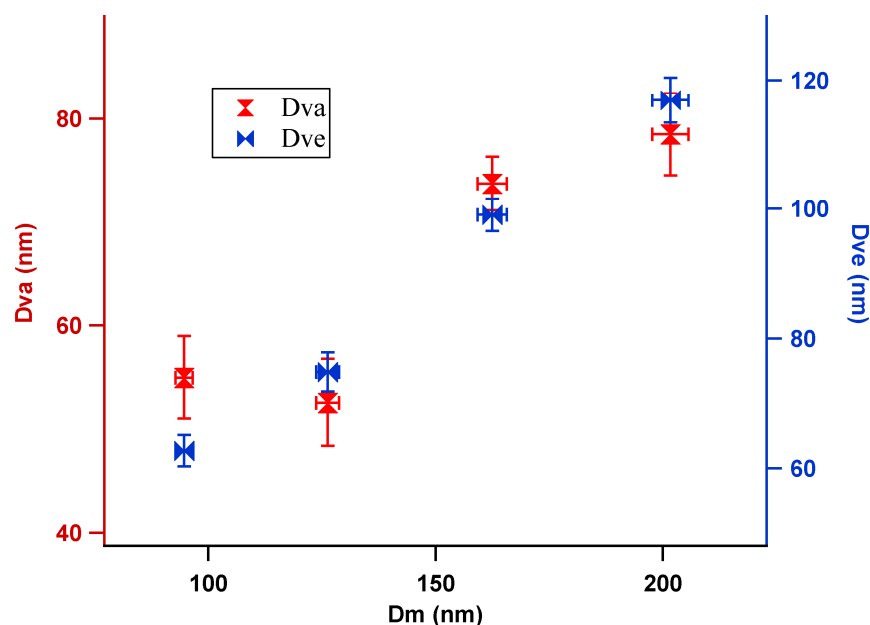


**Figure 3.11 Relationship among mobility diameter (Dm), vacuum aerodynamic diameter (Dva) and volumetric equivalent diameter (Dve) for mono-disperse soot particles**

The significant discrepancy between $D_{va}$ and $D_m$ indicates that the miniCAST-generated soot particles are highly fractal. Compared to the direct black carbon mass measurement technique such as Couette Centrifugal Particle Mass Analyzer (CPMA), the measurement error of the AMS-SMPS method on particle mass is less than 20%. Therefore the corresponding error on $D_{ve}$ should be no more than 7%.

### 3.3.4.1.3  Impact of Uptake on Particle Size

Uptake of volatile inorganic and organic species in gas phase is one of the fundamental mechanisms for the growth of particulate matter. In this study, significant growth of soot particles from condensation of VOC can be detected in term of particle size increase by the AMS and SMPS measurements, while a thin coating can only be detected as PM mass increase with the AMS. As shown in Figure 3.12, particle size distribution in mobility diameter from the SMPS measurements remains essentially the same when 6.9 ppm naphthalene was mixed with the denuded soot particles. These observations suggest that uptake of unsaturated naphthalene vapor by the combustion soot particles under ambient condition may be a thin coating on the soot surface and therefore the particle growth is undetectable from the SMPS measurement.
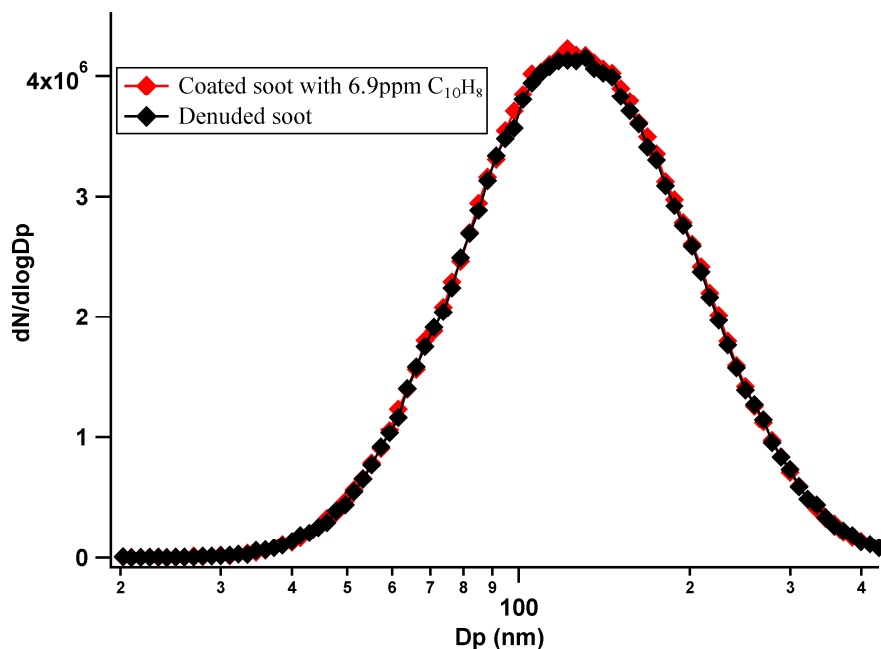
**Figure 3.12 Particle size distributions in mobility diameter from the SMPS measurements**

The AMS measurement allows another investigation of soot particle growth. Since the AMS detects the volatile and semi-volatile composition of combustion soot particles, in principle completely denuded soot particles cannot be monitored by this technique. However there is always a trace amount of organic PM left on the denuded soot particles. In our case, about 0.1% of the denuded soot particle mass is semi-volatile organic species. As shown in Figure 3.13, introducing VOC vapor results in significant increase in measured organic PM mass, while the particle size distribution in aerodynamic diameter remains the same. This observation from the AMS is consistent with that from SMPS. It again suggests that the mass of VOC due to uptake by the soot particles is small but measureable compared to the total soot mass.
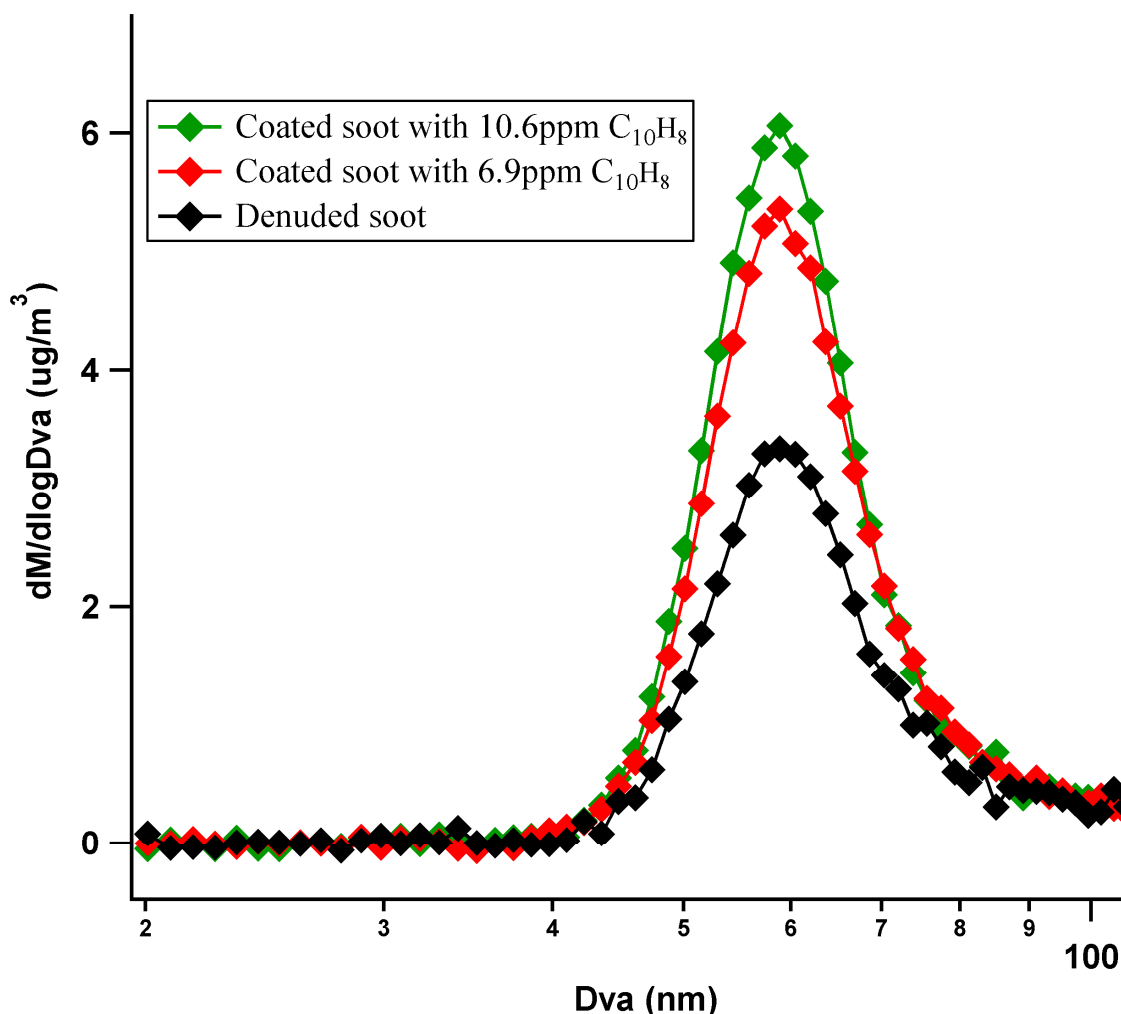
**Figure 3.13 Particle size distribution of denuded and naphthalene-coated soot particles**

### 3.3.4.1.4 Results and Discussion

According to equation (5), a linear fit of $\Delta n$ vs $cnA_dN/(4F_g)$ yields the effective uptake coefficient, $\gamma_{obs}$. This requires the simultaneous measurements on VOC concentration ($n$), particle size ($A_d$), and VOC mass on PM ($\Delta n$). As shown in Figure 3.14, the effective uptake coefficient naphthalene of was then determined to be $(1.56\pm0.05)\times10^{-6}$ in this study, with the correlation coefficient $R^2 = 0.956$. The uncertainty of the uptake coefficient represents $1\sigma$ precision of the fitting without the consideration of systematic uncertainty. The naphthalene concentrations in gas were measured by the HFID from 3 to 11 ppm, with an experimental uncertainty of 0.1ppm.
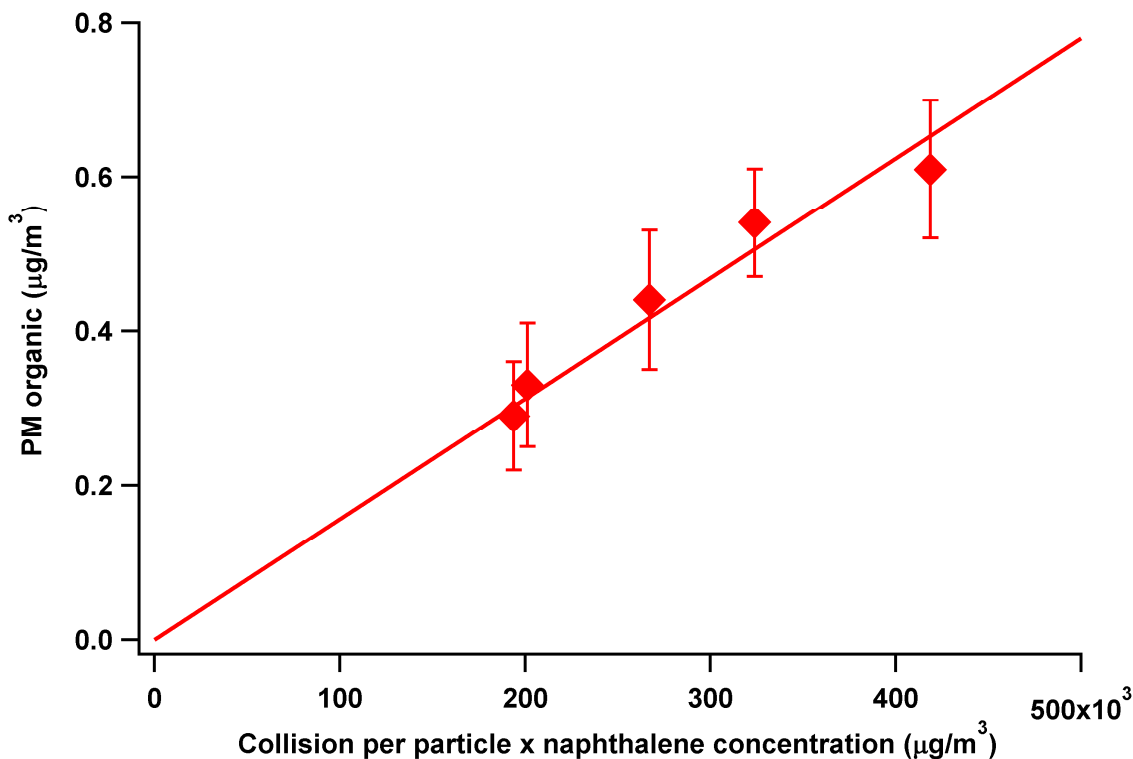
**Figure 3.14 Determination of uptake coefficient of naphthalene based on a kinetic model**

This quantitative analysis on uptake coefficient of naphthalene on soot is based upon two critical assumptions: 1) soot surface area determination from AMS-SMPS methodology; and 2) transmission efficiency of unity for the aerodynamic lens. The first assumption has been discussed in the previous section. A direct measurement on soot surface area is technically difficult. On the other hand, its nature of fractal dimension requires geometric or physical assumption to convert the measured particle size into volume or surface area. The applied AMS-SMPS method has been proved in the past as an efficient and reliable approach to determine volumetric equivalent diameter for the soot particles.

With regard to the second assumption, aerodynamic lens systems have been widely used to generate collimated narrow particle beams since they were invented by Liu et al. in 1995 (Liu et al. 1995a and 1995b). The collimated particles are subject to certain loss due to impact and diffusion. Particle loss of the aerodynamic lens systems are usually evaluated by experimental measurements or numerical simulations. The aerodynamic lens is considered highly efficient in focusing spherical particles in the size range of 40-700 nm. In this study, transmission loss of aerodynamic lens was not evaluated and corrected. A comparison study by Liu et al. with model calculations and laboratory measurements on transmission efficiency suggests that for the particles of 60 nm in aerodynamic diameter, the efficiency is approximately 15%. However due to the fractal nature of soot particles and the lack of combustion soot size standard, it is difficult to evaluate transmission efficiency of soot inside the applied aerodynamic lens. Corrected by this efficiency, the uptake coefficient of naphthalene by combustion soot particles is $(1.11\pm0.03)\times10^{-5}$.

Raja and Valsaraj studied uptake of gas-phase naphthalene by micron-size fog droplet and found that the mass accommodation coefficient is $4.0\times10^{-4}$ at 22°C, greater than that predicted by gas-water phase equilibrium. Our results show that uptake of gas-phase naphthalene

64

by the denuded combustion soot particle is smaller than that by micron-size water droplet even though soot particle is generally considered hydrophobic. Hennings and coworkers investigated hygroscopic growth and activation of miniCAST soot particles by succinic acid and sulfuric acid. Their results demonstrate that there is no particle growth or activation with the volatile species in nitrogen as carrier gas, indicating a very small uptake coefficient, consistent with our observation. Compared to the surface of micron-size water droplet, combustion soot particles generated by the miniCAST seem inert to the adsorption of gas-phase hydrocarbon compounds.

### 3.3.4.2 Uptake investigations on a variety of organic compounds

### 3.3.4.2.1 Physical properties of the studied organic compounds

The uptake study on soot particles yields the mass accommodation coefficient for the VOCs, which is defined as the probability of a gaseous molecule sticking on soot surface. Based on the discussion in the previous section, the determined uptake coefficient in this study equals the mass accommodation coefficient if the impact of gas-phase diffusion is negligible. Uptake of organic gas phase species by ethylene glycol, 1-octanol, and 1-methylnaphthalene has been extensively investigated by Zhang and coworkers (2003). They found that uptake coefficients of water-soluble species such as HCl by 1-methylnaphthalene is less than $10^{-3}$ compared to 0.44 and 0.47 for m-xylene and α-pinene, respectively. It appears that chemical affinity of the interface and physical properties of organic compounds play significant roles in uptake kinetics.

Solubility of naphthalene in water is merely 30 mg/L at ambient conditions (*i.e.* nearly insoluble). As with the rest of the PAHs in this investigation, it is considered hydrophobic. In this study, in addition to the measurement on uptake of naphthalene, a number of water-insoluble and soluble volatile organic compounds were also investigated for their uptake properties. These compounds include 1-methylnaphthalene ($C_{11}H_{10}$) and 2,6-dimethylnaphthalene ($C_{12}H_{12}$), which are derivatives of naphthalene and water-insoluble; propylene glycol ($C_3H_8O_2$) and phenol ($C_6H_6O$), which are organic alcohols and water-soluble; 1-nonanol ($C_9H_{20}O$), another organic alcohol but slightly water-soluble (~1 g/L); dodecane ($C_{12}H_{26}$), tetradecane ($C_{14}H_{30}$) and hexadecane ($C_{16}H_{34}$), all water-insoluble paraffins.

At ambient conditions, all the species yield an appreciable vapor pressure from 2.8 Pa for 2,6-dimethylnaphthalene to 61 Pa for phenol. Because of the relatively low vapor pressures of 2,6-dimethylnaphthalene (2.8 Pa) and 1-nonanol (4.0 Pa) at room temperature, the vaporization tube was slightly heated at keep the temperature 5-10°C above room temperature for the two compounds in order to generate a well-detectable vapor for the HFID measurement. For all the studied compounds, vapor pressures of the mixing soot/VOC flow were below saturation limit so that condensational growth of the VOCs on the soot particles would not occur. A thin coating on soot particles through uptake process would occur and be measured using the AMS.

### 3.3.4.2.2 Results from laboratory measurements

The methodology used to determine uptake coefficient for these compounds was the same as we described in the previous section. In brief, The SMPS measures particle size in mobility diameter and concentration; the AMS determines particle size in aerodynamic diameter and semi-volatile composition coated on soot particles; and the HFID measures the VOC concentration from the mixed soot/VOC flow. The mixing ratio of the soot and VOC flows was

controlled to yield the VOC concentration between 20 – 150 ppm C. The miniCAST generated soot particles had the same size distribution for all the VOCs tested.

Most of the studied compounds gave similar data quality from the SMPS, AMS and HFID measurements to naphthalene. For instance, a portion of the AMS and HFID measurements on phenol is shown in Figure 3.15. The green line is the measured total PM organic mass from the AMS without correction of transmission efficiency and the red line is the measured phenol concentration in the mixed soot/VOC flow by the HFID. The obtained PM organic mass responded almost simultaneously to the variation of phenol concentration, indicating that the response delay due to the large wall area of sampling tube is negligible in this case. Experimental uncertainty is approximately 0.2 $\mu$g m$^{-3}$ for the AMS measurement and 0.1 ppm C for the HFID measurement.
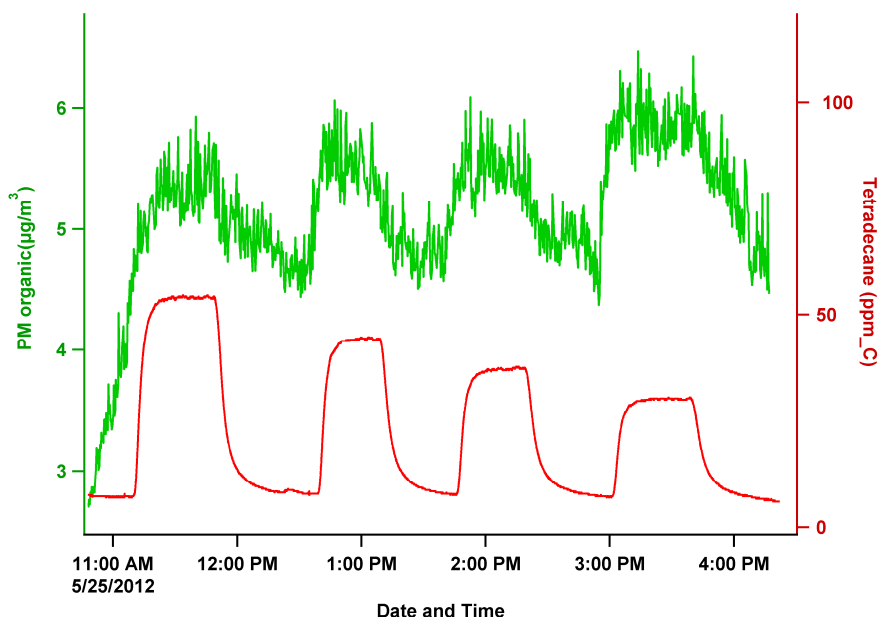


**Figure 3.15 A portion of HFID and AMS measurements on uptake of phenol**

The wall effect (*i.e.* coating of the VOC on the walls of the mixing tube), affected the measurement of alkanes more than the other compounds. As demonstrated in Figure 3.16, the gaseous tetradecane concentration (red line) reached to equilibrium very slowly after the introducing of the VOC flow was turned on and off, compared to phenol and other VOCs. The exponential decay time for tetradecane was approximately three minutes compared to a half minute for naphthalene. Furthermore, the measured PM organic mass (green line) does not seem to achieve steady state during the variation of the gaseous tetradecane concentration. Dodecane and hexadecane gave similar results as tetradecane. This result suggests that the wall effect is not negligible for the paraffins. Due to the difficulty in thoroughly evaluating the magnitude of the wall effect, we will not provide quantitative analysis on the paraffins.
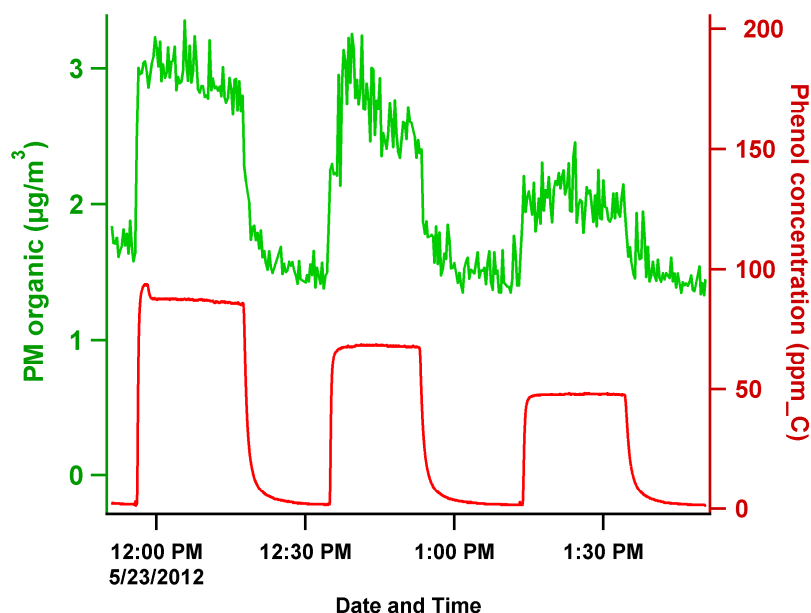
**Figure 3.16 A portion of HFID and AMS measurement on uptake of tetradecane**

Similar to naphthalene, all the applied VOCs gave rise to a thin coating on the soot surface which resulted in a non-detectable growth on the particle size using the SMPS. As shown in Figure 3.17, the increase in gaseous 1-methylnaphthalene concentration led to the increase in total PM organic. However, the particle size distribution remains the same with a peak position at $D_{va}$ = 56 nm. Below the saturation limit, the introduced VOCs can only be adsorbed by the soot surface while no condensational growth would happen under such a condition. The adsorbed mono-layer or multi-layer organic compounds contributes a very small mass increase compared to the total soot mass. Thus no particle size change was observed in these studies. On the other hand, if the VOC concentration rises above the saturation vapor pressure, significant particle size growth would be observed, as we will demonstrate in Section 3.3.4.3.

67
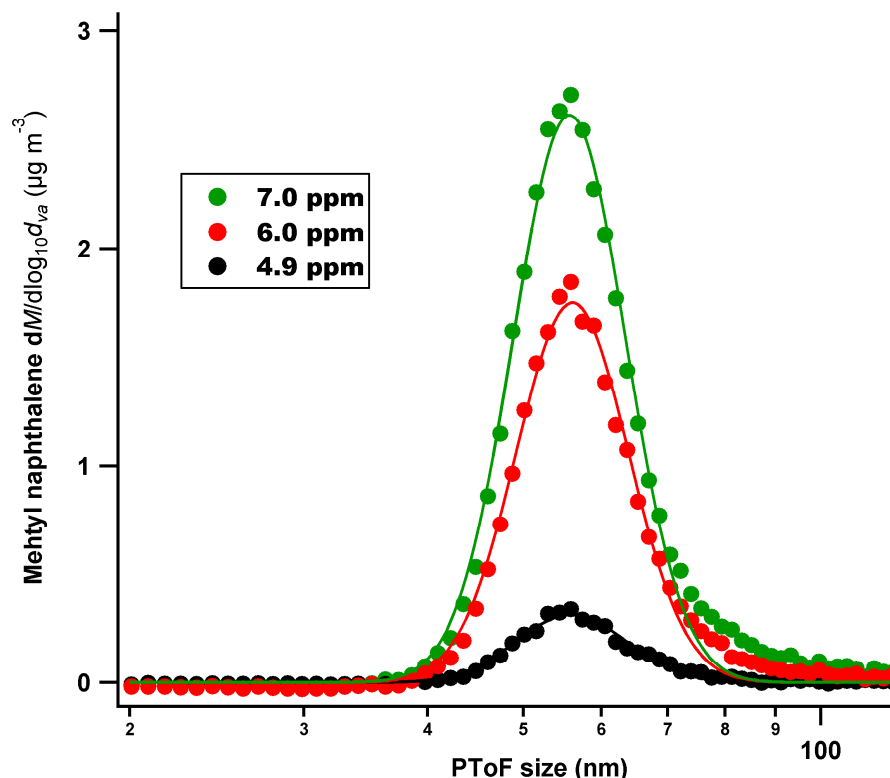
**Figure 3.17 Size distribution of naphthalene-coated soot particles**

### 3.3.4.2.3  Determination of uptake coefficient

Uptake coefficients of the studied VOCs by soot particles, $\gamma_{obs}$, were determined through a linear fitting according to the kinetic model discussed in the previous section. In the analysis, soot surface area was obtained from the AMS-SMPS approach, while the PM organic mass from the AMS measurement was corrected for the transmission efficiency of aerodynamic lens, which was obtained via laboratory evaluation in a previously published study. As shown in Figure 3.18, the fitting results indicate a large difference in uptake coefficient. The data points in red come from naphthalene and its derivatives and those in green are from water-soluble species. The fitted uptake coefficient varies from $(7.4\pm0.9)\times10^{-6}$ for propylene glycol to $(1.79\pm0.06)\times10^{-4}$ for 2,6-dimethylnaphthalene. Difference in physical and chemical properties leads to the variation in uptake coefficient.
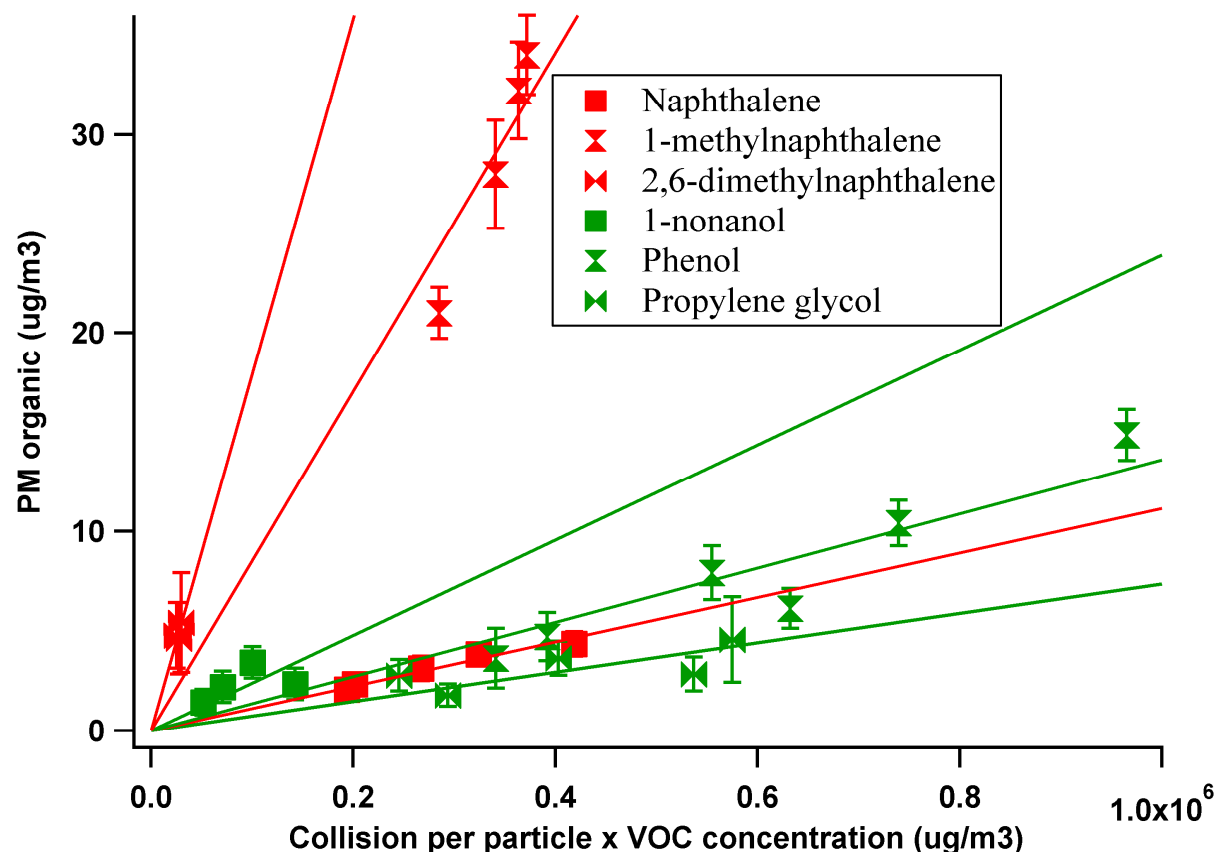
**Figure 3.18 Determination of a variety of VOCs via linear fit based on a kinetic uptake model**

The fitted uptake coefficient was listed in Table 3.2 for comparison. It appears that in general water-soluble species have a lower uptake coefficient than water-insoluble PAHs. For example, 1-nonaol has similar vapor pressure (4.0 Pa) and molecular weight (214) as 2,6-dimethylnaphthalene (v.p.= 2.8 Pa and MW = 264), but its uptake coefficient, $(2.4\pm0.5)\times10^{-5}$, is more than six times lower than that of 2,6-dimethylnaphthalene ($(1.79\pm0.06)\times10^{-4}$). This observation is consistent with the conventional thought that combustion soot particles are usually hydrophobic so hydrophobic hydrocarbons like PAH and alkanes have larger uptake coefficient than the water soluble species such as alcohols and organic acids.

Although the studied naphthalenic compounds are similar in vapor pressure, molecular weight, solubility, and chemical properties, the obtained uptake coefficients are very different. The uptake coefficient is only $(1.11\pm0.03)\times10^{-5}$ for naphthalene, but six times higher for 1-methylnaphthalene and 15 times higher for 2,6-dimethylnaphthalene. Since the uptake model already takes the VOC concentration (vapor pressure) into account, the results suggest that crystalline naphthalene is different from amorphous organic compounds in uptake ability by combustion soot particles due to crystal lattice interaction.

**Table 3.2 List of obtained uptake coefficients**

|  | $\gamma_{obs}$ |
|---|---|
| Naphthalene | $(1.11\pm0.03)\times10^{-5}$ |
| 1-methylnaphthalene | $(8.5\pm0.4)\times10^{-5}$ |
| 2,6-dimethylnaphthalene | $(1.79\pm0.06)\times10^{-4}$ |
| 1-nonanol | $(2.4\pm0.5)\times10^{-5}$ |
| Propylene glycol | $(7.4\pm0.9)\times10^{-6}$ |
| Phenol | $(1.36\pm0.09)\times10^{-5}$ |

Fresh combustion soot is typically considered as hydrophobic and this statement has been proved experimentally in the past through aging the soot particles, which has been found to increase the soluble fraction. To further quantify the observed correlation between uptake coefficient and solubility in water, we presented this inverse correlation in a logarithm plot, as shown in Figure 3.19. The logarithm of the uptake coefficient has a linear inverse correlation with the logarithm of solubility in water, in g $L^{-1}$. The slope of the linear fit is -0.32±0.01 and the correlation coefficient, R, is 0.999, implying a very strong correlation. This plot suggests that a phenomenological power-law relation exists between uptake coefficient of VOC on denuded combustion soot particle and solubility of VOC in water. Therefore we found in this study that hydrophobicity of fresh soot can also be represented by the inverse power-law correlation between uptake of VOC on soot and solubility in water, which directly links adsorption on soot surface to hydrophobicity. Such correlation may vary for different chemical compounds.
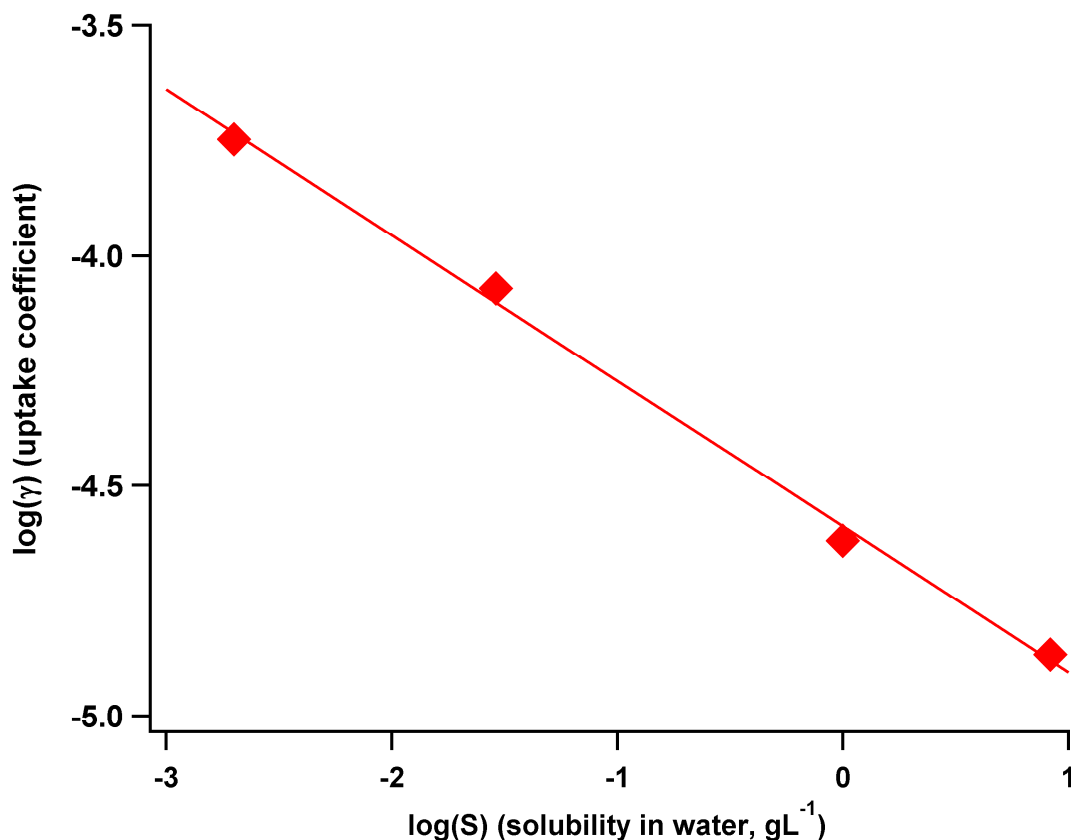


**Figure 3.19 Inverse correlation between uptake coefficients of VOCs and aqueous solubility**

### 3.3.4.3 Significant Particle Growth via Condensation

Adipic acid is a hydrophilic, water-soluble, oxygenated organic compound, which is a solid at room temperature. Its vapor pressure at ambient condition is around $9.8 \times 10^{-6}$ Pa, almost six orders of magnitude less than methyl-naphthalene. It is clear that adipic acid should be considered as non-volatile. In this study, with a concentration of about 1 ppm at the mixing point with the soot stream, adipic acid vapor appears highly super-saturated inside the sampling tube.

Four different mono-disperse (50, 90, 120, 160 nm) as well as four different poly-disperse soot particle sizes were selected to investigate the condensation of adipic acid on the soot surface. Figure 3.20 is the timeline showing adipic acid vapor on and off during the investigation on mono-disperse soot particles. When adipic acid was off, the mono-disperse denuded soot particles were represented by a flat line in both geometric mean diameter (GMD) and volumetric mean diameter (VMD), and the rest in the figure corresponds to turning on adipic acid vapor. Size of the soot particles in GMD and VMD increased significantly after introducing adipic acid to the denuded soot.
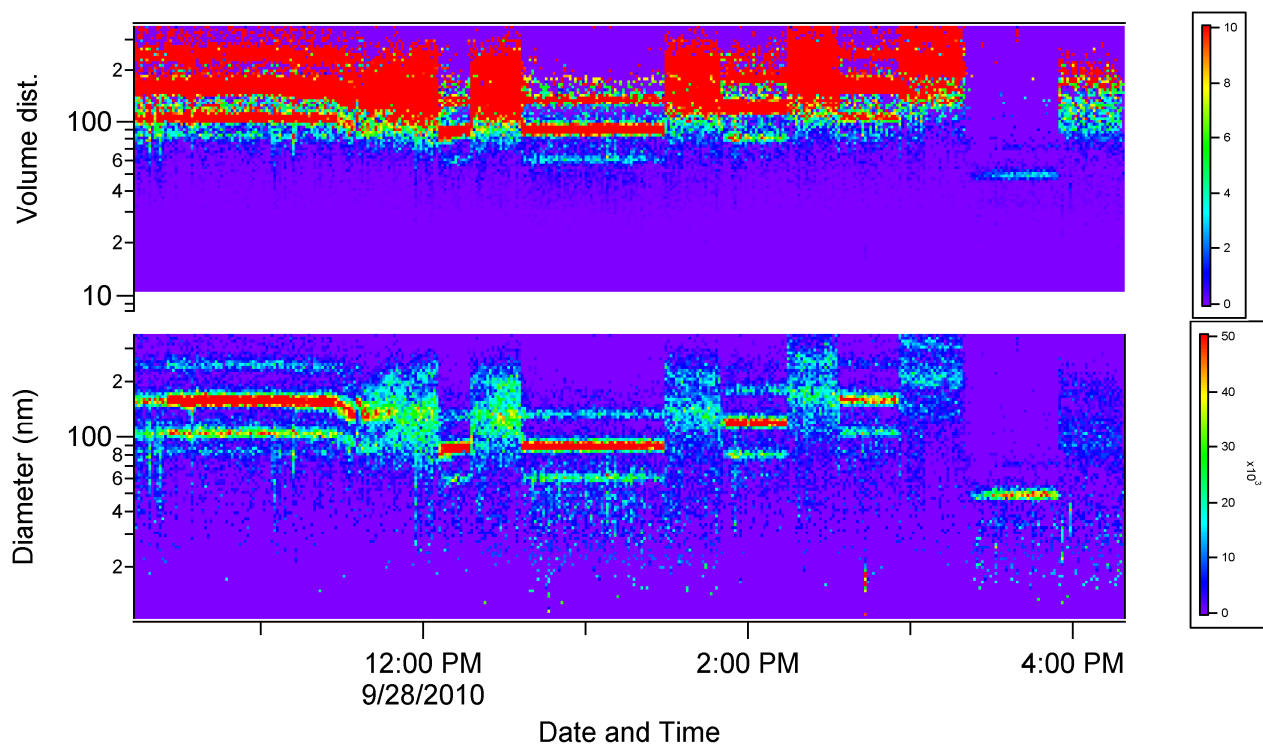


**Figure 3.20 GMD and VMD variation of mono-disperse soot particles in response to VOC introduction. The flat areas are those for the uncoated soot and the rest for the coated soot**

The primary objective of the experiment was to provide values of critical parameters for the organic soot coating model. The microphysical model developed in Section 2 evaluates the time-wise evolution of particulate matter given that we provide the time-series profiles of temperature, pressure, and dilution fraction. Therefore, to apply the microphysical model, a fluid/heat-transfer model representing the experimental setup must be developed.

Comparing experimental results with the predictions from microphysical modeling, we obtained the critical parameters of wet and dry accommodation coefficients ($\alpha_w$ and $\alpha_d$). Due to the condition of super-saturation at ambient condition for the mixed adipic acid vapor, $\alpha_w$ becomes predominant in particle growth as discussed in the previous section. With mixing ratio

of adipic acid = 1 ppm, the best prediction from simulation was generated with both $\alpha_w$ and $\alpha_d$ = 0.027. As shown in Table 3.3, for all the four different mono-disperse soot size, the predictions from microphysical modeling agree extremely well with the experimental measurements within our experimental uncertainty. The study on poly-disperse soot particles provided similar agreement between experiment and microphysical simulation. It indicates that the microphysical modeling is a practically useful tool in the investigation on VOC condensation on the combustion soot particles.

**Table 3.3 Comparison between microphysical simulation and experimental measurements for adipic acid ($\alpha_w = \alpha_d = 0.027$)**

| Initial soot size (nm) | Coated soot size (nm) | |
|---|---|---|
| | Simulation | Experiment |
| 50 | 91.5 | 91.4 |
| 90 | 140.8 | 140.7 |
| 120 | 174.9 | 181.1 |
| 160 | 218.2 | 216.7 |

Docosane is long-chain paraffin with a low vapor pressure similar to adipic acid at ambient condition. It contains no oxygen and its electric dipole moment is zero, so the compound is entirely hydrophobic and cannot be mixed with water. With our current VOC delivery apparatus, controlling the mixing ratio of docosane at the mixing point with soot stream was more difficult than controlling adipic acid. It appeared that there might be a strong wall effect inside the mixing tube, which tended to complicate the condensation procedure of docosane. Therefore, our concentration measurements were only accurate to approximately 0.5 ppm compared to the estimated 0.2 ppm for adipic acid.

From the SMPS measurements, particle growth was clearly detected for the mono-disperse soot particles after mixing with the introduced docosane vapor. As shown in Figure 3.21, GMD of the denuded soot particles was increased from 90 nm to about 146 nm after mixing with docosane vapor at a concentration of 0.4 ppm. The size distribution of the coated soot particles became poly-disperse, similar to the previous SMPS observation on condensation of adipic acid vapor.
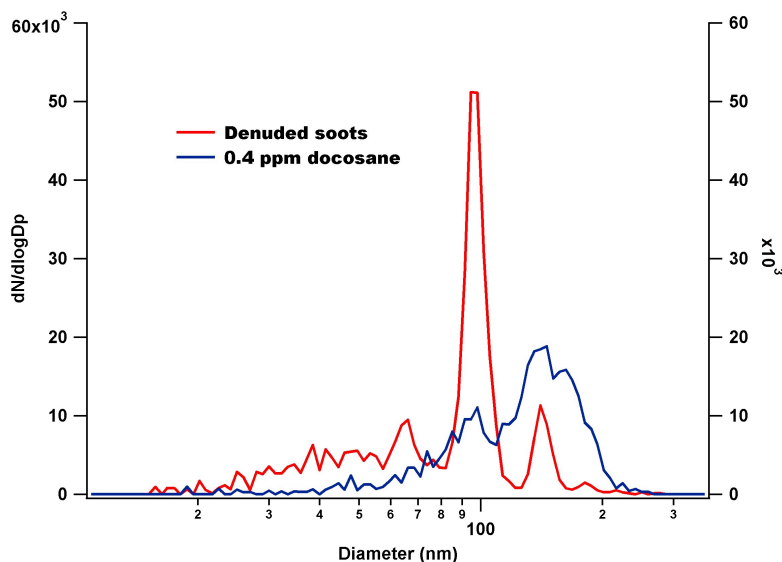
**Figure 3.21 SMPS observation of particle growth of docosane vapor (~0.4 ppm) on 90 nm denuded soot particles**

Table 3.4 presents the comparison between experimental results and simulation predictions. The applied $\alpha_w$ and $\alpha_d$ equal to 0.01 in the simulation, in which $\alpha_w$ dominates the condensation procedure due to super-saturation. As mentioned above, due to the relatively large uncertainty on the concentration of docosane vapor, the predictions from simulation agree only qualitatively with the experimental results. Further improvement in controlling docosane vapor is necessary to achieve better agreement.

**Table 3.4 Comparison between microphysical simulation and experimental measurements for docosane ($\alpha_w = \alpha_d = 0.01$)**

| Initial soot size (nm) | Mixing ratio (ppm) | Coated soot size (nm) | |
|---|---|---|---|
| | | Simulation | Experiment |
| 50 | 1.8 | 111.1 | 101.8 |
| 90 | 0.4 | 114.8 | 145.9 |
| 120 | 0.1 | 131.2 | 156.8 |
| 120 | 1.8 | 202.7 | 209.1 |
| 160 | 1.0 | 213.6 | 174.7 |

## 3.4   Summary

We investigated the uptake of a variety of water-soluble and water-insoluble volatile organic compounds by soot from a propane flame via a simultaneous measurement of VOC vapor concentration and volatile PM organic mass. The uptake coefficient for naphthalene was determined to be $(1.11\pm0.06)\times10^{-5}$, comparable to that of $NO_2$, but three orders of magnitude less than that of sulfuric acid. Our results imply that, compared to sulfuric acid, uptake of naphthalene is not an efficient mechanism to activate fresh combustion soot. We also observed that the particle condensational growth due to the uptake of VOCs is negligible in terms of both mobility diameter and vacuum aerodynamic diameter.

Investigating the dependence of uptake coefficients on water-solubility, we found that hydrophobicity of fresh soot can also be represented by an inverse power-law correlation

between uptake of VOC on soot and solubility in water, which directly links adsorption on soot surface to hydrophobicity.

# 3.5 References

Cross, E. S., Onasch, T. B., Ahern, A., Wrobel, W., Slowik, J. G., Olfert, J., Lack, D. A., Massoli, P., Cappa, C. D., Schwartz, J. P., Spackman, J. R., Fahey, D. W., Sedlacek, A., Trimborn, A., Jayne, J. T., Freedman, A., Williams, L. R., Ng, N. L., Mazzoleni, C. Dubey, M., Brem, B., Kok, G. L., Subramanian, R., Freitag, S., Clarke, A., Thornhill, D., Marr, L. C., Kolb, C. E., Worsnop, D. R., and Davidovits, P. 2010. Soot Particle Studies - Instrumental Inter-Comparison – Project Overview. *Aerosol Sci. Tech.*, 44, 592-611.

Davidovits, P.; Hu, J. H.; Worsnop, D. R.; Zahnister, M. S.; and Kolb, C. E. 1995. Entry of Gass Molecules into Liquids. *Faraday Discuss.*, 100, 65-82.

DeCarlo, P. F., Slowik, J. G., Worsnop, D. R., Davidovits, P., and Jimenez, J. L. 2004. Particle Morphology and Density Characterization by Combined Mobility and Aerodynamic Diameter Measurements. Part 1: Theory. *Aerosol Sci. Tech.*, 38, 1185-1205

Finlayson-Pitts, B. J. and Pitts, J. N. 1997. Tropospheric air pollution: Ozone, airborne toxics, poly-cyclic aromatic hydrocarbons, and particles, *Science*, 276, 1045–1052.

Huffman, J. A.; Ziemann, P. J.; Jayne, J. T.; Worsnop, D. R.; and Jimenez, J. L. 2008. Development and Characterization of a Fast-Stepping/Scanning Thermodenuder for Chemically-Resolved Aerosol Volatility Measurements. *Aerosol Sci. & Technol.*, 42, 395-407.

Jayne, J. T.; Leard, D. C.; Zhang, X.; Davidovits, P.; Smith, K. A.; Kolb,C. E.; and Worsnop, D. R. 2000. Development of an Aerosol Mass Spectrometer for Size and Composition Analysis of Submicron Particles, *Aerosol Sci. Technol.*, 33, 49-70.

Knighton, W. B., Rogers, T.; Wey, C. C.; Anderson, B. E.; Herndon, S. C.; Yelvington, P. E.; and Miake-Lye, R. C. Application of Proton Transfer Reaction Mass Spectrometry (PTR-MS) for Measurement of Volatile Organic Trace Gas Emissions From Aircraft. Journal of Propulsion and Power. **2007**, 23, 949-958.

Liu, P., Ziemann, P. J., Kittleson, D. B., and McMurry, P. H. 1995a. Generating Particle Beams of Controlled Dimensions and Divergence: I. Theory of Particle Motion in Aerodynamic Lenses and Nozzle Expansions, *Aerosol Sci. Technol.* 22, 293–313.

Liu, P., Ziemann, P. J., Kittleson, D. B., and McMurry, P. H. 1995b.Generating Particle Beams of Controlled Dimensions and Divergence: II. Experimental Evaluation of Particle Motion in Aerodynamic Lenses and Nozzle Expansions, *Aerosol Sci. Technol.* 22, 314–324.

Ramanathan, V., Crutzen, P. J., Kiehl, J. T., and Rosenfeld, D. 2001. Atmosphere - Aerosols, climate, and the hydrological cycle, *Science*, 294, 2119–2124.

Slowik, J. G., Stainken, K., Davidovits, P., Williams, L. R., Jayne, J. T., Kolb, C. E., Worsnop, D. R., Rudich, Y., DeCarlo, P. F., and Jimenez, J. L. 2004. Particle Morphology and Density Characterization by Combined Mobility and Aerodynamic Diameter Measurements. Part 2: Application to Combustion-Generated Soot Aerosols as a Function of Fuel Equivalence Ratio. *Aerosol Sci. Tech.*, 38, 1206-1222.

Spicer, C. W.; Holdren,M. W.; Smith,D. L.; Hughes, D. P.; and Smith, M.D. Chemical composition of exhaust from aircraft turbine engines. Journal of Engineering for Gas Turbines and Power. **1992**, 114(1), 111-117.

Worsnop, D. R.; Zahniser, M. S.; Kolb, C. E.; Gardner, J. A.; Watson, L. R.; Van Doren, J. M.; Jayen, J. T.; and Davidovits, P. 1989. Temperature Dependence of Mass Accommodation of $SO_2$ and $H_2O_2$ on Aqueous Surfaces. *J. Phys. Chem.*, 93, 1159-1172.

Zhang, H. Z.; Li, Y. Q.; Davidovits, P.; Williams, L. R.; Jayen, J. T.; Kolb, C. E.; and Worsnop, D. R. 2003. Uptake of Gas-Phase Species by 1-Octanol. 2. Uptake of Hydrogen Halides and Acetic Acid as a Function of Relative Humidity and temperature *J. Phys. Chem. A*, 107, 6398-6407.

# 4  Characterization of Lubrication Oil Emissions from Aircraft Engines

## 4.1   Significance of Lubrication Oil Emissions

Typical modern gas turbine engines use two or more spools rotating at different speeds to optimize the thermodynamic/aerodynamic cycle performance of the engine. This sophisticated rotating machinery requires oil to lubricate and cool the bearings and other engine parts. A pressure pump continuously circulates the oil and a scavenging system cleans and returns the oil to a tank for reuse. Generally oil consumption is low and depends primarily on the efficiency of the seals. However the lubrication system must be vented to the atmosphere to allow the pressurized system to circulate oil. Oil loss due to the "breather" vent is typically controlled by using an oil demisting system which centrifugally recycles the oil drops larger than ~1 μm in diameter and returns that mass to the oil reservoir. Oil droplets that are smaller than the effective cut size of the demisting system in principle can escape in the breather air vented overboard.

Although lubrication oil has been identified as an important source of organic particulate matter (PM) emissions from gasoline and diesel engines (Rogge et al. 1993), a gas turbine engine lubrication system is typically not considered as a potential source of PM emissions. PM emissions from gas turbine engines are typically viewed to be products of the combustion process, such as black carbon soot particles (Schlager *et al*. 1997; Anderson *et al*. 1998; Paladino *et al*. 1998; Schumann *et al*. 2002). However recent PM emission measurements on aircraft engines, especially detections based upon characteristic mass fragment signatures, have strongly suggested the presence of lubrication oil in the organic PM emitted from aircraft engines (Onasch et al. 2009). Because of the appreciably low volatility of lubrication oils, any emitted oil vapor or drops will add to the condensed mass and thus contribute to the organic PM in the wake of the aircraft. Although the high fuel efficiency of modern aircraft engines results in low organic PM emissions from combustion, the results from previous exhaust characterization measurements suggest that the lubrication system may be a much greater contributor to the organic PM than the engine exhaust for some aircraft engines.

Base fluids of aircraft lubrication oils in general are synthetic fatty acid esters with small amounts of specialized performance additives. They are safe when handled and used according to the manufacturers' specifications. However the vented lubrication oil can cause water pollution and the additives can be toxic to human beings. Toxicity of aircraft oil additives such as tricresyl phosphate (TCP), which is considered a neurotoxin, has been investigated by several research groups (Craig & barth 1999; van Netten 1999; and Winder & Balouet 2002) which recommend that the toxicity of lubrication oils should be more carefully evaluated. Due to the high thermal and chemical stabilities of lubrication oils, which are required by the extreme temperature conditions (turbine inlet temperature more than 1500°C) inside aircraft engines, emissions of synthetic aircraft lubrication oil may have extended environmental lifetimes.

To characterize and quantify lubrication oil emissions, we carried out the first-ever systematic investigation of the physical and chemical properties of the aerosol emitted from the over-board breather vent of several aircraft engines using several highly sensitive PM-detecting instruments. The study was performed from July 22 to July 25, 2009 at the Pratt & Whitney (P&W) engine test facilities in Middletown, CT. The investigated chemical and physical properties were primarily total particulate mass, particle size distribution, total particle number

count, optical extinction, and chemical composition of the particles. Because the demisting systems of aircraft engines are designed to recycle lubrication oil droplets larger than ~1 μm, we selected PM detection techniques suitable to measure particles from 6 to 3000 nm in diameter. In addition a sampling system capable of dilution was utilized to condition the aerosol concentration prior to measurement. As listed in Table 4.1, the deployed measurement instruments include: (1) Compact Time-of-Flight Aerodyne Mass Spectrometer (C-TOFAMS, Aerodyne Research, Inc.), (2) Tapered Element Oscillating MicroBalance (TEOM, Thermo Electron Co., Model 1105), (3) Engine Exhaust Particle Sizer (EEPS, TSI, Model 3090), (4) Condensation Particle Counter (CPC, TSI, Model 3022A), and (5) Ultra High Sensitivity Aerosol Spectrometer (UHSAS, Droplet Measurement Technologies).

## 4.2   Measurements on three Aircraft Engines under Performance Test at P&W

Three high-bypass turbofan aircraft engines, representing two different distinct engine model types, were examined for lubrication oil emissions in this study. The engines were under the performance evaluation by the original equipment manufacturer (OEM), so their operation was not specifically designed for our study. The tested engine was mounted to a test stand inside a P&W Engine Test Cell and remained stationary during its entire test program. In an individual test, engine power was increased from idle to take-off through several specific power settings, and then decreased through the same steps back to idle. A typical aircraft engine performance timeline is illustrated in Figure 4.1. Each power setting lasted from 2 to 15 minutes, during which PM measurements were averaged. The flow rate of the breather air vented overboard is almost linear with respect to engine thrust, as determined by the engine operator. According to our on-site measurements, the temperature of the lubrication oil exhaust increases appreciably with engine thrust, from 30°C at low idle to about 100°C at high power. On the other hand, the pressure of the same exhaust increases by around 7000 Pa with increasing engine thrust.
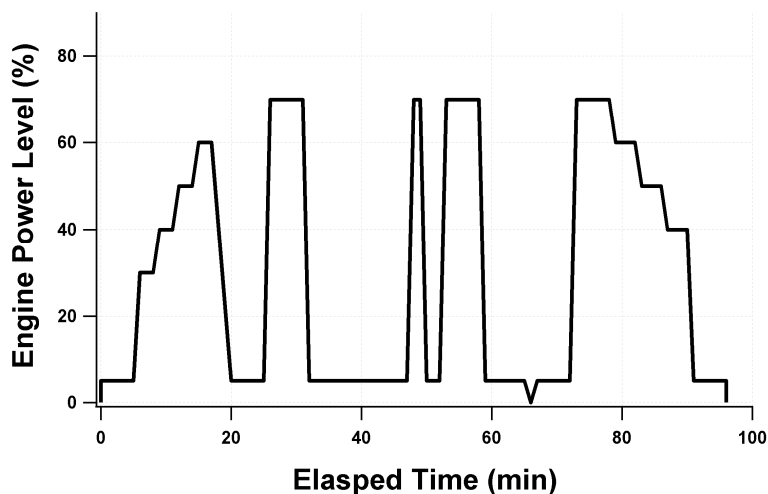


Figure 4.1 Engine verification timeline applied in this study. At the 65th minute of operation, the engine was unintentionally turned off

To sample lubrication oil exhaust without introducing any interference to the oil venting system, we designed the PM collecting and diluting apparatus, as shown in Figure 4.2. A small amount of the vented breather flow (<1%) was collected by an L-shaped 1/2" stainless tube inserted into the overboard vent line downstream of the demisting system. The 3/8" tube was

surrounded by a concentric 5/8" tube and recessed 1". The larger tube provided a controlled flow of dry, particle-free nitrogen to dilute the oil sample. Dilution ratios as high as several thousand were used to match lubrication oil PM sample concentrations with the dynamic range of the selected PM measurement instruments.
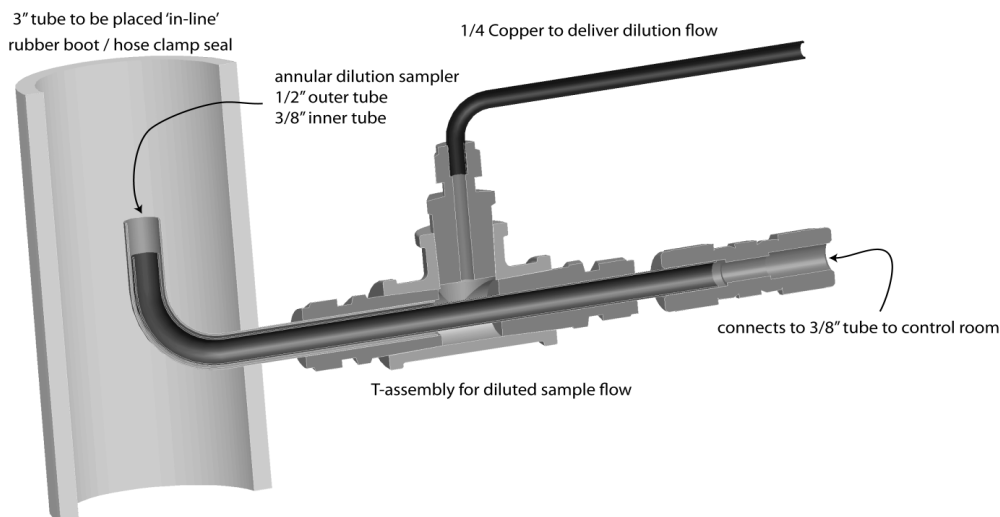


**Figure 4.2 Sampling and dilution apparatus used to collect particulate matter emitted from the oil system overboard breather vent**

After dilution with nitrogen gas, the collected breather flow sample was drawn through 30 ft of 3/8" stainless tubing into the control room where it was split to the individual measurement instruments. The primary PM measurement instruments used in the study are listed in Table 4.1. Because this investigation was the first dedicated study on PM emission of lubrication oil from modern aircraft engines, little was known about the quantitative or even qualitative nature of such emissions, i.e. PM mass and size distributions. As the knowledge on lubrication oil emissions from aircraft engines was limited, we chose a set of measurement instruments to cover a very broad dynamic range in terms of particle concentration, mass and size.

The C-TOFAMS was used to measure both particle size distributions in the volume domain and the volatile chemical composition of the lubrication oil PM emissions (Jayne et al. 2000) with a dynamic range from 0.05 to 100 $\mu$g m$^{-3}$. It measures the particle size in vacuum aerodynamic diameter ($D_{va}$) from 40 to 1000 nm. As discussed in the following section, the ultra-high sensitivity of the C-TOFAMS required significant dry nitrogen dilution because of the high concentration of lubrication oil in the breather air vented overboard.

The EEPS and UHSAS were deployed to measure the number-based, size distribution of oil droplets less than 500 nm and 1000 nm in diameter respectively. Among the deployed PM measurement instruments, the EEPS measures particles in mobility diameter, while the UHSAS measures optical extinction of the particles, which is a function of volume equivalent diameter, $D_{ve}$, and refractive index of the particles. The current UHSAS measurements on $D_{ve}$ were calibrated with latex spheres which have the real part of refractive index, $n = 1.57$ and the imaginary part of index of refractive index = 0.

**Table 4.1 List of the applied PM measurement instruments in this study**

| Instrument | Dynamic Range | Particle Size (nm) | Measured Properties |
|---|---|---|---|
| Compact Time-of-Flight Aerodyne Mass Spectrometer (C-TOFAMS) | $0.05 - 100 \ \mu g/m^3$ | $40 - 1000$ | Mass spectrum of chemical composition, aerodynamic diameter |
| Condensation Particle Counter (CPC) | $0 - 10,000,000$ $particle/cm^3$ | $7 - 3000$ | Number count |
| Engine Exhaust Particle Sizer (EEPS) | $200 - 100,000,000$ $particle/cm^3$ | $6 - 500$ | Particle size distribution in mobility diameter |
| Tapered Element Oscillating MicroBalance (TEOM) | $0.2 \ mg/m^3$ – several $g/m^3$ | | PM mass |
| Ultra High Sensitivity Aerosol Spectrometer (UHSAS) | $0 - 18,000$ $particle/cm^3$ | $60 - 1000$ | Optical extinction |

The TEOM, the least sensitive instrument in this study, measured total PM mass. The lower detection limit of the TEOM is ~ 200 $\mu g \ m^{-3}$, so for all the engine power settings from low idle to high power, the TEOM measurements were made without dilution. The CPC was used to provide a direct measurement of total particle number. It enabled us to briefly study lubrication oil exhaust at idle conditions without diluting the collected sample to the CPC, and thus make a correspondence between the CPC and the TEOM.

Detection sensitivity of the C-TOFAMS, CPC, EEPS and UHSAS is several orders of magnitudes higher than that of TEOM, so all instruments except for TEOM require dry nitrogen dilution. Dilution flows of 22 and 24 liter per minute (LPM) were applied for the engine idle, while 26 and 28 LPM were used for the higher powers.

To positively identify lubrication oil from its ion fragment signatures in the mass spectrum, a laboratory test on the lubrication oil samples from the engines used in the P&W field test was performed. Oil aerosols were generated with a nebulizer and then size-selected at 250 nm using a differential mobility analyzer (DMA, TSI, mode 3081), with the sample mass concentration controlled around 5 $\mu g \ m^{-3}$. The nebulized mono-disperse oil aerosols were later analyzed with a C-ToFAMS using the same instrumental settings as those applied in the field measurements. As presented in the next section, the laboratory mass spectrometric results on pure lubrication oil droplets provide valuable information on identification of lubrication oil from the PM emission of oil vent flow.

## 4.3   Evaluation of Emission Indices and Particle Size Distributions

This collaborative study represented the first systematic investigation of lubrication oil particulate emissions from modern aircraft engines. It provided detailed insights into PM emission, particle size distribution, and power influence upon both particle composition and size.

Since no instrument applied here is capable of covering the entire particle concentration range from no dilution to the highest dilution, the determination of dilution ratio in this study was based on the measurements of particle mass and concentration. In particular, particle mass from the sample was measured with the TEOM without dilution and then with a dilution flow of 22 LPM. Without dilution, the PM concentration determined by the TEOM was 469 ± 40 mg m$^{-3}$, while it was 3.5 ± 0.5 mg m$^{-3}$ with the dilution flow of 16 LPM. A dilution ratio of 134 ± 22 was obtained from these results. In this case, the uncertainty of the dilution ratio is dominated by the precision of the TEOM measurement, which was affected by the limited time on each test

point. Several factors including water condensation, which may not be severe in the lubrication oil system, could also impact the accuracy of the determined dilution ratio.

In the case of high dilution flows, the effect of dilution on the CPC and EEPS measurements is presented in Figure 4.3. The measured particle concentrations were a highly nonlinear function of the nitrogen diluents flow rate, indicating that a precise dilution ratio cannot be obtained through measurements of flow rate. Dilution ratio was determined by the CPC measurements of particle count. For example, the difference in dilution ratio between a dilution flow rate of 16 and 22 LPM was $7.8 \pm 1.2$ by the CPC measurements, where the uncertainty only indicates the precision of the CPC measurements. Since the dilution ratio with a dilution flow rate of 16 LPM was $134 \pm 22$ from the TEOM measurements, we determined that the dilution ratio with dilution flow of 22 LPM was therefore $1045 \pm 240$. Dilution ratios at other flow rates were then determined via the same methodology.
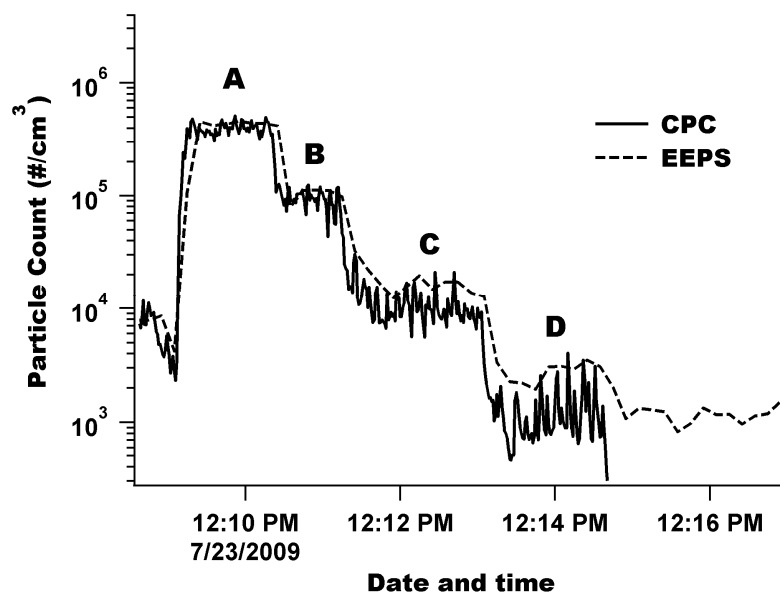


**Figure 4.3 Dilution effects on lubrication oil emissions measured by CPC and EEPS with dry nitrogen dilution flow of (A) 22 LPM; (B) 24 LPM; (C) 26 LPM; and (D) 28 LPM. The tested engine is at idle condition**

Lubricants used in modern high-performance aircraft engines are generally specialized synthetic oils whose base stocks are usually a mixture of $C_5 - C_{10}$ fatty acid esters of pentaerythritol and dipentaerythritol. Nearly four decades ago, Tou reported that under electron impact ionization, polyfunctional pentaerythritol derivatives exhibit extensive ion fragmentations and no information on the molecular ion can be obtained (Tou 1972). Therefore identification of lubrication oil must be primarily based on its characteristic ion fragmentation patterns. As illustrated in Figure 4.4, lubrication oils showed ion fragmentation patterns close to those of saturated long-chain hydrocarbons, with a homologous series of 14 mass-unit intervals starting at m/z = 29. Unlike the regular ion fragmentation pattern of alkyl ion $C_nH_{2n+1}^+$ of the long-chain hydrocarbons such as decane ($C_{10}H_{22}$) in Figure 4.4C (NIST Chemistry WebBook), the mass spectrum of lubrication oil is characterized by the significantly weaker ion signals at m/z = 71 and 99 than the rest of the series. Similar discrete and characteristic fragmentation patterns between lab test and field measurement, as shown in Figure 4.4, confirm that the detected PM emissions from aircraft overboard breather vent came predominantly (>95%) from the aircraft lubrication oil.

Degradation of lubrication oil during aircraft engine operation as a result of friction and/or pyrolysis would change the oil's chemical composition (Wang et al. 2004). The C-ToFAMS is capable of detecting the variation due to oil degradation by monitoring changes in ion fragment patterns. In this study, we discovered that ion fragmentation patterns in mass spectra of oil from the tested aircraft engines and the nebulized oil aerosols in the laboratory are quite similar, as shown in Figure 4.4, which suggests that the degree of degradation of lubrication oil during our entire engine test might be negligible.
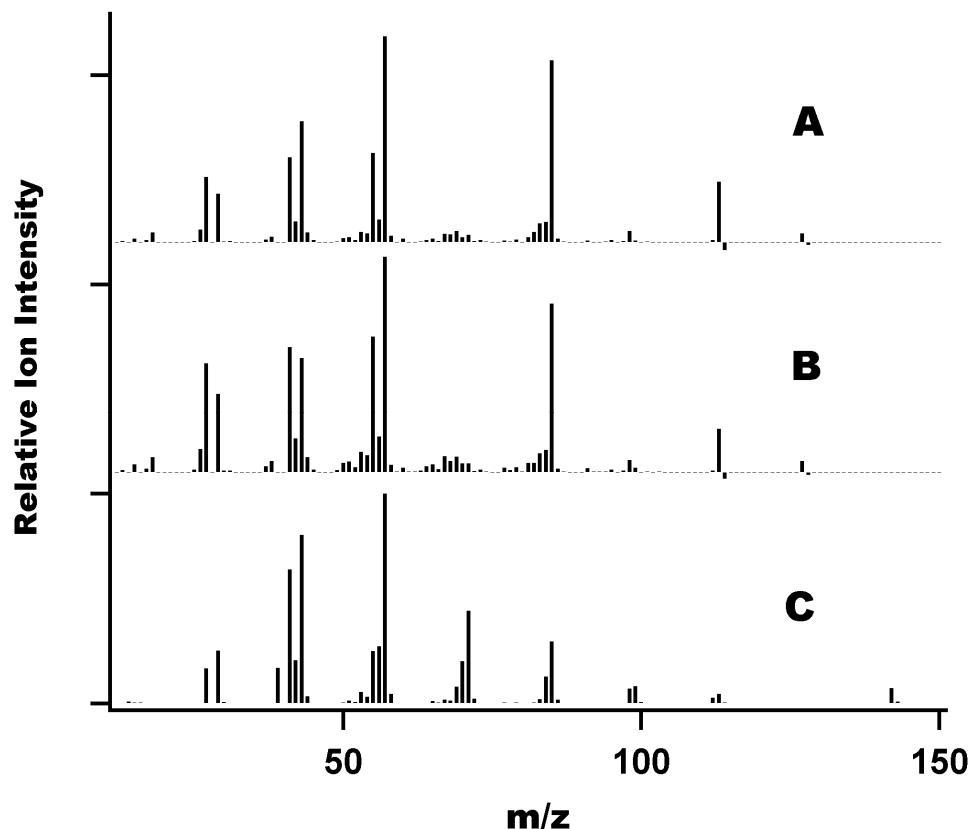


**Figure 4.4 Mass spectra of lubrication oil droplets: (A) measured in the laboratory from nebulized lubrication oil microspheres (250 nm is diameter); (B) measured from the PM exhausts of lubrication oil demisting system at idle; and (C) the mass spectrum of decane ($C_{10}H_{22}$) from the NIST Chemistry WebBook. The similarity between the two spectra (A) and (B) indicates PM exhausts from the lubrication oil demisting system are lubrication oil particles**

The high dilution ratios that were required in this experiment made the uncertainty in the dilution ratio greater than desired. However, we found that at engine idle conditions, particle size distributions measured by the C-TOFAMS, EEPS and UHSAS are insensitive to variation in dilution, suggesting that sampling line microphysical processing has a minor effect on overall particle physical properties.

The size of the emitted oil particles from an aircraft engine lubrication system is expected to be limited by the cyclonic separator of the demisting system. As illustrated in Figure 4.5, $D_{ve}$ measured by the UHSAS was 281 ± 9 nm at energy idle, compared to $D_{va}$ of 260 ± 3 nm by the C-TOFAMS. The C-TOFAMS measured $D_{va}$ with a low-pressure aerodynamic lens. In the free-molecular regime like the aerodynamic lens, $D_{va}$ equals $D_{ve} \times \rho$ for a spherical particle. Here the density, $\rho = 0.93$ gcm$^{-3}$ for the tested lubrication oil, so $D_{ve} = 281 ± 9$ nm from the UHSAS

corresponds to $D_{va}$ = 261 ± 8 nm, showing our measurements on particle size by C-TOFAMS are in good agreement with those from UHSAS at engine idle.
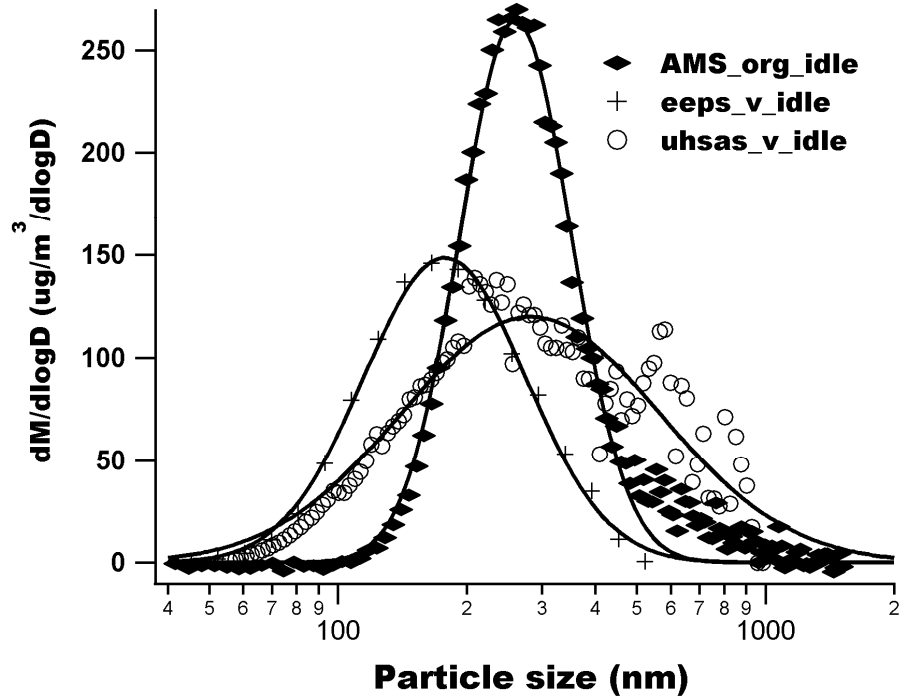


**Figure 4.5 Particle size distributions of organic PM emitted from the lubrication oil demisting system at idle, measured by Compact Time-of-Flight Aerodyne Aerosol Mass Spectrometer (C-TOFAMS), Engine Exhaust Particle Sizer (EEPS), and Ultra High Sensitive Aerosol Spectrometer (UHSAS). The solid lines are lognormal fitting results**

At higher engine power, $D_{ve}$ from the UHSAS and $D_{va}$ from the C-TOFAMS were 350 ± 8 nm and 272 ± 4 nm, respectively. The determined particle size from the UHSAS is about 20% larger than that from the C-TOFAMS. The discrepancy in particle size distribution between C-TOFAMS and UHSAS is believed to arise from differences in instrumental dynamic range and cut-off efficiency of the C-TOFAMS aerodynamic lens. Regardless, it is clear from this study that as engine power increases from idle to high thrust, the emitted lubrication oil particles slightly shift to larger sizes.

At engine idle, $D_{ve}$ determined by the EEPS measurement is 178 ± 3 nm, which is very similar to that determined at higher engine power. The EEPS measures particle counts by monitoring the electric mobility of particles, so it is in principle more sensitive to smaller particles. In the past, we found in several aircraft engine tests that this technique tended to underestimate the concentration of particles larger than 100 nm. We therefore believe that the C-TOFAMS and UHSAS provide more accurate detection and better information on mass or volume for particles larger than 200 nm than does the EEPS.

Total PM mass of lubrication oil in the vented stream at idle condition was directly measured by the TEOM technique without dilution. The emission characteristics of a combustion source is usually evaluated in terms of emission index (EI), which is mass ($EI_m$) or number ($EI_n$) of the emitted pollutant per mass fuel consumed, in the unit of g kg$^{-1}$ or mg kg$^{-1}$ for PM mass. In this study, unlike the usual determination of fuel mass from measuring the exhausted gas $CO_2$ concentration, the amount of the consumed fuel was provided directly by the original equipment manufacturer (OEM) engine control crew. The C-TOFAMS measurements, with a dilution flow

82

of 22 LPM, gave an $EI_m$ of $3 \pm 1$ mg kg$^{-1}$ at idle compared to an $EI_m$ of $10 \pm 2$ mg kg$^{-1}$ from the TEOM without dilution. In spite of the significant uncertainty in the determined dilution ratio (which is not taken into account in the above error bar), C-TOFAMS and TEOM provide the results of lubrication oil emissions of the same order of magnitude. At engine idle, the EI of lubrication oil in the exhaust was thus estimated in the range of 2-12 mg kg$^{-1}$. The EI of the volatile PM organic of the RB211-535 engines, being used on some Boeing 757 airplanes, is 10 $\pm 3$ mg kg$^{-1}$, and the non-volatile soot EI is $50 \pm 20$ mg kg$^{-1}$ (Timko et al. 2010). Our current measurements indicate the contributions from lubrication oil could be significant in the total aircraft PM emissions at engine idle.

Total PM emissions from lubrication oil exhaust also depend upon engine power setting. At high power, $EI_m$ of $33 \pm 7$ mg kg$^{-1}$ was determined from the TEOM measurement, compared to those of $510 \pm 63$ mg kg$^{-1}$ for the RB211-535, which is the highest in this type of high-bypass turbofan engines (Timko et al. 2010).

At engine idle, the measured $EI_n$ was $(1.6 \pm 0.3) \times 10^8$ kg$^{-1}$, compared to $(1.3 \pm 0.5) \times 10^{14}$ kg$^{-1}$ for the RB211-535 engine. Aviation fuels contain high concentrations of sulfur-bearing compounds (~100-1000 ppm in JetA fuel). The high-temperature and high-pressure combustion results in the formation of sulfuric acid. The total PM number of aircraft engines is dominated by the nucleation-mode particles made of sulfuric acid and other volatile species, which are approximately 10-20 nm in diameter (Corporan et al. 2007; Timko et al. 2010). The lubrication oil PM we detected from the deoiler is more than one order of magnitude larger in diameter than the combustion-generated nucleation-mode particles. The contribution from lubrication oil to the total PM number of aircraft engines seems negligible.

## 4.4   Field Measurements

The field measurements at Midway International Airport (MDW) and O'Hare International Airport (ORD) in Chicago were performed on February 17-18, 2010 with the help of Southwest Airlines, United Airlines and the City of Chicago. Emission plumes of the aircraft were investigated using a variety of gaseous and particulate measurement instruments located on board the Aerodyne mobile laboratory (Kolb et al. 2004; Herndon et al. 2005). Engine exhaust plumes were sampled through 1-inch outside-diameter stainless tubing in front of the laboratory and drawn into individual instruments. During the field measurement period, the Aerodyne Mobile Laboratory was located at downwind locations to monitor air advected from the active taxiways (30-150m). The measured meteorological conditions (e.g., wind speed and direction) were used to choose the mobile lab location. A camera located in front of the mobile lab provided additional information for aircraft identification and attribution of the plume origin.



**Figure 4.6 Field measurements on PM emissions from in-service commercial aircraft exhaust at O'Hare International Airport in Chicago**

The gaseous measurements of CO, NO and $NO_2$ were used to assess the engine state. Emission index of CO (EI-CO) decreases with engine power, while EI-$NO_x$ increases, so the ratio of EI-CO/EI-$NO_x$ is a very reliable indicator of engine power.

The particle measurement instruments employed during these tests included a Multi-Angle Absorption Photometer (MAAP) (Thermo Environmental), a Condensation Particle Counter (CPC, Model 3776, TSI) and an Engine Exhaust Particle Sizer (EEPS, Model 3090, TSI).  These instruments provided information about particle absorption, number density, and mobility-based size distribution. Carbon dioxide concentration measurements were provided by a Li-Cor 820 $CO_2$ analyzer.

A HR-ToFAMS was deployed to detect semi-volatile organic PM from aircraft engine exhaust. At present, AMS is the only available instrument capable of providing quantitative size and chemical mass loading information simultaneously in real-time for sub-micron aerosol particles (50-700 nm). It measures the non-refractory PM composition of the particles through thermal ablation on a hot metal surface followed by mass spectrometric detection of the vaporized compounds. Technical details of the AMS have been described in previous publications.

### 4.4.1 Characteristic Ion Fragmentation Pattern of Lubricating Oils

To characterize lubrication oil with the AMS, we performed a dedicated laboratory investigation of lubrication oils from ExxonMobil and BP. Based on industrial marketing materials, the market share of ExxonMobil and BP for aviation lubrication oil is more than 83%. The oil samples were provided by the commercial airlines that took part in the APEX 1-3 (Aircraft Particle Emissions Experiment) field missions. The base stocks of lubrication oils are essentially a mixture of $C_5 - C_{10}$ fatty acid esters of pentaerythritol, whose structure is shown in Figure 4.7. Each of the four branches of fatty acid moieties contain between 5 and 10 carbon atoms depending on the synthesis procedure. Although the presence of the molecular ion has been considered as the most important information of analytical mass spectrometry, Tou reported more than three decades ago that under electron impact ionization (70 eV), polyfunctional pentaerythritol derivatives exhibit extensive ion fragmentation and no information on the molecular ion can be obtained. Therefore identification of lubrication oil from the observed mass spectrum must be primarily based on its specific ion fragmentation pattern.
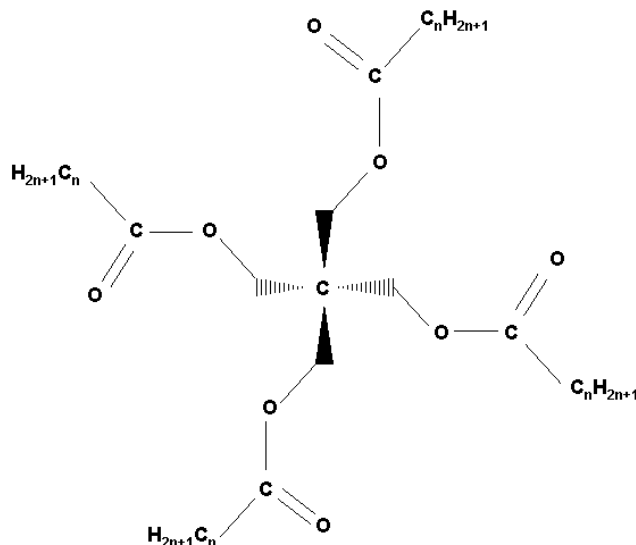


**Figure 4.7 Molecular structure of fatty acid ester of pentaerythritol, the main base stock of aircraft lubrication oils**

In the laboratory study, a continuous flow of lubrication oil aerosol was generated with a pneumatic nebulizer and then size-selected to a diameter of 250 nm by a Differential Mobility Analyzer (DMA, TSI, mode 3081). The nebulized mono-disperse oil aerosol was then introduced into a HR-ToF AMS. The laboratory results provide a direct comparison to the field measurements.

Mono-disperse aerosols of two aircraft lubrication oils showed a characteristic ion fragmentation pattern from the laboratory AMS measurements, as shown in Figure 4.8 (A and B). The mass spectra of lubrication oils are compared to the decane ($C_{10}H_{22}$) mass spectrum obtained from NIST Chemistry WebBook. Since kerosene-based aviation fuel is a mixture of hydrocarbons with a carbon number distribution between 8 and 16, we chose decane as a suitable reference. Similar to decane (Figure 4.8 C), two homologous series of 14 atomic mass unit (amu) intervals starting at m/z = 27 and 29, which are the so-called $\Delta = 0$ and 2 series (McLafferty & Turecek 1993), are apparent for both oil samples. Compared to the same series of decane, the

stronger Δ = 0 series for lubrication oils indicates the presence of oxygenated alkyl chains as one of the major moieties of lubrication oils.
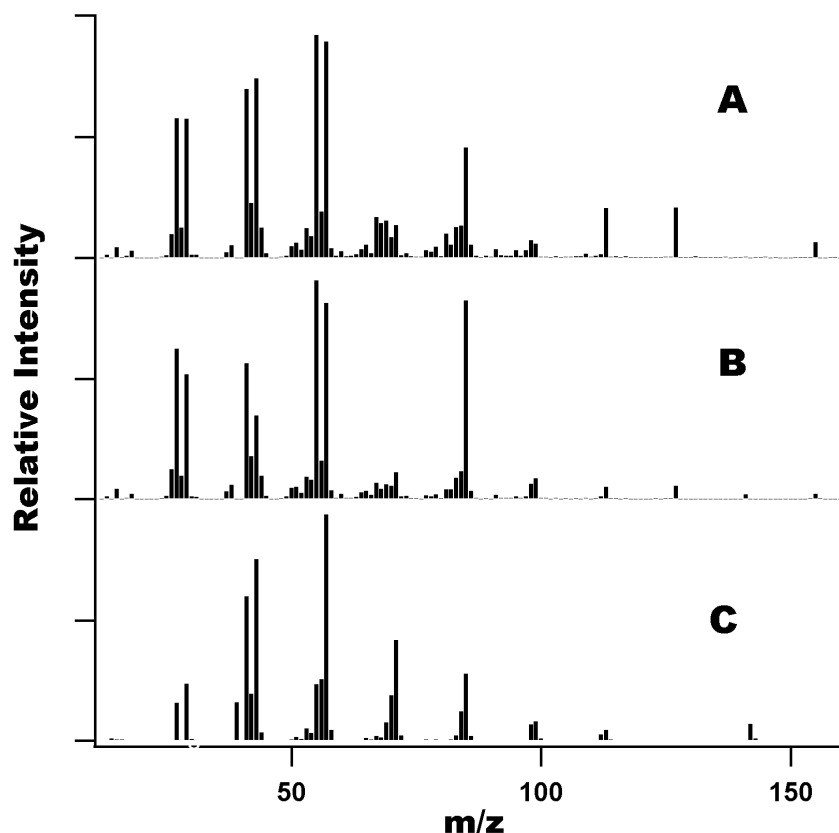


**Figure 4.8 Characteristic mass spectra of mono-disperse oil droplets in 250 nm diameter obtained from C-ToF AMS measurements with: (A) lubrication oil from BP; (B) lubrication oil from Mobil Oils; and (C) NIST standard mass spectrum of decane ($C_{10}H_{22}$). Because the significant difference in ion fragmentation pattern between aircraft lubrication oil and long-chain alkanes, the ratio of I(85)/I(71) will be considered as the mass marker in the AMS measurements to identify lubrication oil**

However, unlike the mass spectra of *n*-alkanes such as decane, the mass spectra of lubricant oils give significantly different fragmentation patterns at the mass range above m/z = 57, specifically the ion signal at m/z = 85, but also m/z = 113, 127, and 155. Even though an ion signal at m/z=85 is common for both alkanes and oils, the ratio of m/z=85 over m/z=71 allows their unambiguous differentiation. The less abundant ion signals at m/z = 113, and 127 vary appreciably between the two studied lubrication oils, probably a result of slightly different synthetic procedures and raw materials.

According to the early mass spectrometric study on aliphatic and aromatic esters (Sharkey et al. 1959; McLafferty & Gohlke 1959), C-O bond cleavage is one of the dominant pathways to generate fragment ions under electron impact ionization. From our AMS measurements on aircraft lubrication oils, the C-O bond breaking to form $C_nH_{2n+1}CO^+$ is the primary ion fragmentation pathway. This mechanism was verified in this study by using a high-resolution HR-ToF AMS. The HR-ToF AMS is capable of distinguishing $C_4H_9CO^+$ from $C_6H_{13}^+$ based upon their slightly different masses (85.070 vs 85.102 amu). We found that the pronounced m/z = 85 peaks in mass spectra of lubrication oils were primarily due to $C_4H_9CO^+$, which came from the C-O cleavage of $C_5$ fatty acid ester. The high-resolution MS measurement

suggests that $C_5$ fatty acid esters of pentaerythritol are the major components of the base fluids, in agreement with the specifications from the manufacturers. By comparison to m/z = 85, the signal at m/z = 71 is very weak, consistent with the lack of the $C_4$ fatty acid ester moiety in lubrication oil.

The two major brands of lubrication oils in the market yield different values for the ion intensity (peak area) ratio of m/z = 85 over m/z = 71, I(85)/I(71). The ratio of I(85)/I(71) for the BP sample is 3.7±0.2 (Figure 4.8A) and 8.6±0.5 for the sample from ExxonMobil (Figure 4.8B). For $n$-alkanes like decane, this ratio is about 0.66. This significant difference in I(85)/I(71) between lubrication oil and n-alkanes allows the AMS to make rapid identification of organic PM emissions that contain a large portion of aircraft lubrication oil. In addition, lubrication oil from BP yields appreciable ion fragments at m/z = 113 and 127, while for the ExxonMobil oil these ion peaks are negligible. In the following analysis, we assume that the engine combustion process yielded organic PM with an I(85)/I(71) ratio of 0.66 as decane. The oil contribution was identified base on a threshold, such that any measured value of I(85)/I(71) larger than 0.66 indicates the presence of lubrication oil.

We investigated the mass spectra of mono-disperse oil droplets from 100 to 350 nm and did not observe any noticeable difference in the spectra across this range of particle size. However, a dependence of lubrication oil ion fragmentation on source temperature has been observed in the laboratory investigation. In this study, the lubrication oil droplets were generated via atomization of lubrication oil at different heating temperature. The AMS measurement indicates that the ratio I(85)/I(71) decreases slightly with the heating temperature due to thermal pyrolysis. Therefore, the temperature to which the emitted oil is exposed is one of the limiting factors for the quantification of lubrication oil emissions. For example, the exhaust temperature of CFM-56 7B22 engine at idle condition is about 400°C.

### 4.4.2   Identification of Lubrication Oils from Aircraft Engine Exhaust Plumes at MWD and ORD

#### 4.4.2.1 Plume Measurements at MDW

While at Chicago Midway Airport (MDW) on February 17, 2010, engine exhaust plumes were identified using $CO_2$, CO and $NO_x$ time series measurements. The particle number concentration from the CPC, black carbon concentration from the MAAP, and the particle size information from the EEPS were also recorded. The AMS quantified the non-refractory mass loading and composition of semi-volatile organic PM present in the exhaust plumes. All of the identified plumes described in this work were due to near-idle engine operation based on CO and $NO_x$ concentrations: the ratio EI-CO/EI-$NO_x$ is significantly larger than unity at idle operation. Tail numbers were recorded and used to verify the visual identification of engine/airframe.

A segment of the exhaust plume data set is presented in Figure 4.9, in which the plume event #2 was marked by a significant increase in the $CO_2$, particle and black carbon concentrations, as well as organic PM. Since the AMS measures particles from 50 nm to 700 nm in diameter, the detected organic PM emissions were primarily associated with black carbon soot emissions since volatile nucleation mode particles are mostly smaller than the AMS measurement range. The rest of the observed plume events shown in Figure 4.9 showed increases in $CO_2$ and particle concentrations, while the signals in the MAAP and AMS measurements were below the instrumental detection limits.
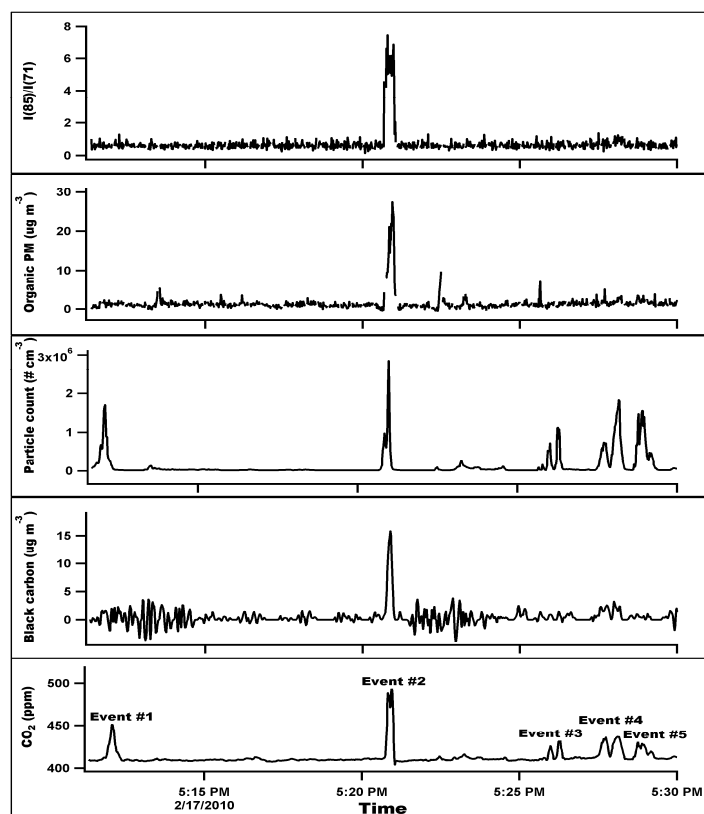
**Figure 4.9 A portion of the results from the field measurements on in-service commercial aircraft, which was performed at MWD on February 17, 2010**

In this study, the detection limit of the MAAP was about 3 μg m$^{-3}$ for 15s integration, while the detection limit was approximately 50 ng m$^{-3}$ for the AMS. This observation indicates that the low AMS signal is related to a low soot concentration. Due to the limitation of particle transmission efficiency decreasing at small particle sizes in the AMS, we cannot determine the composition of nucleation mode particles, which contribute significantly to by CPC measurements. For event #2, the ratio of I(85)/I(71) was determined to be approximately 5.9±0.8, indicating predominant contribution from lubrication oil to organic PM.

To identify the type of lubrication oil in use, we obtained the full organic PM mass spectra of the individual plume by integrating the AMS measurements through each plume and subtracting the ambient background from the resulting spectra, and then compared the obtained plume mass spectra with the standards of the two lubrication oils (Fig. 4.8A and 4.8B). We identified the type of lubricant oil applied for the aircraft and the results are listed in Table 4.2. Since we identified from the AMS measurement that the applied lubrication oil for event #2 was from ExxonMobil, which gives I(85)/I(71) = 8.60, the lubrication oil contribution to organic PM is determined to be approximately 66±10% by assuming that the organic PM from engine combustion yields I(85)/I(71) of 0.66.

**Table 4.2 Emission indices of organic PM (EI$_m$-org) and black carbon (EI$_m$-BC) due to the observed aircraft engine plume events as well as the determined oil contribution to organic PM. Events 1 – 5 are obtained from MDW while 6 – 12 from ORD**

| Event | Engine | EI$_m$-org (mg kg$^{-1}$) | EI$_m$-BC (mg kg$^{-1}$) | I(85)/I(71) | Oil Type | Oil contribution |
|---|---|---|---|---|---|---|
| 1 | CFM56-7B24 | - | - | - | - | - |
| 2 | BR715C1-30 | 386±49 | 200±47 | 5.9±0.8 | ExxonMobil | 0.66±0.10 |
| 3 | CF34-3B1 | - | - | - | - | - |
| 4 | CFM56-7B24 | - | 95±54 | - | - | - |
| 5 | PW150A | - | - | - | - | - |
| 6 | PW4077 | 8±1 | 39±6 | 1.1±0.5 | ExxonMobil | 0.05±0.06 |
| 7 | V2522-A5 | 10±2 | 206±10 | 3.7±0.7 | ExxonMobil | 0.38±0.09 |
| 8 | PW2037 | 13±2 | 214±9 | 3.5±1.0 | ExxonMobil | 0.36±0.13 |
| 9 & 10 | PW2037 & CF34-3B1 | 12±2 | 141±8 | 4.1±1.1 | BP | 1.00±0.35 |
| 11 | AE3007A1P | - | 117±31 | - | - | - |
| 12 | CF4-8E5G01 | 46±2 | - | 2.4±0.4 | BP | 0.55±0.13 |

The emission characteristics of a combustion source is usually evaluated in terms of emission index (EI), which is mass of the emitted pollutant per mass fuel consumed, in the unit of mg kg$^{-1}$ for PM mass. In this study, EI of organic PM (EI-org) measured by the AMS and black carbon (EI-BC) by the MAAP were calculated via the following equation (Timko et al. 2010):

$$EI(\frac{mg}{kg\ fuel}) = \frac{\Delta M}{\Delta C(CO_2)} \frac{T}{P} \times 4478$$

where $\Delta M$ is the measured mass in μg m$^{-3}$, $\Delta C(CO_2)$ is the difference between the sample and ambient $CO_2$ concentrations (in ppm), $T$ is the sampling temperature in Kelvin, and $P$ is the pressure (in torr). Based on the characteristic EI-$CO_2$ of 3160 g/kg fuel for conventional aviation fuel and neglecting engine combustion inefficiency, we calculated the emission indices of organic PM and black carbon for the observed plume events and listed the results in Table 4.1.

During the field measurements at MWD, the signal of organic PM and black carbon emissions for a large number of the plume events were below the instrumental sensitivity, except

for event #2, in which we measured more than one order of magnitude higher EI-org compared to the previously published results. The analysis above demonstrates that the predominant contribution to organic PM in event# 2 came from lubrication oil.

### 4.4.2.2 Plume Measurements at ORD

On February 18, 2010, analogous measurements were conducted at Chicago O'Hare International Airport (ORD). Figure 4.10 presents exhaust emission data for seven engine events (labeled as Events #6-12), all of which were taxiing based on the CO and $NO_x$ emission indices. The near constant delay (~60 seconds) between the appearance of the taxiing aircraft in the center of the video camera frame and wind speed-based estimates of the advection distance corroborate that these events were from taxiing aircraft with engines operating near-idle.
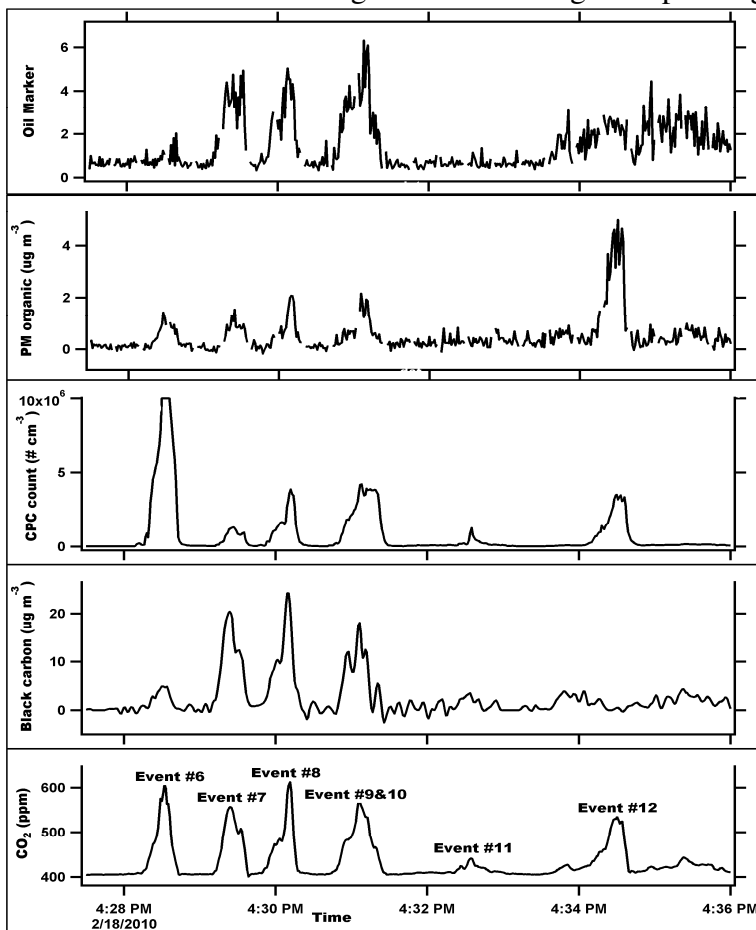


**Figure 4.10 A portion of the results from the field measurements at ORD**

The sources of the plume events described in Figure 4.10 are listed in Table 4.2. We observed more than one hundred plumes events during the two campaigns, but a large number of them were contaminated with other ground activities. The presented plume events are periods with little interference. The emission plume, event #6 in Figure 4.10, was generated by a PW4077 engine installed on a Boeing 777-222(ETOPS) airframe. Events #9 and #10, arrived too close to one another and are indistinguishable from each other in the measurements. Mass spectra of the organic PM obtained for all the plume events were obtained and compared to the

90

laboratory results to determine which type of lubrication oil was used. The determined oil type is also listed in Table 4.2, showing that both BP and Mobil lubrication oils were in common usage.

Given that I(85)/I(71) was approximately 1.1 for event #6 (Fig. 4.10), the oil contribution to the organic PM emission was small for this long-range wide-body aircraft. On the contrary, events #9&10, which were both due to small regional jet, show a significant lubrication oil contribution to the organic PM. Based on the determined I(85)/I(71) ratio and lubrication oil type, we calculated the contribution of lubrication oil to organic PM and presented the results in Table 4.2. Our results indicate that the oil contribution to the total organic PM EI ranges from 5 to 100% depending on engine type and condition.

### 4.4.3   Issues related to quantification of lubrication oil contribution to organic PM

A number of factors need to be considered when quantifying lubrication oil contribution to organic PM emissions. Since there are two common aircraft lubrication oils, the mass marker, I(85)/I(71), can only provide quantitative information after the applied lubrication oil has been determined. Therefore, the mass spectra of organic PM must be obtained to determine the oil type before the oil contribution can be calculated. However, in cases with low lubrication oil composition, the determination of oil type becomes difficult because of the experimental uncertainty in the AMS measurements. We could only provide an estimate in such cases.

## 4.5   Summary

This work has demonstrated that aircraft engine lubrication oil emitted from aircraft deoiling system can be an important emission vector of semi-volatile hydrocarbon mass that does not have to do with the combustion process. Synthetic lubricants are designed to be thermally and chemically stable to prevent degradation from corrosion and oxidation, especially for those made up of pentaerythritol esters that contain a shorter-chain alkanoyloxy group (Nakanish *et al.* 1997). Emitting such organic PM into the upper troposphere and lower stratosphere could have significant environmental impact. Emissions in and around airports can also contribute to degradation of local air quality. It is noteworthy, however that this study finds that the oil recycling techniques employed in the demisting technologies tested in this work are actually highly efficient in reducing oil particle emissions at and above the designed cut-off size.  It may be possible to further improve the demisting efficiency without significant energy cost by dramatically reducing the emissions of lubrication oil in the sub-micron size mode. Further investigations of the lifetime, atmospheric fate and the optical properties of these lubrication oil PM emissions formed in the wake of engines are important in evaluating the short- and long-term impact upon the atmosphere and local air quality.

The field study on in-service commercial aircraft engine exhaust reveals the unambiguous identification of lubrication oil constituents in organic PM emissions from taxiing commercial aircraft. Comparing the AMS field measurements of various commercial aircraft engine exhausts with those from the well-controlled mono-disperse lubrication oil aerosols generated in the laboratory, we found that lubrication oil was clearly present in the organic PM emissions from the commercial aircraft engine exhausts and could become the predominant composition in some of the cases. The intensity ratio of I(85)/I(71) from the AMS measurements serves as an excellent mass marker of lubrication oils. Although the quantitative correlation between lubrication oil emissions and engine model, thrust, age, and ambient conditions is still

under investigation, this study demonstrates that lubrication oil emission can be a significant component of organic PM in aircraft engine exhaust.

## 4.6 References

Anderson, B. E.; Cofer, W. R.; Bagwell, D. R.; Barrick, J. W.; Hudgins, C. H.; Brunke, K. E. 1998. Airborn Observations of Aircraft Aerosol Emissions I: Total Nonvolatile Particle Emission Indices. *Geophys. Res. Lett.*, 25, 1689-1692.

Corporan, E.; DeWitt, M. J.; Belovich, V.; Pawlik, R.; Lynch, A. C.; Gord, J. R.; Meyer, T. R. 2007. Emissions Characteristics of a Turbine Engine and Research Combustor Burning a Fischer-Tropsch Jet Fuel. *Energy Fuels.*, 21, 2615-2626.

Craig, P. H.; Barth, M. L. 1999. Evaluation of the Hazards of Industrial Exposure to Tricresyl Phosphate: a Review and Interpretation of the Literature. *J. Toxicol. Environ. Health, Part B.*, 2, 281-300.

Herndon, S. C.; Jayne, J. T.; Zahniser, M. S.; Worsnop, D. R.; Knighton, B.; Alwine, Lamb, B. K; Zavala, M.; Nelson, D. D.; McManus, J. B.; Shorter, J. H.; Canagaratna, M. R.;Onasch, T. B.; and Kolb, C. E. 2005. Characterization of urban pollutant emission fluxes and ambient concentration distributions using a mobile laboratory with rapid response instrumentation, *Faraday Discuss.***,** 130, 327-339.

Jayne, J. T.; Leard, D. C.; Zhang, X.; Davidovits, P.; Smith, K. A.; Kolb,C. E.; Worsnop, 2000. D. R. Development of an Aerosol Mass Spectrometer for Size and Composition Analysis of Submicron Particles, *Aerosol Sci. Technol.,* 33, 49-70.

Kolb, C. E.; Herndon, S. C.; McManus, J. B.; Shorter, J. H., Zahniser, M. S.; Nelson, D. D.; Jayne, J. T.; Canagaratha, M. R.; and Worsnop, D. R. 2004. Mobile Laboratory with Rapid response Instruments for Real-Time Measurements of urban and Regional Trace Gas and Particulate Distributions and Emissions Source Characteristics. *Environ. Sci. Technol.*, 38, 5694-5703.

McLafferty, F. W. and Gohlke, R. S. 1959. Mass Spectrometric Analysis: Aromatic Acids and Esters. *Anal. Chem.*, 31, 2076-2082.

McLafferty, F. W. and Turecek, F. Interpretation of Mass Spectra, 4th Ed., University Science Books, Mill Valley, CA, 1993.

Nakanish, H.; Onodera, K.; Inoue, K.; Yamada, Y.; Hirata, M. Oxidation Stability of Synthetic Lubricants. *Lub. Eng.* **1997**, 53, 29-37.

NIST Mass Spec Data Center, S.E. Stein, director, "Mass Spectra" in NIST Chemistry WebBook, NIST Standard Reference Database Number 69, Eds. P.J. Linstrom and W.G. Mallard, National Institute of Standards and Technology, Gaithersburg MD, 20899.

Onasch, T. B.; Jayne, J. T.; Herndon, S.; Worsnop, D. R.; Miake-Lye, R. C.; Mortimer, I. P.; Anderson, 2009, B. E. Chemical Properties of Aircraft Engine Particulate Exhaust Emissions. *J. Propul. Power,* 25, 1121-1137.

Paladino, J.; Whitefield, P.; Hagen, D.; Hopkins, A. R.; Trueblood, M. 1998, Particle Concentration Characterization for Jet Engine Emissions Under Cruise Conditions. *Geophys. Res. Lett.*, 25, 1697-1700.

Rogge, W. F.; Hildermann, L. M., Mazurek, M. A.; Cass, G. R.; Simoneit, B. R. 1993. Sources of Fine Organic Aerosol. 2. Noncatalyst and Catalyst-Equipped Automobiles and Heavy-Duty Trucks. *Environ. Sci. Technol.,* 27, 636-651.

Schlager,H.; Konopka, P.; Schulte, P.; Schumann, U.; Ziereis, H.; Arnold, F.; Klemm, M.; Hagen, D. E.; Whitefield, P. D.; Ovarlez, J. 1997. *In Situ* Observation of Air Traffic

Emission Signatures in the North Atlantic Flight Corridor. *J. Geophys. Res.*, 102, 10739-10750.

Schumann, U.; Arnold F.; Busen, R.; Curtis, J.; Karcher, B.; Kiendler, A.; Petzold, A.; Schlager, H.; Schroder, F.; Wohlfrom, K. H. 2002. Influence of Fuel Sulfur on the Composition of Aircraft Exhaust Plumes: The Experiments SULFUR 1-7. *J. Geophys. Res.*, 107, 4247.

Sharkey, A. G. Jr.; Shultz, J. L.; and Friedel, R. A. 1959. Mass Spectra of Esters. *Anal. Chem.*, 31, 87-94.

Timko, M. T.; Onasch, T. B.; Northway, M. J.; Jayne, J. T.; Canagaratna, M. R.; Herndon, S. C.; Wood, E. C.; Miake-Lye, R. C.; Knighton, W. B. 2010. Gas Turbine Engine Emissions-Part II: Chemical Properties of Particulate Matter. *J. Eng. Gas Turbine & Power*., 132, 061505/1-15.

Tou, J. C. 1972. Comparative Studies of Electron-Impact (EI) and Field Ionization (FI) Mass Spectra of Pentaerythritol Derivatives. *Org. Mass. Spectrem.*, 6, 833-841.

Van Netten, C. 1999. Multi-elemental Analysis of Jet Engine lubricating Oils and Hydraulic Fluids and Their Implication in Aircraft Air Quality Incidents. *The Sci. of the Total Environ.*, 229, 125-129.

Wang, D.; Mousavi, P.; hauser, P. J.; Oxenham, W.; Grant, C. S. 2004. Novel testing System for Evaluating the Thermal Stability of Polyol Ester Lubricants. *Ind. Eng. Chem. Res.*, 43, 6638-6646.

Winder, C.; Balouet, J.-C. 2002. The Toxicity and Commercial Jet Oils. *Environ. Res. Sect. A.*, 89, 146-164.

# 5   Condensation on Soot in the Exhaust of a Combustor Sector Rig

A systematic test was performed with a high pressure arc sector combustor rig located in the Jet Burner Test Stand (JBTS) at UTRC on July 19, 23, and 25, 2012.  This combustor rig is a test article used to evaluate hardware performance and when burning Jet A, provides PM emissions typical of gas turbine engines.  The partitioning of non-volatile and volatile particle emissions as well as the speciation of the volatiles provides a dataset that would be useful to determine necessary parameters for the microphysics modeling.  In addition to condensation experiments performed with the miniCAST burner, the sector rig test provides parameters to the model which are not easily obtained from other sources.  The deployed instruments include C-ToF AMS, SMPS, MAAP, CPC, and CAPS$_{ex}$ to investigate a variety of physical and chemical properties for both non-volatile and volatile PM emissions.

## 5.1   Description of the Facility and Test Setup

The combustor at the UTRC Jet Burner Test Stand (JBTS) is a full size test article consisting of 5 fuel nozzles in a 120 degree sector rig.  The combustor is placed in a pressure vessel allowing inlet pressures up to 300 psia and inlet temperatures to 1000 F.  A rotation emission rake system of 5 discrete sampling probes allows gaseous and particulate sampling to be performed. Jet A gas turbine fuel was used for our testing; the fuel sulfur content for this fuel sample was determined to be 656±1 ppm.

## 5.2   Sampling Setup

The burner exhaust sample is extracted at the exit plane of the combustor with five probes bundled together to average out the effect of sampling location.  The probes were stationary behind the middle combustor nozzle although the test stand had a capability to sweep the probe across the sector.  The five samples are mixed to one stream before it is split again into a gas sampling line and a particle sampling line.  The gas sampling line is an undiluted and heated line that feeds gaseous species measurement instruments.  The gaseous species measurement includes $CO_2$, CO, $O_2$, NO, $NO_2$, and total hydrocarbon.  The gas sampling line also feeds a filter sampling system that is used to measure Smoke Number according to ARP 1179.  The particle sampling line has a pressure control valve that regulates the flow entering Dekati diluter (typically between 0 to 15 PSIG).  The exhaust sample is diluted with dry nitrogen in the Dekati diluter by a factor of 3 to 11.  The dilution nitrogen may or may not be heated.  The Dekati diluter dumps some flow after dilution, and the diluted sample has some positive pressure head to travel through the sampling line (typically about 0.3 PSIG when using ½" transfer line and about 1.0 PSIG for ¼" line).  The sampling line is a 60-feet long stainless steel tubing.  We had two different sampling lines, one with ½" OD and 0.44" ID, and another with ¼" OD and 0.18" ID.  The ¼" line can be either heated or left at room temperature.  Because the ¼" line is bundled with the dilution nitrogen going into Dekati diluter, they must be heated or unheated at the same time.  The ½" is a separate line, and it does not have a heater.  Therefore, the sampling configuration can be one of the following four:
  A) Cold ¼" line, cold dilution
  B) Cold ½" line, cold dilution

C) Cold ½" line, hot dilution

D) Heated ¼" line, hot dilution

We tested for 3 or 4 dilution ratios for each sampling configuration.

The diluted sample was analyzed with 2 suites of instruments:

1) $CO_2$ meter (with a HEPA filter in front), SMPS, and MAAP

2) CPC, CAPS extinction monitor, and AMS

Between the suites 1 and 2, there was a 25 feet section of ¼" OD, 0.18" ID copper tubing (unheated). Figure 5.1 shows the schematic of the sampling setup, and Table 5.1 lists the specifications of the instruments used.
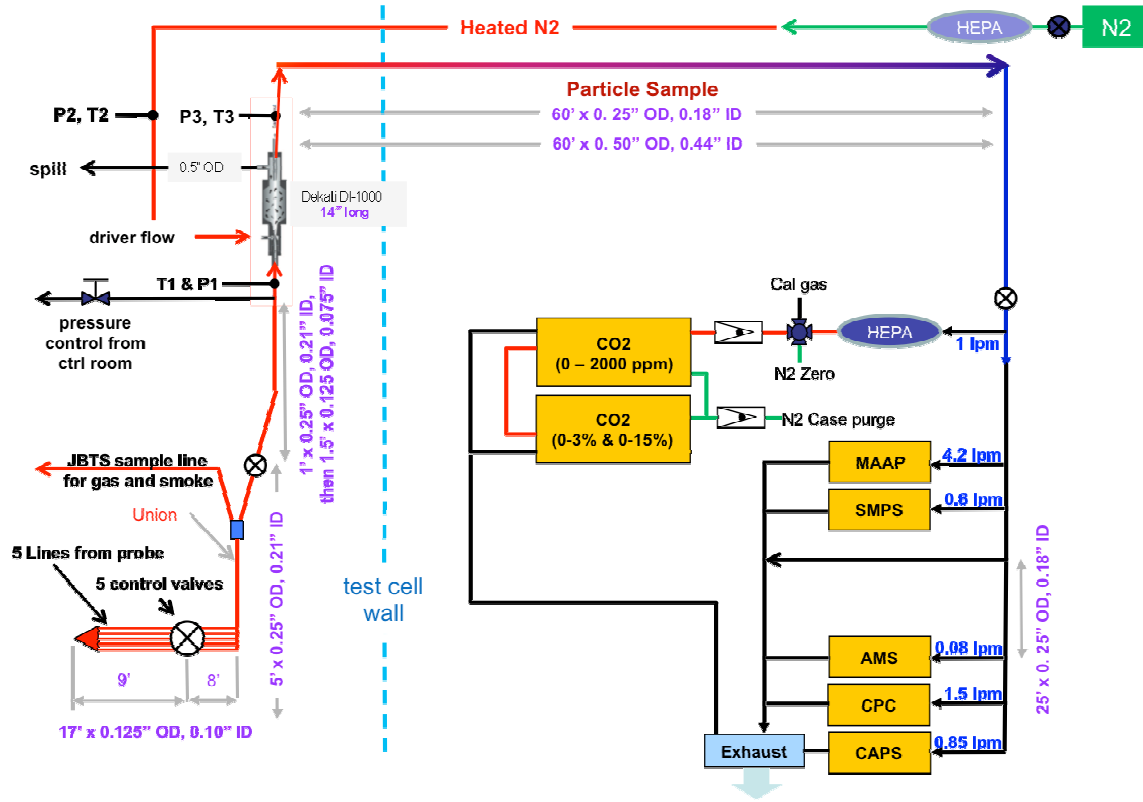


**Figure 5.1 Schematic of the sampling setup**

**Table 5.1 Specifications of the instruments**

| Instrument | Parameter measured | Unit reported | Detection range | Time resolution (s) |
|---|---|---|---|---|
| ARI C-ToF AMS | Size-resolved particle mass and composition | $\mu g/m^3$ | 80-1000 nm | ~10 |
| TSI CPC 3022 | Number concentration | $\#/cm^3$ | $0-10^7$ (>7 nm) | 1 |
| Thermo Electron MAAP 5012 | Black carbon mass | $\mu g/m^3$ | $> 5\ \mu g/m^3$ | ~1.5 |
| ARI Cavity Attenuated Phase Shift (CAPS) spectrometer | Total extinction | $Mm^{-1}$ | | |
| TSI SMPS (DMA 3080 + CPC 3025A) | Size-resolved number concentration (dN/dlogDp) | $\#/cm^3$ | 10-300 nm | 60 |
| Nondispersive intrared (NDIR) $CO_2$ meter | CO2 concentration | % | 0-3 % | 1 |

# 5.3   Results and Discussion

## 5.3.1   Effect of burner operating conditions

To understand and characterize the burner, we sampled the burner exhaust using the sampling configuration C, described in Section 5.2.  We kept the dilution ratio within a narrow range between 3 and 5, and changed the burner operating conditions such as the inlet temperature and pressure, and fuel-to-air-ratio.  The inlet temperature (T3) and pressure (P3) were changed from low to medium, and to high powers, to simulate different engine power settings, from idle to take-off.  At each power setting, the fuel-to-air ratio was varied.  Table 5.2 lists the burner operation conditions that we tested, and the corresponding emissions indices (EI) of gas and PM emissions at each condition.

**Table 5.2 Burner operating conditions and corresponding EI of gas and PM emissions**

| Power | P3 (Pa) | T3 (K) | Fuel-air ratio | EI NOX (g/kg) | EI CO (g/kg) | EI HC (g/kg) | EIn (#/kg) | EI BC (mg/kg) |
|-------|---------|--------|----------------|---------------|--------------|--------------|------------|---------------|
| low | 466869.9 | 518.4 | 0.0103 | 4.96 | 27.61 | 4.197 | 9.88E+11 | 0.064 |
| low | 482557.5 | 518.2 | 0.0128 | 5.50 | 36.56 | 0.410 | 2.35E+12 | 0.078 |
| low | 485162.5 | 517.3 | 0.0165 | 4.18 | 36.23 | 0.150 | 7.46E+12 | 0.085 |
| low | 482056.1 | 519.7 | 0.0184 | 3.68 | 41.16 | 0.108 | 1.27E+13 | 0.174 |
| low | 487508.3 | 519.3 | 0.0201 | 3.36 | 33.50 | 0.084 | 2.74E+13 | 0.515 |
| low | 486270.9 | 520.0 | 0.0224 | 3.18 | 29.15 | 0.070 | 4.99E+13 | 1.253 |
| low | 488976.2 | 519.5 | 0.0240 | 3.01 | 26.02 | 0.044 | 9.54E+13 | 2.914 |
| medium | 1222446.4 | 639.8 | 0.0100 | 10.14 | 5.38 | 0.110 | 4.83E+11 | 0.048 |
| medium | 1231043.3 | 638.2 | 0.0130 | 11.24 | 9.94 | 0.090 | 5.67E+11 | 0.016 |
| medium | 1217128.1 | 638.9 | 0.0187 | 6.37 | 10.56 | 0.064 | 3.29E+12 | 0.066 |
| medium | 1215603.3 | 640.0 | 0.0202 | 5.97 | 9.55 | 0.036 | 1.06E+13 | 0.150 |
| medium | 1227247.3 | 640.1 | 0.0224 | 5.42 | 7.74 | 0.041 | 3.86E+13 | 1.020 |
| medium | 1243509.6 | 640.6 | 0.0261 | 5.50 | 7.06 | 0.039 | 2.02E+14 | 9.908 |
| medium | 1235965.0 | 641.1 | 0.0296 | 5.66 | 9.36 | 0.037 | 3.52E+14 | 33.199 |
| medium | 1243821.6 | 641.6 | 0.0335 | 5.89 | 16.66 | 0.054 | 6.52E+14 | 108.418 |
| high | 1720032.3 | 729.8 | 0.0140 | 21.54 | 4.88 | 0.046 | 4.54E+11 | 0.147 |
| high | 1721575.3 | 730.3 | 0.0181 | 14.46 | 4.06 | 0.035 | 3.83E+12 | 0.101 |
| high | 1720010.0 | 699.2 | 0.0219 | 9.61 | 3.51 | 0.019 | 4.43E+13 | 1.108 |
| high | 1731841.2 | 700.8 | 0.0260 | 9.13 | 3.19 | 0.012 | 2.18E+14 | 11.399 |
| high | 1715104.9 | 699.7 | 0.0279 | 9.23 | 4.03 | 0.018 | 4.07E+14 | 31.755 |
| high | 1733536.8 | 701.1 | 0.0300 | 9.36 | 5.90 | 0.012 | 5.40E+14 | 63.741 |
| high | 1753414.2 | 700.3 | 0.0315 | 9.72 | 8.15 | 0.014 | 6.10E+14 | 99.451 |

The emissions indices (EI) of gaseous species in Table 5.2 are plotted in Figure 5.2.  As expected, the total NOx (a) increases with engine power due to higher combustion temperature, but as the engine power is increased, CO (b) and total hydrocarbon (c) EIs are reduced because the combustion efficiency is enhanced.  Figure 5.3 shows the PM EIs.  For PM measurements, less variation is seen between the engine powers, and the PM emissions increase with increasing fuel-to-air ratio.  In real aircraft engines, both the PM number and black carbon mass EI generally increase with power.  Figure 5.3 (a) and (b) suggest that the increased black carbon EI

in the real aircraft engines at high power is mainly due to increased fuel-air ratio associated with high power operation.  Figure 5.3 (c) shows that the black carbon mass EI increases faster than the number EI, indicating that larger particles are formed for fuel-rich combustions.



(a)

(b)

(c)
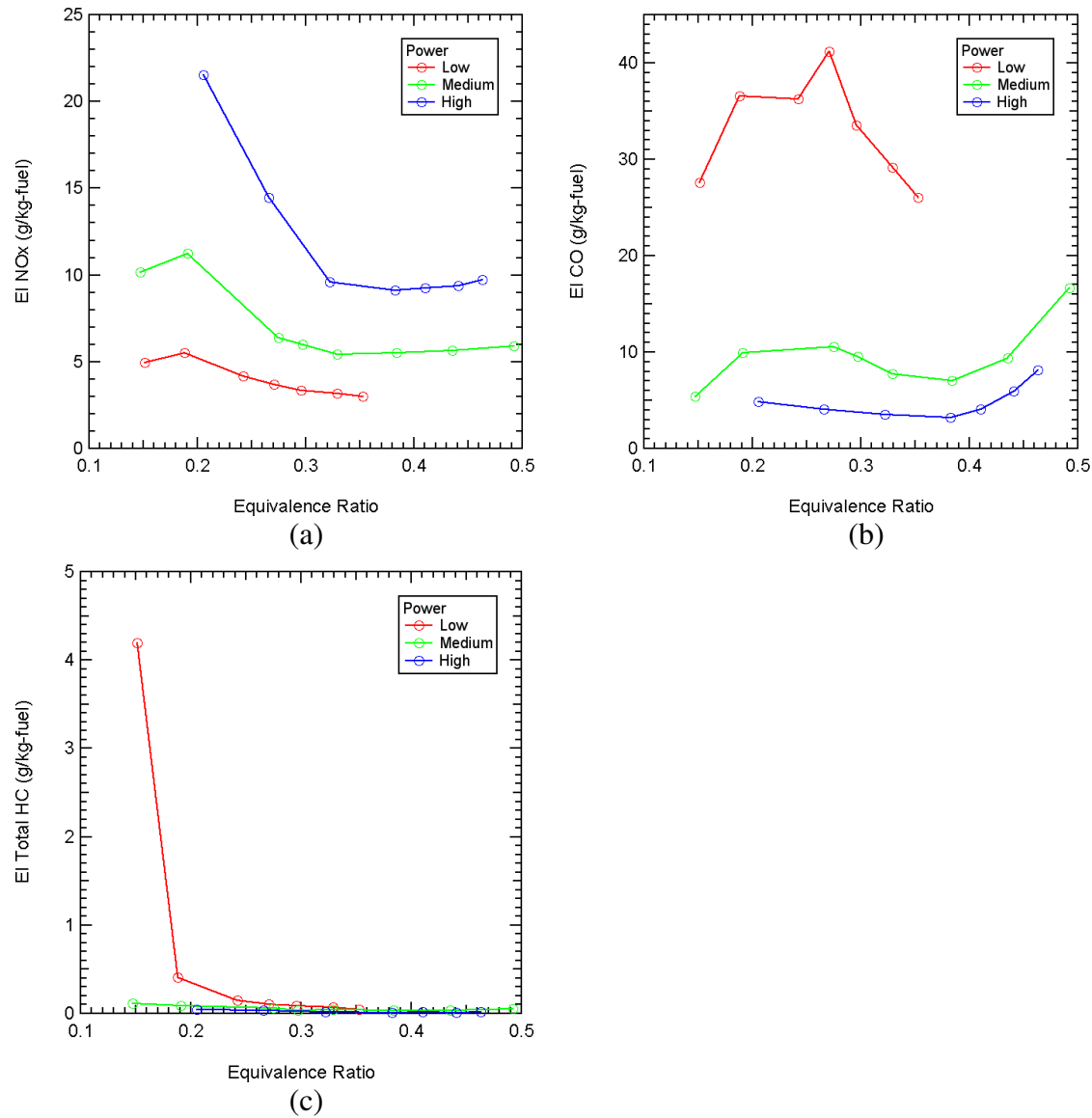
**Figure 5.2 Emissions indices (EI) of (a) NOx, (b) CO, and (c) total hydrocarbon vs. fuel-air equivalence ratio**
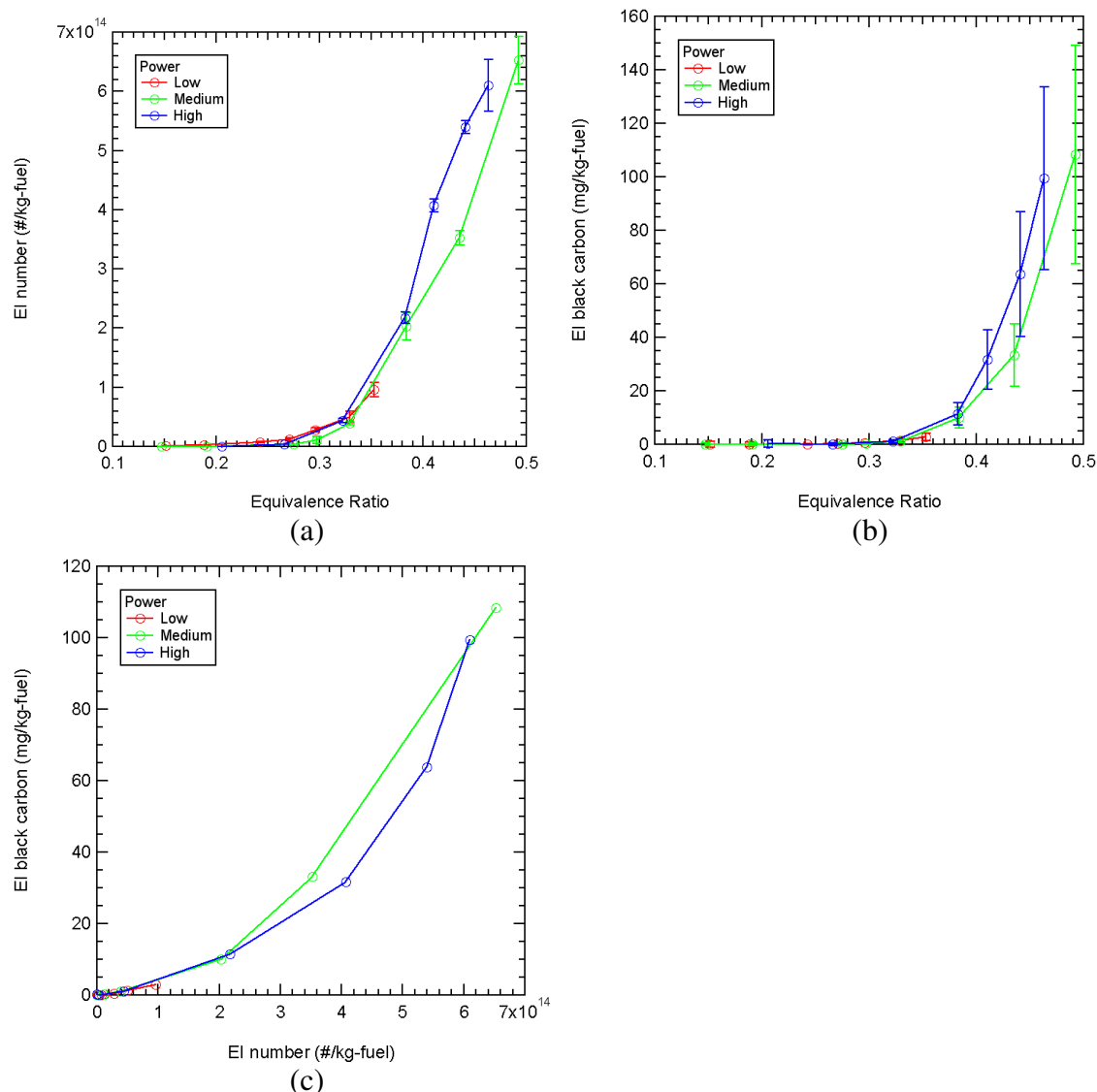
**Figure 5.3 Emissions indices (EI) of (a) PM number and (b) black carbon mass vs. fuel-air equivalence ratio, and (c) EI black carbon vs. EI number**

### 5.3.2 Effect of sampling configuration

At two different power settings, we kept the burner at constant operation and varied the sampling configuration. Figure 5.4 shows the EIs of the PM species when the burner setting was at medium power (1.2MPa and 640K combustor inlet pressure and temperature, with a fuel-to-air ratio of 0.028). Figure 5.4 (a) and (b) implies that the PM number and black carbon mass are not significantly affected by the dilution ratio or dilution temperature. The variance is mainly due to the different sampling line size, and we believe that the difference is due to different loss rate to the sampling line walls. Not much difference can be seen for the organic coating of soot particles. However, the EI of PM sulfates is significantly increased (by more than a factor of 4) by using cold dilution (Figure 5.4 (c)).

98
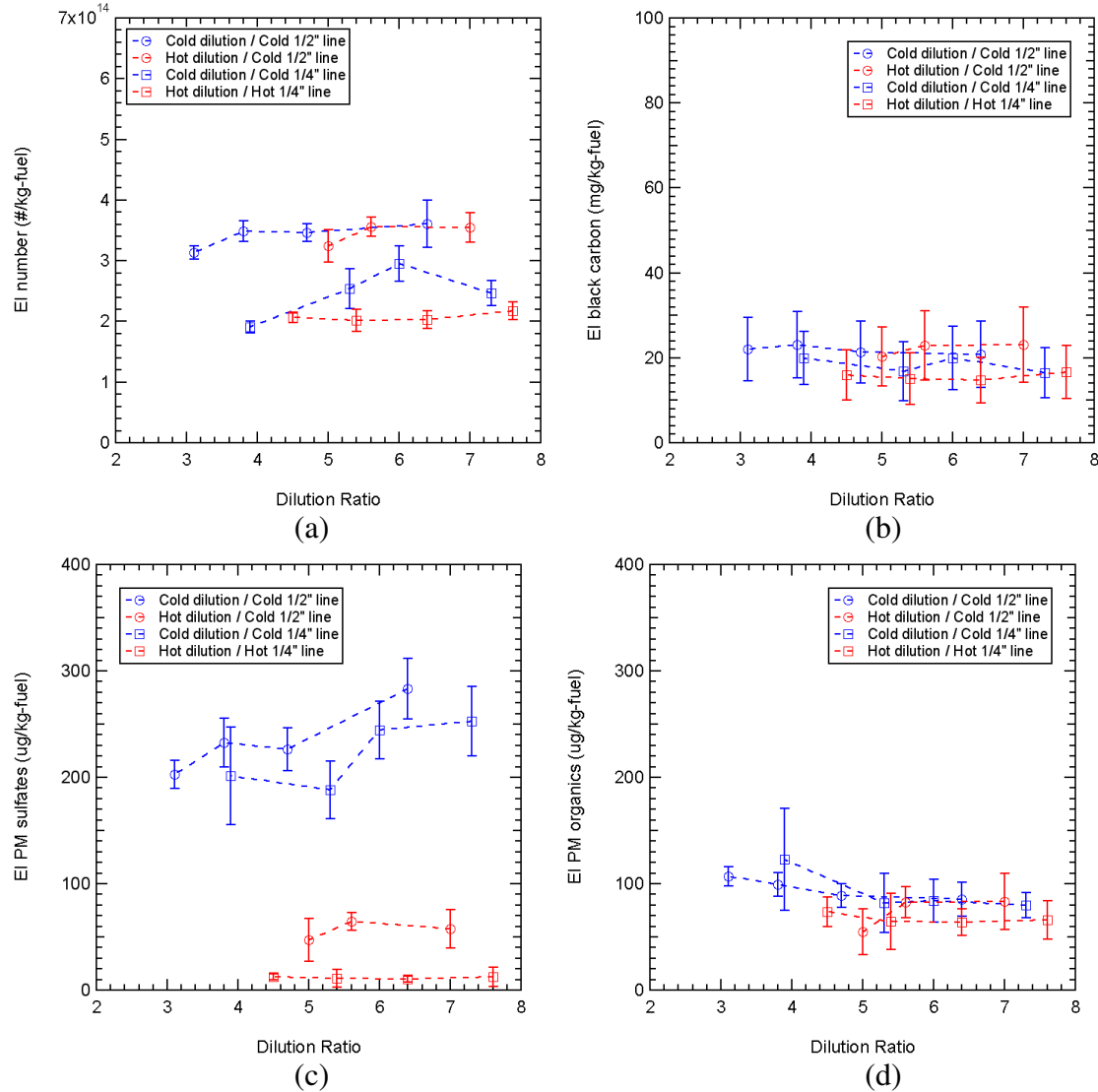
**Figure 5.4 EIs for (a) PM number, (b) black carbon mass, (c) PM sulfates, and (d) PM organics for the burner operating at 1.2MPa of inlet pressure, 640K of inlet temperature, and 0.028 of fuel-air ratio**

Figure 5.5 shows the EIs of the PM species when the burner setting was nominally at sea-level take-off power (1.7MPa and 700K of combustor inlet pressure and temperature) with a fuel-to-air ratio of 0.030. Compared with the medium power condition, the PM number and black carbon EIs are increased, about a factor of 2 for the number and a factor of 3 for the mass. For the high power, it appears that there is a more difference in the PM number and black carbon mass EIs between the hot and cold dilutions cases, and it may be due to the fact that we heated the Dekati dilutor itself when we turned on the heating on this day. For the medium power condition experiments, the final segment of the heater that heats the Dekati dilutor failed, and could not be used. PM organics follow a very similar trend as the black carbon mass, about a factor of 3 increase from the medium power. However, PM sulfates are not by affected by the power change. This is because the volatile sulfates are almost fully converted to the particle phase even for the low soot setting (medium power) in this sampling configuration, so additional soot surface area does not lead to more condensation. The fraction of the organics converted from the vapor phase to particle phase is small, and therefore the additional soot surface can

facilitate more condensations of organic species. This argument will be discussed in more detail in Section 5.4.
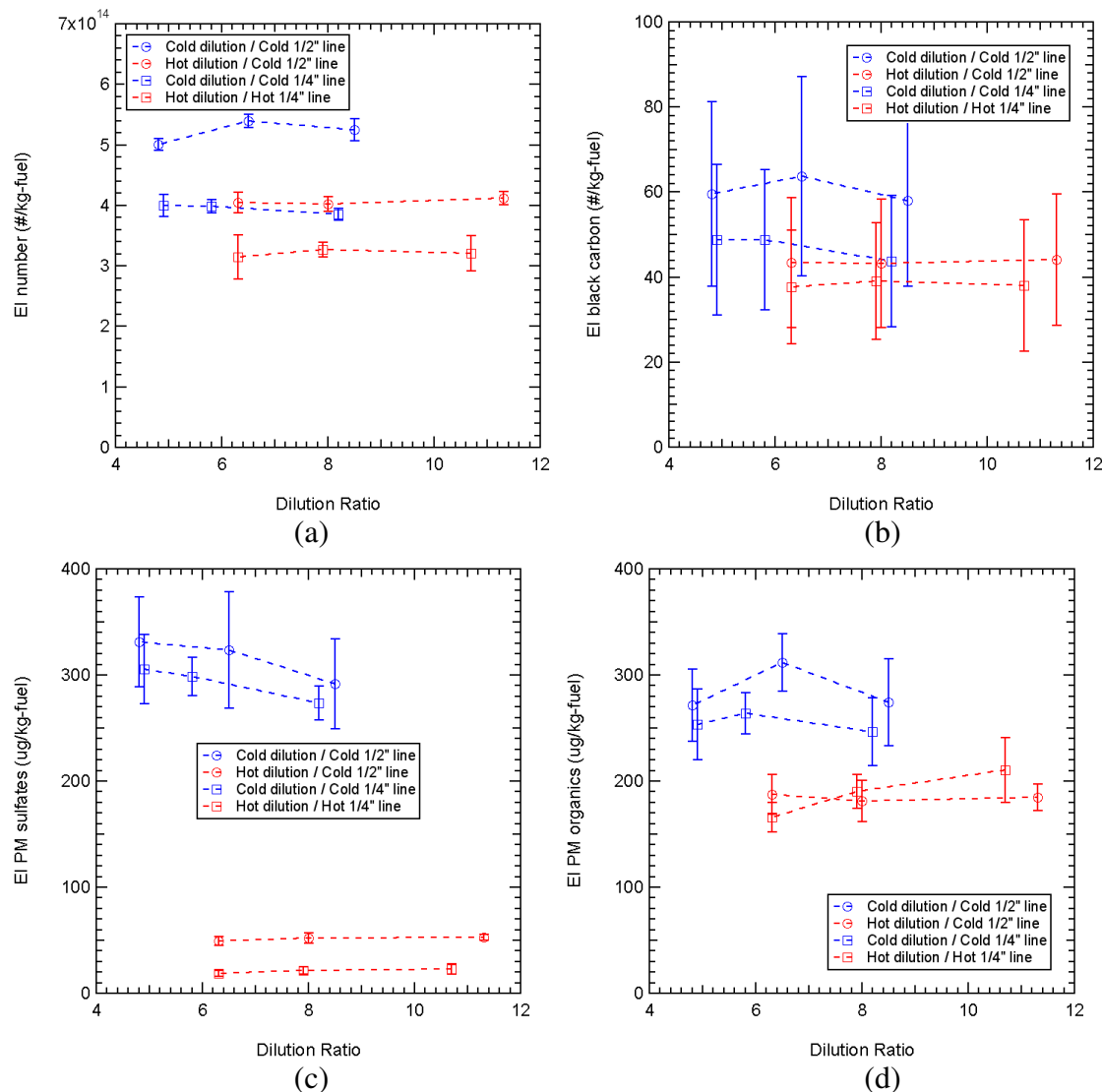


Figure 5.5 EIs for (a) PM number, (b) black carbon mass, (c) PM sulfates, and (d) PM organics for the burner operating at 1.7MPa of inlet pressure, 700K of inlet temperature, and 0.030 of fuel-air ratio

### 5.3.3 Further test on the effect of dilution temperature

In Section 5.3.2, the effect of the dilution nitrogen temperature was discussed. To study the temperature effect more carefully, we performed a test in which we maintained the burner operating conditions and dilution conditions constant, but only changed the temperature of the dilution nitrogen gradually from 380K to 325K over 45 minutes time span. For this test, the burner inlet temperature was 700K, inlet pressure 1.76MPa, and fuel-to-air ratio 0.030 (high power). The ½" cold sampling line was used. Figure 5.6 shows the time series data for the test. It can be seen that the AMS sulfates signal increases as the dilution nitrogen temperature decreases while all other conditions are constant. This indicates that more sulfates condense and coat on the soot particles when the dilution is cooler. The AMS organics slightly decreases as the dilution temperature decreases, implying that the coating partitioning changes. These results

are consistent with the observation and explanation described in Section 5.3.2, and also with our microphysical simulation results described in Section 2.
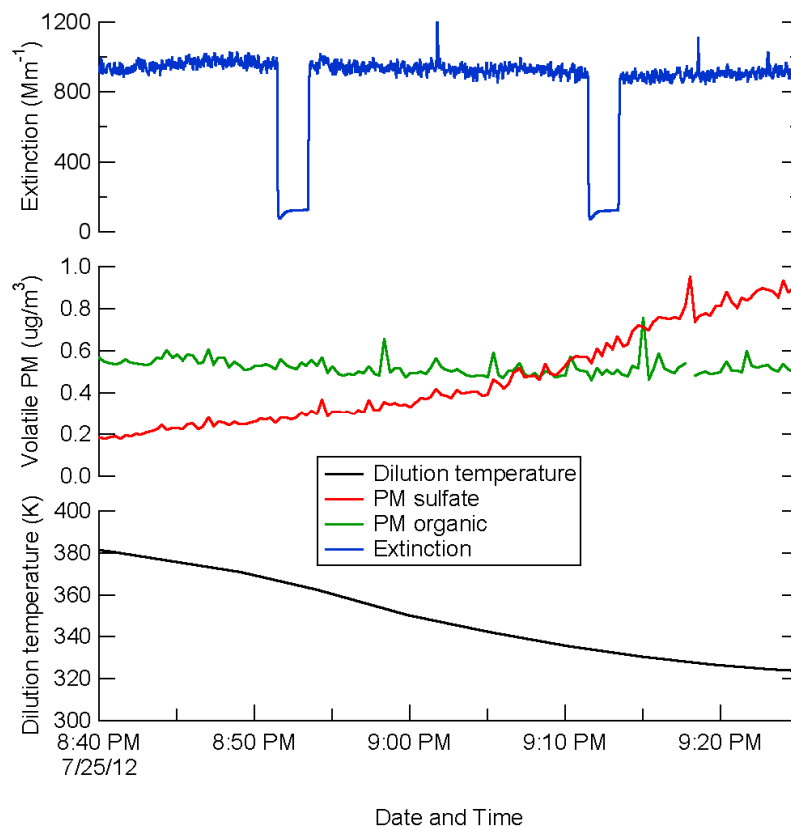


**Figure 5.6 Time series data for changing dilution temperature while keeping the burner operation and dilution ratio constant**

## 5.4 Microphysical Modeling

In this section, two sets of microphysical simulations are performed, one to examine the difference between the medium and high power settings, and another to see the dilution temperature effect. The microphysical simulation code described in Section 2 was used. The organic species included in the simulation and the relative composition among them are shown in Figure 5.7, which basically follow the argument described in Section 2.
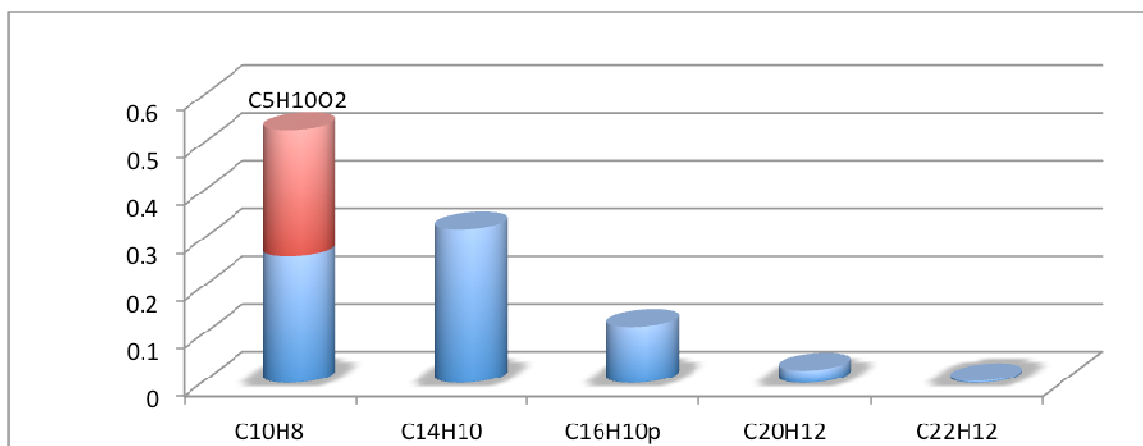
**Figure 5.7 Hydrocarbon species included in the model, and their relative composition**

A few simulations with the nucleation/coagulation mode turned on revealed that the homogeneous mode was not important, and it was turned off in the subsequent simulations.

### 5.4.1   Medium vs. high power setting

The main differences between the two power settings are soot loading and total hydrocarbon concentration.  The high power condition has higher soot concentration and lower total hydrocarbon concentration than the medium power condition.  To investigate the effect of these changes, two microphysical simulations were performed for:

1) $1 \times 10^7$ cm$^{-3}$ soot concentration, 0.6 ppm total hydrocarbon, 5.8% $CO_2$ to simulate the medium power condition
2) $3 \times 10^7$ cm$^{-3}$ soot concentration, 0.4 ppm total hydrocarbon, 6.6% $CO_2$ to simulate the high power condition

The sampling line configuration of ½" cold line with cold dilution (setup B described in Section 5.2) with a dilution ratio of 5 was used.  Figure 5-8 shows the temperature profile calculated for the case, using a 1-dimensional heat transfer calculation based on a fully-developed turbulent flow assumption.

**Figure 5.8 Temperature profile for the microphysical simulation run representing a cold ½" sampling line with a cold dilution at a factor of 5**

Table 5.3 lists the simulation results for the two cases. The high power condition shows higher EI for organics even though the initial vapor phase organics concentration was lower than that for the medium power condition. It is because the condensation of organic species was limited by the available soot surface, not by the vapor phase concentration, so larger soot surface area accommodated more organics condens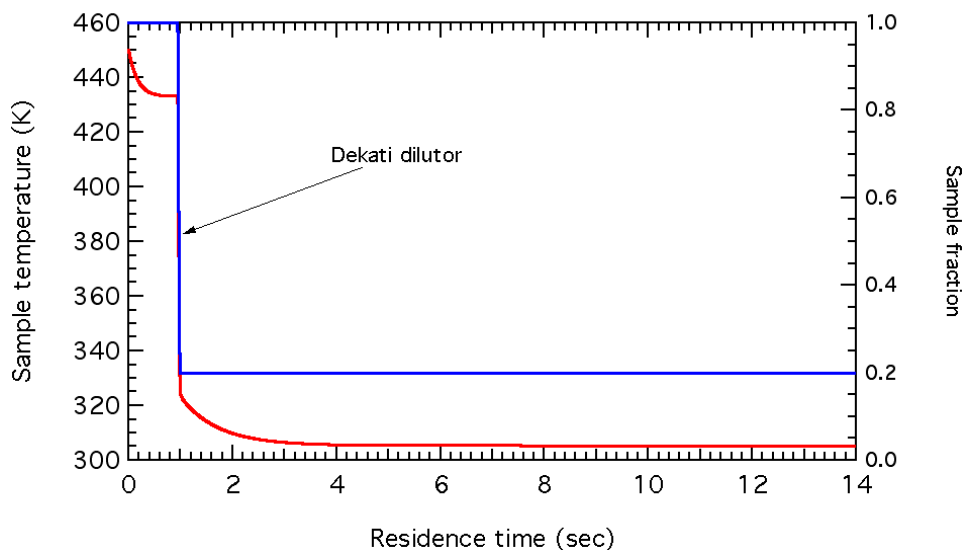ation. For the sulfates, however, almost all sulfates are already converted to the particle phase even for the low soot (medium power) condition, and more surface area does not promote more sulfates condensation. This trend is consistent with the experimental results shown in Figures 5.3 and 5.4.

**Table 5.3 Microphysical simulation results for power settings representing medium and high**

| Power | EI sulfates | EI organics |
|-------|-------------|-------------|
| Medium | 356.01 µg/kg | 327.26 µg/kg |
| High | 346.97 µg/kg | 334.16 µg/kg |

### 5.4.2 Hot dilution vs. cold dilution

In Section 5.3.3, it was shown that the cold dilution generates more sulfates coating on the soot particles. A set of simulations was performed for a hot (110 °C) dilution case and a cold (45 °C) dilution case, and the results are shown in Table 5.4. The simulations are for a burner condition representing the high power setting: $2 \times 10^7$ cm$^{-3}$ soot concentration and 0.4 ppm initial organics concentration. The simulation results capture the trend that the sulfates EI increases as the dilution temperature decreases from 110 °C to 45 °C, but the change is not as dramatic as the experimental results where it showed a factor of 5 times difference. Also, the organics EI increases as well with the cold dilution, which is the opposite trend as the experiments, but the amount of increase is smaller than the sulfates. We currently do not have a full explanation for this slight discrepancy between the experiments and the simulations. Some possibilities are 1) gaseous and/or particle loss to the sampling line walls, 2) incorrect mass accommodation coefficients, and 3) the included 6 hydrocarbon species not representing the burner exhaust.

**Table 5.4 Microphysical simulation results for hot dilution and cold dilution cases**

| Dilution temperature | EI sulfates | EI organics |
|---|---|---|
| 45 $^{o}$C | 285.19 µg/kg | 74.01 µg/kg |
| 110 $^{o}$C | 276.87 µg/kg | 71.99 µg/kg |

## 5.5  Summary

A systematic measurement of particulate matter was performed with a combustor sector rig at a wide range of burner operation conditions and with 4 different sampling configurations. It was found that the dilution ratio is not an important factor when sampling particulates.  For non-volatile soot particles, the dilution temperature does not significantly affect the measurements, but the sampling line diameter does.  For volatile PM such as sulfates and organics, both the dilution temperature and sampling line diameter have significant impacts on the measurements. .  It was experimentally observed and numerically explained that the amount of sulfates coated on the soot particles increases when using colder dilution gas. Because the sulfates are readily converted to particle phase regardless of the amount of available soot surface area, sulfates EI was not changed by different soot conditions (different power setting). However, the condensation rate of the organic species is much lower than the sulfates, making the soot surface availability a rate limiting factor, and the organics EI increases with increasing black carbon number and mass.  This trend was captured by the microphysical simulations

## 5.6  Reference

SAE ARP 1179: Aircraft Gas Turbine Engine Exhaust Smoke Measurement, 1997.

# 6  Summary and Conclusions

This project was a multi-component effort that drew on the expertise of university research scientists, private sector research scientists, and aircraft engine manufacturers. The work spanned a range of elements from theoretical model development through laboratory scale experiments and industrial hardware development test facilities to full scale engine testing.  There was excellent synergy between the various components of the project, which ensured that the basic research components were addressing important questions for engineering application and that the industrial tests were done with a fundamental understanding of the underlying processes. Several of the research questions that were addressed during this project:

- *How do unburned low volatility hydrocarbons contribute to the number, size and mass of particle emissions from aircraft engines ?*
- *How do aerosols evolve in the engine plume ?*
- *What properties of volatile species control condensation and particle growth ?*
- *What is the quantity and role of lubrication oil emitted by an engine ?*

Significant advances were made on all fronts, and this report and the associated archival journal publications will provide a useful resource for the documented understanding of volatile PM emissions from aircraft engines.

Each of the main facets of the overall project is summarized below along with the important conclusions for each. For the overall project:

1. *A more complete understanding of volatile PM emissions from gas turbine engines has been obtained*
2. *A modeling tool is available that can quantitatively predict how organic and sulfate emissions contribute to volatile PM formation and growth.*

This model has been demonstrated to be applicable for full scale gas turbine engines, which will allow future technology decisions to be evaluated for volatile PM emissions. In addition, this understanding and these tools will allow better and more quantitative assessments of how aircraft emissions can contribute to emissions inventories around military bases so that more accurate and realistic environmental impact assessments can be made.

**Model Development and Applications:** In this project, a detailed microphysical model previously developed to study PM evolution in near-field aircraft emitted plumes was extended to study soot microphysics and homogeneous particle nucleation in the presence of organic emissions. Our new formulation includes (1) organic vapor activation on soot surface, (2) organic vapor condensation on activated soot surface, (3) independent unary nucleation of water-insoluble organic vapors, and (4) condensation of water-soluble and water -insoluble organic vapors on homogeneous sulfuric acid-water droplets. Several organic surrogate species mimicking organic emissions from modern gas turbine engines were selected for our modeling study, and methodologies estimating chemical and physical properties of the aerosols containing complex mixtures of sulfuric acid, water, and various organic molecules were also developed. Our modeling study suggests that:

- *soot size, ambient conditions (temperature and relative humidity levels), organic emissions levels, and organic mass accommodation coefficients all have effects on the amount of organic coatings on soot.*

Homogeneous particle formation is primarily driven by binary sulfuric acid-water nucleation, and water insoluble organic species significantly contribute the size growth of the homogeneous droplets. Competition between soot surfaces and homogeneous particles for organic vapors exists, and the partitioning between the two modes is determined by the ambient conditions, engine operation, and emissions levels.

This model was used to plan the laboratory studies and the sector rig test, and was used to analyze the resulting data from those measurements. By comparing the model predictions with the experimental results, parameters in the model (mass accommodation coefficients) were refined to better represent the observed microphysical evolution. Further, such exercising of the model allowed it to be tested in an operational setting and to be shown to be a good tool for estimated volatile PM emissions from military gas turbine engines.

**Laboratory Studies:** A laboratory study of volatile organic compound (VOC) coatings on combustion soot particles resulted in the determination of uptake coefficients for a variety of VOCs. Uptake is a critical parameter in the microphysical process of gas to particle evolution, since under controlled experimental conditions the uptake coefficient can be considered equivalent to the dry mass accommodation coefficient. We found that:

- *a phenomenological power-law correlation exists between the uptake coefficient of VOCs on combustion soot particles and the solubility of VOCs in water, therefore:*
- *the more soluble the VOC is in water, the less likely the VOC will coat on the fresh soot surface.*

This is in agreement with the common thinking that fresh combustion soot is hydrophobic.

In general, uptake coefficients are difficult to measure experimentally since the simultaneous determination of species concentration in both gaseous and particulate phases is required. Thus, the phenomenological correlation developed under this project allows

- *estimates to be made of the uptake coefficient for most organic compounds based solely on aqueous solubility, which has been widely studied.*

In the future, this correlation may also be very useful for air quality assessment, when both soot and VOCs are involved.

**Engine Oil PM:** A dedicated engine test at a Pratt & Whitney Test Facility and field measurements at Chicago's O'Hare International Airport and Midway International Airport have quantified aircraft engine lubrication oil as a significant emission vector of semi-volatile hydrocarbon mass that does not have to do with the combustion process.

- *The contribution of lubrication oil to total PM organic emissions ranges from 5% to 100% based on engine type, age, and maintenance.*

In general, new aircraft engines generate much lower emissions of lubrication oil than the old types of engines. It is noteworthy, however that this study finds that the oil recycling techniques employed in the demisting technologies tested in this work are highly efficient in reducing oil particle emissions at and above the designed cut-off size of approximately 1μm. It may be possible to further improve the demisting efficiency without significant energy cost to reduce the emissions of lubrication oil in the sub-micron size mode. Further investigations of the lifetime, atmospheric fate and the optical properties of these lubrication oil PM emissions formed in the wake of engines operating aloft are important in evaluating the short- and long- term impact upon atmosphere.

**Sector Rig Tests:** Particulate matter (PM) emissions from a 4-nozzle high-pressure combustor sector rig were determined over a range of burner operation conditions using 4 different sampling configurations to study the condensation of VOCs on soot.

- *For volatile PM such as sulfates and organics, both the dilution temperature and sampling line diameter (residence time) have significant impacts on the measurements.*
- *It was experimentally observed and numerically explained that the amount of sulfates coated on the soot particles increases when using colder dilution gas.*

Because the sulfates readily condense on the soot even for low soot conditions, sulfate concentration was not changed by different soot concentrations (different power setting). However, the condensation rate of the organic species is much lower than the sulfates, making the soot surface availability a rate-limiting factor, and the organics concentration increases with increasing black carbon number and mass. This trend was captured by the microphysical simulations, which demonstrate that the models developed in this project are applicable to the regimes encountered in full-scale military engines.

In these the combustor sector rig experiments, the mass accommodation coefficients, which are critical parameters in the microphysical model, were determined with higher fidelity.

- *With the updated mass accommodation coefficients, the microphysical simulation method can now quantitatively determine the organic PM emissions, as well as the sulfate PM emissions, from aircraft engines.*

This is an important contribution to understanding the total PM emissions from military gas turbine engines and the major objective of the overall project.

# Appendix: Publications and Presentations

**Publications**

*In-print:*

Yu, Z., Liscinsky, D. S., Winstead, E. L., True, B. S., Timko, M. T., Bhargava, A., Herndon, S. C., Miake-Lye, R. C., Anderson, B. E. (2010). Characterization of Lubrication Oil Emissions from Aircraft Engines. *Environ. Sci. Technol.*, 44:9530-9534.

Yu, Z., Ziemba, L. D., Onasch, T. B., Herndon, S. C., Albo, S. E., Miake-Lye, R. C., Anderson, B. E., Kebabian, P. L., and Freedman, A. (2011). Direct Measurement of Aircraft Engine Soot Emissions Using a Cavity-Attenuated Phase Shift (CAPS)-Based Extinction Monitor. *Aerosol Sci. Technol.*, 45:1319-1325.

Yu, Z., Herndon, S. C., Ziemba, L. D., Timko, M. T., Liscinsky, D. S., Anderson, B. E., Miake-Lye, R. C. (2012). Identification of Lubrication Oil in the Particulate Matter Emissions from Engine Exhaust of In-service Commercial Aircraft. *Environ. Sci. Technol.*, 46: 9630-9637.

*Submitted:*

Liscinsky, D. S., Yu, Z., True, B. S., Peck, J., Jennings, A. C., Wong, H-W., Franklin, J., Herndon, S. C., Miake-Lye, R. C. (submitted). Uptake of Naphthalene by Combustion Soot Particles. *Combust. Flame*.

Yu, Z., Liscinsky, D. S., True, B. S., Peck, J., Jennings, A. C., Wong, H-W., Jun, M., Franklin, J., Herndon, S. C., Waitz, I., Miake-Lye, R. C. (submitted). Uptake Coefficients of Several Volatile Organic Compounds by Combustion Soot Particles and its Correlation with Hydrophobic Effect. *Environ. Sci. Technol.*

**Presentations**

"Tackling a moving target: chemical and microphysical evolution of particulate emissions from aircraft engines", S. C. Herndon, Wong, H.-W., Yu, Z., Timko, M. T., Wood, E. C., Miake-Lye R. C., Knighton, W. B., Beyersdorf, J. A. and Anderson, B. E. American Geophysical Union Meeting, 2009. *Abstract and presentation to Aviation session.*

"Evolution of Aircraft Engine Emissions in the Atmosphere" S.C. Herndon. Partners in Environmental Technology Technical Symposium & Workshop, 2009. *Abstract and presentation to Aircraft Emissions: Future Impacts and Alternative Fuels session.*

"Modeling of hydrocarbon-containing aerosols in near-field aircraft emission" M. Jun, Wong, H.-W., Peck, J., Waitz, I. A., and Miake-Lye, R. C., Aviation Climate Change Research Initiative Symposium, 2011. *Abstract and presentation to Contrails: Simulations and Comparison session.*

"Quantification of Hydrocarbon Condensation on Combustion Soot Particles" D. Liscinsky, Z. Yu, S. Herndon, J. Franklin, J. Peck, H.-W. Wong, M. Jun, I. Waitz, B. True, M. Colket, A. Bhargava, B. Sen, R. Miake-Lye, American Association for Aerosol Research Conference, 2011. *Abstract and presentation to 30th Annual conference in Orlando FL, Oct. 3-7, 2011.*

"Quantification of Hydrocarbon Condensation on Combustion Soot Particles" D. Liscinsky, Z. Yu, S. Herndon, J. Franklin, J. Peck, H.-W. Wong, M. Jun, I. Waitz, A. Jennings, B. True, M. Colket, R. Miake-Lye, Eastern States Section of the Combustion Institute, 2011. *Abstract and presentation Fall Technical Meeting Oct. 9-12*, 2011

"Contrails and Smoke Trails to Exhaust Particle Processes: A Brief History of Aircraft Particulate Emissions" Miake-Lye, R. C., Partners in Environmental Technology Technical Symposium & Workshop, 2011. *Abstract and presentation to Impact of Particulate Emissions from Gas Turbine Powered Aircraft session.*

"Aircraft Emissions Characterization" R.C. Miake-Lye, Airport Council International – North America. *Abstract and presentation to 2012 Environmental Affairs Conference in Las Vegas, NV, 16-19 April 2012.*

"Quantifying the Composition of Volatile Particulate Matter Emissions from Aircraft Engine" Z. Yu, H.-W. Wong, J. Peck, S.C. Herndon, M. Jun, I.A. Waitz, D.S. Liscinsky, A. Jennings, B.S. True, A. Bhargava, M. Colket, B. Sen, L.D. Ziemba, E.L. Einstead, B.E. Anderson. Transportation, Atmosphere, and Climate Conference (TAC-3). *Prien am Chiemsee, Germany 25-28 June 2012*

**Posters**

"Fusing model results and measurements to quantify the contributions of sulfate and organic emissions to particles emitted from military aircraft engines" Wong, H.-W., Jun, M., Liscinsky, D., Yu, Z., Cross, E., Fortner, E., True, B., Bhargava, A., Herndon, S., Onasch, T., Waitz, I., Colket, M., and Miake-Lye, R., Partners in Environmental Technology Technical Symposium & Workshop 2009 Poster Session.

"Novel characterization of lubrication oil emissions from military aircraft engines" Liscinsky, D., Yu, Z., Winstead, E., True, B., Timko, M., Herndon, S., Anderson, B., Miake-Lye, R., and Bhargava, A, Partners in Environmental Technology Technical Symposium & Workshop 2009 Poster Session.

"Development of a detailed microphysical model to simulate the formation of hydrocarbon-containing aerosols emitted from military aircraft engines" H.-W. Wong, M. Jun, I. Waitz, D. Liscinsky, J. Peck, S. Herndon, M. Colket, Z. Yu, B. True, J. Franklin, R. Miake-Lye, Partners in Environmental Technology Technical Symposium & Workshop 2010 Poster Session.

"Quantitative Measurements of Hydrocarbon Condensation on Soot Particles" D. Liscinsky, Z. Yu, S. Herndon, B. True, H.-W. Wong, M. Jun, J. Franklin, J. Peck, A. Bhargava, B. Sen, I. Waitz, M. Colket, R. Miake-Lye, Partners in Environmental Technology Technical Symposium & Workshop 2010 Poster Session.

"Characterization of Lubrication Oil Emissions from Aircraft Engine" Z. Yu, D. Liscinsky, A. Bhargava, L. Ziemba, E. Winstead, B, Sen, B. True, M. Timko, S. Herndon, R. Miake-Lye, and B. Anderson, Partners in Environmental Technology Technical Symposium & Workshop 2010 Poster Session.

"Development of a detailed microphysical model to simulate the formation of hydrocarbon-containing aerosols emitted from military aircraft engines" H.-W. Wong, M. Jun, I. Waitz, D. Liscinsky, J. Peck, S. Herndon, M. Colket, Z. Yu, B. True, J. Franklin, R. Miake-Lye, Partners in Environmental Technology Technical Symposium & Workshop 2011 Poster Session.

"Quantification of Hydrocarbon Condensation on Combustion Soot Particles" D. Liscinsky, Z. Yu, S. Herndon, B. True, A. Jennings, H.-W. Wong, M. Jun, J. Franklin, J. Peck, I. Waitz, M. Colket, R. Miake-Lye, Partners in Environmental Technology Technical Symposium & Workshop 2011 Poster Session.

"Characterization of Lubrication Oil Emissions from Aircraft Engine" Z. Yu, D. Liscinsky, L. Ziemba, E. Winstead, B. True, M. Timko, S. Herndon, R. Miake-Lye, and B. Anderson, Partners in Environmental Technology Technical Symposium & Workshop 2011 Poster Session.

**Other**

"Microphysical modeling of ultrafine hydrocarbon-containing aerosols in aircraft emissions" Mina Jun, Thesis, Department of Aeronautics and Astronautics, Massachusetts Institute of Technology, Cambridge, MA, June 2011.